VPL as an Analytical Tool for Semi-Automated Detection and Mapping of Masonry Decay

Sant’Antonio Church
2025 - 2026

Politecnico di Torino
Master’s Degree Course in Architecture For Heritage

From Point Cloud to HBIM: VPL as an Analytical Tool for Semi-Automated Detection and Mapping of Masonry Decay

A case study of the Sant’Antonio Church in Martina Franca

By
Mahtab Fallah

Supervisor
Prof. Elisabetta colucci

Co-Supervisors
Prof. Paolo Piumatti
Prof. Daniele Dabbene

in a collaboration with
Politecnico di Bari
Prof. Domenica Costantino
Prof. Vincenzo Saverio Alfio

2025-2026

Acknowledgements

Above all, I would like to thank my supervisor, **Prof. Elisabetta Colucci,** who has been much more than a professor to me. Her support, trust, and encouragement have shaped not only this thesis, but also the direction of my academic and personal growth. More than anything, I am grateful for the humanity and kindness she has always shown me. I owe her more than words can express.

I would also like to sincerely thank my co-supervisor, **Prof. Paolo Piumatti**, for his guidance, support, and valuable contribution throughout the development of this thesis; and I am also very grateful to **Prof. Daniele Dabbene** for his valuable feedbacks and perspective on architectural conservation, which helped me approach my work more critically.

I am also deeply grateful to **Prof. Domenica Costantino**, **Prof. Vincenzo Saverio Alfio**, and **Dr. Alfredo Restuccia Garofalo**, who made my time at Politecnico di Bari feel like more than just an academic experience. Their kindness, warmth, and hospitality made those six months in Puglia truly special to me. Puglia gave me people, places, and moments that made me feel at home in a way I will never forget, **e forse una parte di me è rimasta lì**.

A special place in these acknowledgements belongs to my nephews, **Sam** and **Diyar**. You bring a kind of joy into my life that makes everything I work for feel more meaningful. More than anything, I hope I can always be part of what makes you happy.

I cannot thank **my parents** and **my brothers**, **Mohsen**, **Mohammad**, and **Mehdi**, enough. Everything I have been able to dream and achieve was possible because you were always there behind me. You gave me the freedom to go further than I ever thought I could. You made it possible for me to fly, and every achievement of mine carries a part of your support, sacrifice, and love.

And finally, for **all of my friends**, thank you for surviving every thesis crisis, every existential conversation, every moment of self-doubt, and every mental breakdown along the way.

This thesis may have my name on its cover, but it belongs to all of you.

To **Sama**, and to those who were never afraid to stand against the darkness and sacrificed their lives and their freedom so that one day, **light may return to our home, Iran.**

Abstract

Accurate **3D metric surveys** have become an essential part of **built heritage conservation** for documenting complex historical architectures. However, despite their importance, a primary **challenge** is the **disconnection** of different types of data across isolated environments. Specifically, advanced decay mapping methods, such as semi-automated techniques like machine-learning-based methods, are often developed in **computer science environments**. This creates a significant interoperability **gap**, as these tools are usually detached from standard architectural workflows. Consequently, transitioning such diagnostic outputs into architectural practice is not a common practice; the resulting data often lacks editability, requiring technical expertise, which limits their practical application for conservation specialists. To address this issue, this thesis develops an **integrated** and **reproducible digital workflow** centered on **Rhinoceros** and **Grasshopper** as the **VPL** tool, on the complex historic architecture of the **Church of Sant'Antonio dei Cappuccini** in Martina Franca, Italy.

The methodology begins with a **multi-sensor 3D survey** combining aerial **UAV photogrammetry** and a **handheld Mobile Mapping System** (MMS) to record high-fidelity geometric datasets. Then, these point clouds are transformed into an **as-built NURBS model** that preserves structural irregularities and deformations rather than forcing geometric regularization. In the next phase of the methodology, a **Visual Programming Language** (VPL) framework is designed in Grasshopper to perform **semi-automated masonry decay mapping** by processing **RGB values** extracted from orthophotos. The resulting vector boundaries are directly projected onto the 3D model to function as a reliable diagnostic support tool for experts. In addition, comparative evaluations confirm that this parametric workflow significantly reduces processing time compared to manual 2D CAD drafting while maintaining high metric accuracy.

Ultimately, **this thesis demonstrates** that a **parametric workflow** not only accelerates the decay mapping process but also successfully centralizes these **multidisciplinary** datasets into an **interactive web-based platform**, creating a **unified**, **replicable**, and **scalable** framework for new analytical features that can be developed into a **complete digital tool** to **support heritage conservation** across different case studies.

Key words

Built Heritage; Point Cloud; Multi-Sensor 3D Metric Survey; NURBS As-Built Modelling; Visual Programming Language (VPL); RGB-Based Decay Detection; Semi-Automated Masonry Decay Mapping; Web-Based 3D Visualization

. Acknowledgements
. Abstract
. Key words
. Table of contents

.01 Introduction

1.1 Background and Problem Statement
1.2 Aim, Objectives, and Research Questions
1.3 Key Concepts and Definitions
    1.3.1 Digital Documentation and 3D Metric Survey of built Heritage
    1.3.2 As-Built NURBS Modelling and Reality-Based Representation
    1.3.3 Visual Programming Languages (VPL) in Architectural Workflows
1.4 Scope and Limitations
1.5 Structure of the Thesis
1.6 Systematic Literature Review
    1.6.1 Search Strategy
    1.6.2 Visualization of the Review Process
1.7 Research Gap

.02 Case Study

2.1 Site Location and Environmental Context
2.2 Historical Background of the Case Study
    2.2.1 Historical Background of Martina Franca
    2.2.2 Historical Background of the Church of Sant’Antonio dei Cappuccini

.03 Survey Metodology

3.1 Introduction
3.2 Survey Objectives
3.3 Survey Workflow
    3.3.1 Instruments and Techniques
    3.3.2 Post-Processing of Point Clouds

.04 Architectural Characteristics

4.1 General Composition
4.2 Exterior Architectural Characteristics
4.3 Interior Architectural Characteristics
4.4 Analysis of Architectural Geometric Forms
    4.4.1 Vaulting System
    4.4.2 Geometry of Openings
    4.4.3 Facade Orthophotos
4.5 Building Diagnosis
    4.5.1 Decay Detection Using a Manual Technique

.05 Geometric Modeling

5.1 Importing and Managing Point Clouds
5.2 Modelling Strategies (Workflow and LOD)
5.3 Accuracy Validation
5.4 Model Limitations and Challenges

.06 VPL-Based Analysits

6.1 Environment and Tools
6.2 RGB-Based Decay Detection
6.3 Final Workflow Definition
6.4 Evaluating the Mapping Methods: Manual vs. Semi-Automated

.07 Final Outputs

7.1 From Questions to Findings
7.2 Web-based Visualisation
7.3 Conclusions
7.4 Discussion and Limitations
7.5 Future Research Perspectives

. Bibliography

1. Introduction

Built heritage conservation requires reliable information from different fields, including architectural studies, metric survey, digital modelling, and condition assessment. This thesis investigates **how** 3D metric survey data, as-built architectural models, diagnostic results, and digital visualisation can be **conneced** in a **single** and **reproducible** workflow. This approach is centred on **Rhinoceros software and Grasshopper environment** and is tested through the case study of the Church of Sant'Antonio dei Cappuccini in Martina Franca. This chapter introduces the **background** and the **main problem** of the research. It then defines the **aim**, **objectives**, and **research questions**, followed by the scope and limitations of the study and the overall structure of the thesis. Finally, the conducted **systematic literature review** is illustrated in the final part of this chapter to define the existing gaps that the thesis can bridge.

1.1 Background and Problem Statement

In recent years, the **integration of multidisciplinary datasets** has transformed the way in which built heritage is documented, analysed, and managed. This development of 3D metric survey techniques has made it possible to generate highly detailed **point clouds**, **orthophotos**, **photographs**, and other forms of **digital documentation**. At the same time, architectural modelling, condition assessment, and web-based visualisation have created new possibilities for supporting conservation and restoration planning. However, one of the main **limitations** of current digital documentation is that geometric data, 3D architectural models, condition assessments, and analytical results are usually generated and managed in different **isolated software environments**. Survey data may be processed in a range of Geospetial software, architectural models may be developed in modelling or BIM software, condition assessments may be documented through 2D solid drawings or external analytical tools, and the final results may be presented through **separate** visualisation platforms. Therefore, this **disconnection** creates significant challenges for the comparison, interpretation, and management of heritage information between different groups of stakeholders. This limitation can be problematic in built heritage conservation, where planning decisions depend on understanding the relationships between surveyed geometry, architectural irregularities, geometric deformations, material conditions, and visible decay patterns, which have cause-and-effect relationships. Although 3D metric data acquisition is improving rapidly, the resulting information is still frequently used only as a **geometric reference**. Its analytical potential for documenting the existing condition of historic buildings is not always fully developed.

To investigate how these different forms of information are currently managed, a systematic literature review was conducted. The critical evaluation of the existing academic works identified a significant research problem: **geometric survey data, architectural models, condition assessments, diagnostic outputs, and visualisation results are generally produced through separate workflows, with limited integration between them.** Existing studies often address individual stages of the process but rarely connect them within the same reproducible and architecture-oriented environment.

To address this problem, this thesis proposes an integrated and reproducible workflow centred on Rhinoceros. The workflow links metric survey datasets with geometric information and material condition of built heritage and subsequently makes the results accessible through a web-based visualisation environment. The Church of **Sant'Antonio dei Cappuccini** in Martina Franca, Puglia, is used as the case study for developing and evaluating the proposed method. The framework begins with multi-sensor data acquisition, using UAV photogrammetry and a handheld Mobile Mapping System to document the exterior and interior areas of the building. The resulting point clouds construct the first geometric and visual record of the church and provide the main reference for the subsequent stages. An as-built model is then developed in Rhinoceros using a NURBS-based modelling approach.

This method aims to preserve the irregularities, deformations, and non-standard architectural characteristics observed in the survey data. Unlike highly idealised modelling approaches, which may replace the surveyed forms with regular and predefined components, the proposed approach maintains a direct relationship between **the point cloud** and the **reconstructed architectural geometry**. Visual Programming Language is subsequently introduced as an analytical tool. **Grasshopper** is used as the main tool to develop semi-automated procedures for **extracting** and **mapping** selected masonry **decay patterns** based on RGB information. The final outputs are integrated with the point clouds, architectural models, orthophotos, survey photographs, and methodological information within an interactive web-based environment. The proposed VPL-based diagnosis framework is **not** intended to replace expert diagnosis. Instead, it supports **repetitive operations** such as data selection, extraction, classification, and mapping. The interpretation and validation of decay categories and geometric conditions remain dependent on visual evidence and specialist assessment. Consequently, the main research problem addressed by this thesis is **the lack of an integrated workflow** capable of connecting metric survey data, as-built architectural modelling, diagnostic analysis, and accessible digital visualisation within the same reproducible process.

1.2 Aim, Objectives, and Research Questions

The main aim of this thesis is to develop and evaluate an integrated and reproducible workflow for supporting evidence-based conservation planning in built heritage. The proposed workflow connects multi-sensor metric survey data, as-built NURBS modelling, VPL-based diagnostic analysis, and web-based visualisation within a Rhino-centred environment.

To achieve this aim, the research follows these operational objectives:

1. To document the exterior and interior geometry of the Church of Sant'Antonio through multi-sensor survey techniques and to produce registered, high-fidelity point clouds.

2. To develop an as-built NURBS model in Rhinoceros that preserves the irregularities, deformations, and non-standard characteristics.

3. To develop a semi-automated Grasshopper workflow for identifying and mapping selected masonry decay patterns from RGB information extracted from orthophotos.

4. To integrate point clouds, as-built models, orthophotos, survey photographs, diagnostic outputs, and methodological information within an interactive web-based environment.

5. To evaluate the reproducibility and accessibility of the workflow for architects and heritage specialists without an advanced computer-science background.

The main research question that is leading this study is:

How can 3D metric survey data, as-built NURBS modelling, VPL-based diagnostic analysis, and web-based visualisation be connected within an integrated and reproducible workflow for supporting the documentation and conservation of built heritage?

This main question is defined through the following research questions:

As-Built Architectural Modelling

RQ1. How can an as-built NURBS model be developed in Rhinoceros from point-cloud data while preserving all the surveyed irregularities, deformations, and non-standard architectural characteristics of the historic building?

VPL-Based Decay Documentation

RQ2. How can Grasshopper and Visual Programming Language be used to semi-automatically identify and map selected masonry decay patterns from RGB information without relying on external computer-vision or machine-learning environments?

Information Integration and Accessibility

RQ3. How can survey datasets, architectural models, diagnostic results, orthophotos, photographs, and methodological information be integrated within a web-based environment?

Efficiency and Accuracy

RQ4. To what extent can the proposed parametric workflow reduce the time required for decay and condition mapping compared with manual procedures while maintaining comparable accuracy?

Reproducibility and User Accessibility

RQ5. To what extent is the proposed workflow reproducible and accessible for architects and built-heritage specialists without an advanced background?

1.3 Key Concepts and Definitions

This section introduces the key concepts and technical terms that shape the methodological framework of the thesis. Since the terms such as digital documentation, point cloud, as-built modelling, and visual programming may have different meanings based on the context, their use within this thesis is also briefly clarified. Therefore, this part provides the definitions necessary for understanding the workflow developed in the following chapters of the thesis.

1.3.1 Digital Documentation and 3D Metric Survey

Digital documentation of built heritage engages the **acquisition**, **processing**, **organisation**, and **representation** of information describing both the geometry and the physical condition of an existing building. Markiewicz et al. (2025) distinguish between geometrical digital documentation, which records the shape, dimensions, and the relationships of architectural elements, and qualitative documentation, which can also describe the physical properties, state of preservation, and visible degradation of the structure. Depending on the survey **objectives** and the **scale** of the documentation, the results can be represented by plans, sections, elevations, orthophotos, point clouds, and three-dimensional models. However, contemporary heritage documentation is no longer limited to producing 2D and 3D drawings; it now also involves collecting and organizing digital data so the building can be studied, conserved, and documented over time.

In this context, a 3D metric survey can be understood as the **reality-based acquisition** of the measurable geometry of an existing object or environment. Remondino (2011) defines reality-based 3D surveying and modelling as the digital recording and reconstruction of existing scenes through active sensors and range data, passive image-based sensors, conventional surveying techniques such as GNSS and total stations, or combinations of all of these methods. In fact, the choice of the technique is dependent on factors such as the required accuracy, object dimensions, accessibility, surface characteristics, equipment, and the purpose of the survey.

Nowadays, the principal product of a 3D metric survey is the point cloud. Point clouds have become the standard format for three-dimensional survey data and can be generated using different acquisition methods. Although these techniques are different in their principles and performance, their point-cloud outputs can be compared, registered, and combined at the same platforms. This characteristic is important for built heritage, where a single acquisition technique is insufficient. For this reason, multi-sensor approaches that are combining range-based and image-based methods have become established in the documentation of architectural heritage (Perfetti et al., 2023).

In this thesis, digital documentation and 3D metric surveys form the **foundation** of the entire workflow. The **Church of Sant'Antonio dei Cappuccini** is documented through a **multi-sensor** strategy, in which **UAV photogrammetry** captures the exterior surfaces and **handheld mobile laser scanning** records the interior spaces. To ensure spatial accuracy, a Total Station was used to acquire local topographic points, while GNSS measurements provided the global Ground Control Points (GCPs). The final registered point clouds serve as the primary reference for the subsequent phases. They support the generation of orthophotos, the geometric reconstruction and validation of the as-built NURBS 3D model, and the VPL-based diagnostic analysis. In summary, digital documentation in this research is understood as a continuous process connecting 3D metric survey data with modelling, building condition analysis, and the final web-based digital visualisation environment.

1.3.2 As-Built NURBS Modelling

NURBS (Non-Uniform Rational B-Splines) are a **mathematical method** for representing smooth and editable curves and surfaces through a set of **control points**, which is suitable for the reconstruction of complex geometries. Acosta et al. (2022) identify the heterogeneous, complex, and irregular morphology of heritage buildings as one of the main difficulties of conventional BIM modelling, since standardised libraries and modelling tools are mostly developed for new construction contexts. Reality-based representation of the built heritage is based on the **exact condition** of an existing building rather than just the idealised or hypothetical geometry. This distinction is particularly appropriate for built heritage, because the **deformation**, **construction irregularities**, **material behaviour**, **later interventions**, and **historical transformations** may change the geometries that are significantly different from the regular architectural primitives. In recent **recommendations** for heritage documentation, an as-built representation is described as a precisely modelled representation of the constructed object that includes its existing construction irregularities and eccentricities (Markiewicz et al., 2025).

A point cloud can record a large amount of metrically accurate information but cannot provide an organised architectural geometry by itself. Di Luggo et al. (2019) describe point-cloud data as a foundation from which support models can be created for special analytical purposes. The comparison between modelling approaches and techniques shows that a NURBS model produced in Rhinoceros from reality-based survey data can closely reproduce the form of the real situation, while the standard BIM environments may have difficulties for representing the particular and irregular configurations of historical architecture with geometric fidelity.

In this thesis, the term of **as-built NURBS model** refers to an editable geometric reconstruction developed directly from the surveyed data of the Church of Sant'Antonio. The objective is **intentionally** different from an idealised reconstruction and the relevant irregularities, asymmetries, deformations, changes in alignment, and non-standard architectural forms recorded in the point clouds are maintained. In this workflow, NURBS geometry is selected because it will combine continuous surface representation and local editability with direct compatibility with the Grasshopper environment used in the subsequent VPL analytical phase. However, the final model does not reproduce every single point of the survey exactly, and it is not automatically a complete HBIM model; it represents a **controlled**, **reality-based geometric foundation** for subsequent diagnostic analysis and information integration.

1.3.3 VPL in Architectural Workflows

VPL, which stands for Visual and graphical programming languages, provides an alternative method for constructing **computational** architectural workflows by using parameters, operations, and their relationships through an accessible graphical structure.

Within architectural environments, Grasshopper is one of the common examples of this approach. Wang et al. (2021) describe Grasshopper as a graphical programming and modelling platform based on node visualisation and demonstrate its use in a parametric heritage-documentation workflow. In this approach, parameter nodes remain visible to the operator, which facilitates modification and error correction, while different input parameters can generate corresponding outputs through predefined algorithmic relationships. This makes the computational procedure not only repeatable but also adjustable without repeating each operation manually. These characteristics make visual programming (VPL) particularly relevant when the operations need to be repeated, modified, or adapted to different datasets. In built heritage, VPL can therefore provide a connection between the geometry and computational operations while keeping the parameters for controlling the process accessible to the user.

In this thesis, **VPL** is used as an **analytical tool** rather than a tool for form generation. Here, Grasshopper provides the computational structure for the semi-automated identification and mapping of selected masonry decay patterns from orthophotos with **RGB information**. However, the workflow is operator-controlled rather than fully automated; the user is responsible for defining the degradation classes, choosing representative colours, adjusting tolerance values, identifying false selections, and validating the final extracted boundaries by comparing with the survey evidence. In this thesis, VPL connects **image-based** documentation, **computational analysis**, and the **3D model**, rather than as a replacement for specialist diagnosis.

1.4 Scope and Limitations

Case Study Scope

This thesis focuses on the Church of **Church of Sant'Antonio dei Cappuccini** in Martina Franca, Puglia. The church was selected as the case study because of its **complex historic geometry**, **irregular** architectural surfaces, visible material **decay**, and the availability of detailed exterior and interior survey datasets and the **lack of documents** to support the **conservation planning**. The research examines both the exterior and interior areas of the church. However, the purpose of the case study is not to provide a complete conservation project or structural assessment of the building. Instead, the church provides a controlled architectural context for developing, testing, and evaluating the proposed digital workflow. As the research is based on a single case study, the results cannot be automatically generalised to every historic building. Nevertheless, the methodological structure is designed to be **reproducible** and **adaptable** to also other built-heritage case studies.

Data Scope
The primary datasets used in this research were generated through **UAV photogrammetry** and **handheld Mobile Mapping System** surveys. These datasets document the exterior and interior geometry of the building and provide point clouds with geometric and RGB information. Orthophotos, survey photographs, registered point clouds, and the reconstructed architectural model are used as the principal **inputs** for the **analytical stages**. The thesis does **not** attempt to integrate every possible type of heritage information, such as historical archives, laboratory material tests, structural-monitoring data, or long-term environmental sensor records; however, it could be possible for future reaserches on this workflow. The point clouds are treated as the main reference. Therefore, the **reliability** of the subsequent **modelling** and **analytical** results depends on the **quality**, **density**, **registration accuracy**, **colour information**, and **spatial coverage** of the **original survey datasets**.

Modelling and Analytical Scope
The modelling stage is **limited** to an **as-built NURBS-based** representation developed in **Rhinoceros**. The objective is to represent the existing architectural geometry while preserving relevant irregularities and deformations. The research does **not** aim to replace the surveyed forms with standardised BIM families or fully regular parametric components. The **diagnostic analysis** focuses on selected masonry decay patterns that can be visually distinguished through **RGB information** contained in **orthophotos**. **Grasshopper** is used to extract areas corresponding to selected colour ranges and convert them into referenced curves representing the approximate boundaries of the observed decay on the exact position on the 3D model.

Limitations of RGB-Based Decay Mapping
The proposed **decay mapping** method is influenced by the **quality** and **consistency** of the **RGB color code information**. Variations caused by lighting conditions, shadows, surface texture, image resolution, moisture, colour similarities, and orthophoto-generation procedures may affect the results. The RGB thresholds **cannot** necessarily be transferred directly from one dataset or building surface to another. They must be **calibrated** according to the visual characteristics of the specific orthophoto and decay category. Consequently, the process is semi-automated rather than fully automated. The extracted boundaries may also contain noise or false selections. Therefore, visual inspection and manual refinement remain necessary. The resulting curves represent support for **decay documentation** and **not** a complete and ready-to-use diagnosis.

Expert Interpretation
This workflow is not intended to replace conservation specialists and experts. The **classification** and **interpretation** of decay patterns is still **dependent** on visual evidence, specialist knowledge, and, where required, additional material or laboratory investigations. The **VPL** procedure supports repetitive tasks such as colour selection, area extraction, curve generation, and data organisation, and it is also adaptable for converting to a web-based visualisation. Final decisions of each decay pattern must still be **validated** by qualified specialists.

Web-Based Integration
The final **web-based environment** is developed primarily as an inspection and communication platform. It allows users to activate and deactivate individual datasets, compare different representations, inspect selected decay categories, and access supporting documentation and add the notes or information that they need to keep and communicate with the other **stakeholders**. However, the platform does **not** have a function as a **complete management system** or archival database. Also, large point clouds and detailed models may require **optimisation** or **subsampling** to maintain acceptable web performance.

1.5 Structure of the Thesis

This thesis is structured as:
First, the thesis presents the **Systematic Literature Review**, examining current research on 3D metric survey, point-cloud documentation,
as-built and NURBS modelling, decay and condition assessment, Visual Programming Languages, HBIM-oriented integration, and web-based heritage visualisation, and identifies the methodological patterns and **the research gap**.
Chapter 2, introduces the case study of the Church of Sant'Antonio di Padova ai Cappuccini in Martina Franca. It describes the site and its surrounding context, historical development, architectural characteristics, exterior and interior composition, vaulting system, and the geometric characteristics of the principal openings and spaces, and decay diagnosis with the manual and traditional method in 2D drawings.
Chapter 3, presents the **surveying methodology**.
It explains the **objectives** of the metric documentation, the **instruments** and **techniques** used for **UAV photogrammetry**, **handheld MMS** surveying, and **topographic control,** as well as the post-processing, registration, density assessment, accuracy evaluation, and finally the generation of the high-fidelity reference datasets.
Chapter 4, describes the **as-built modelling process** developed in **Rhinoceros**. It explains the NURBS-based modelling **strategy**, the **relationship** between the point cloud and reconstructed geometry, and the **technique** used for representing irregular architectural elements, vaults, openings, and non-standard surfaces.

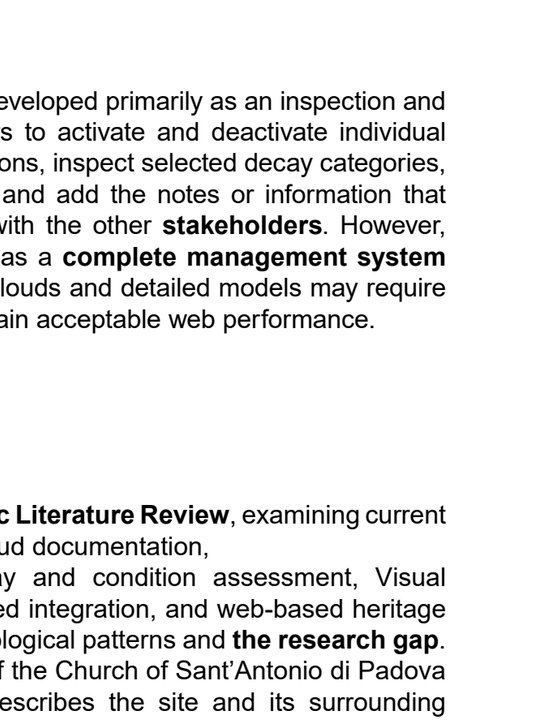


Figure 1.1. The methodological schema of the proposed workflow for built heritage.

Chapter 5, introduces the VPL-based diagnostic analysis developed in Grasshopper environment. It describes the semi-automated extraction and mapping of selected masonry decay patterns based on the RGB values of orthophotos.
Chapter 6, explains the web-based integration of the different datasets. It presents the preparation and organisation of the point clouds, architectural models, decay maps, orthophotos, photographs, and methodological information within the interactive platform.
Finally, **the last chapter** shows the main results and discusses the effectiveness, limitations, reproducibility, and accessibility of the proposed workflow. It also answers the research questions, summarises the principal contributions, and the possible developments for future works.

1.6 Systematic literature review

This **systematic literature review** was done to examine the current methods used for digital documentation, modelling, decay detection and condition analysis, and visualization of architectural heritage. The review is focused on the relationships between 3D metric survey data, as-built and NURBS modelling, decay and damage assessment, visual programming languages, and web-based 3D visualization.
The review is structured through a defined search strategy, followed by the **screening**, **classification**, and **visualization** of selected publications. This process helped to recognize the main limitations in the existing literature and to define the research gap that this thesis wants to address.

1.6.1 Search Strategy

The **search strategy** is a **concept-based** approach. Firstly, before writing the search strings, the main concepts of the thesis that define the scope of the research were identified. These concepts included cultural heritage, point clouds and 3D metric survey, as-built and NURBS modelling, decay and damage assessment, web-based 3D visualization, and Rhino, Grasshopper, and visual programming languages.
For each core concept, a set of **alternative keywords**, **technical terms**, and **common synonyms** were identified in the scientific literature. This phase was necessary because similar research is often described using different terminology across architecture, geomatics, conservation, and computer science.

The search was performed in the Scopus database within the title, abstract, and keyword fields through the TITLE-ABS-KEY command and with a focus on only English-language publications issued after 2014. Therefore, the publication period was limited to 2014–2026.
The search queries for using in the **scopus** website are organized progressively, moving from broad searches to more specific combinations directly related to the proposed methodology. The first query focused on the general relationship between cultural heritage and 3D metric survey and found **3,221** records. The search was then narrowed by integrating as-built, NURBS modelling, resulting in **48** records. A separate query investigated automated and semi-automated decay detection with **90** records.
To investigate the use of visual programming for built heritage condition assessment, the decay mapping was combined with Grasshopper, VPL, visual programming, and Rhinoceros keywords. This more specific query had 6 records.
Web-based visualization was also examined through two levels of queries; a general search concerning web-based visualization in built heritage resulted in **113** records, while a more focused query about web platforms visualization of point cloud and 3D model in the same platform returned 5 records.
Finally, a **highly specific** query combined all the principal concepts of this thesis: **point-cloud data, as-built modeling, VPL-based decay mapping, web-based visualization,** and **architectural heritage**. This query found no results. (The complete search strings, their focus, and the corresponding number of results are reported.)
Then the records were examined through title and abstract screening. Studies outside the field of architectural and built heritage, as well as publications that did not address 3D survey data, as-built modelling, condition assessment, visual programming, or web-based visualization, were excluded. The most recent remaining publications were then evaluated according to their methodological relevance to the development of an integrated workflow connecting metric survey data, architectural modelling, diagnostic analysis, and digital visualization.

Core Concept	Alternative Keywords & Synonyms in the Literature
Cultural Heritage	built heritage, historical monuments, architectural heritage, historic buildings, cultural assets
Point Clouds / 3D metric survey	point cloud, terrestrial laser scanning (TLS), LiDAR, photogrammetry, structure from motion (SfM), reality capture, 3D survey, digital survey, image-based modelling, range-based modelling, multi-sensor survey
As-built Modelling / NURBS Modelling	reverse engineering, as-is modeling, non-idealized modeling, irregular geometry reconstruction, Non-Uniform Rational B-Splines, freeform surface modeling, surface fitting, organic geometry reconstruction
Decay / Damage	decay mapping, deterioration mapping, damage mapping, defect detection, building pathology, condition assessment, condition survey, degradation mapping, weathering mapping, masonry decay, crack detection, damage classification
Web-based 3D Viewers	WebGL, Potree, Three.js, web-based point cloud viewer, online 3D viewer, Web-HBIM, digital twin platform, browser-based visualisation, virtual museum, 3D web GIS
Rhino / Grasshopper / VPL	Rhinoceros 3D, Grasshopper, visual programming language, algorithmic modelling, parametric modelling, computational design

Table 1.1. Core concepts and alternative keywords used in the literature search.

Table 1.2. Scopus search queries and corresponding search results.

Focus	Scopus query (TITLE-ABS-KEY)	Raw results	Purpose
3d metric survey	TITLE-ABS-KEY (("cultural heritage" OR "built heritage" OR "architectural heritage" OR "historic building*") AND ("point cloud*" OR "laser scanning" OR "terrestrial laser scanning" OR "photogrammetry" OR "reality capture")) AND PUBYEAR > 2014 AND PUBYEAR < 2026 AND LANGUAGE (english)	**3221**	
3d metric survey + Asbuilt, Nurbs Modeling	TITLE-ABS-KEY (("cultural heritage" OR "built heritage" OR "historic building*") AND ("point cloud*" OR "laser scanning" OR "photogrammetry") AND ("as-built model*" OR "HBIM" OR "scan-to-HBIM" OR "scan-to-BIM") AND ("NURBS" OR "Grasshopper" OR "Rhinoceros" OR "Rhino" OR "parametric modeling" OR "algorithmic modeling" OR "surface reconstruction" OR "complex geomet*")) AND PUBYEAR > 2014 AND PUBYEAR < 2026 AND (LIMIT-TO (LANGUAGE , "English"))	**48**	
Semi auto, auto decay detection	TITLE-ABS-KEY (("point cloud*" OR "HBIM" OR "3D model*") AND ("decay mapping" OR "deterioration mapping" OR "damage mapping" OR "condition mapping" OR "condition assessment" OR "building pathology") AND ("automat*" OR "semi-automat*" OR "deep learning" OR "machine learning" OR "artificial intelligence" OR "AI" OR "computer vision")) AND PUBYEAR > 2014 AND PUBYEAR < 2026 AND (LIMIT-TO (LANGUAGE , "English"))	**90**	
VPL based decay detection	**TITLE-ABS-KEY (("point cloud*" OR "HBIM" OR "3D model*") AND ("decay mapping" OR "deterioration mapping" OR "damage mapping" OR "condition mapping" OR "condition assessment" OR "building pathology") AND ("Grasshopper" OR "VPL" OR "visual programming" OR "algorithmic" OR "parametric mapping" OR "RhinoCommon" OR "script*")) AND PUBYEAR > 2014 AND PUBYEAR < 2026 AND (LIMIT-TO (LANGUAGE , "English"))**	**6**	**innovative part of thesis**
web based visualisation in built heritage	TITLE-ABS-KEY (("web-based" OR "WebGL" OR "Potree" OR "Three.js" OR "online 3D viewer") AND ("point cloud*" OR "3D model*") AND ("heritage" OR "historic building*")) AND PUBYEAR > 2014 AND PUBYEAR < 2026 AND LANGUAGE (english)	**113**	
web based visualisation of point cloud and model in the same platform	TITLE-ABS-KEY (("web-based" OR "WebGL" OR "Potree" OR "Three.js" OR "online 3D viewer" OR "web-GIS") AND ("point cloud*") AND ("3D model*" OR "HBIM" OR "mesh") AND ("co-visuali*" OR "hybrid visuali*" OR "integrat*" OR "fusion" OR "overlay*" OR "simultaneous* render*" OR "joint* render*") AND ("heritage" OR "historic building*")) AND PUBYEAR > 2014 AND PUBYEAR < 2026 AND (LIMIT-TO (LANGUAGE , "English"))	**5**	
web based visualisation of point cloud,3D model, Decay mapping, survey documentation in the same platform	**TITLE-ABS-KEY (("point cloud" AND ("Rhino" OR "Grasshopper" OR "visual programming") AND ("decay" OR "deterioration" OR "damage") AND ("web-based" OR "WebGL") AND ("heritage" OR "historic building")) AND PUBYEAR > 2014 AND PUBYEAR < 2026 AND LANGUAGE (english)**	**0**	**innovative part of thesis**

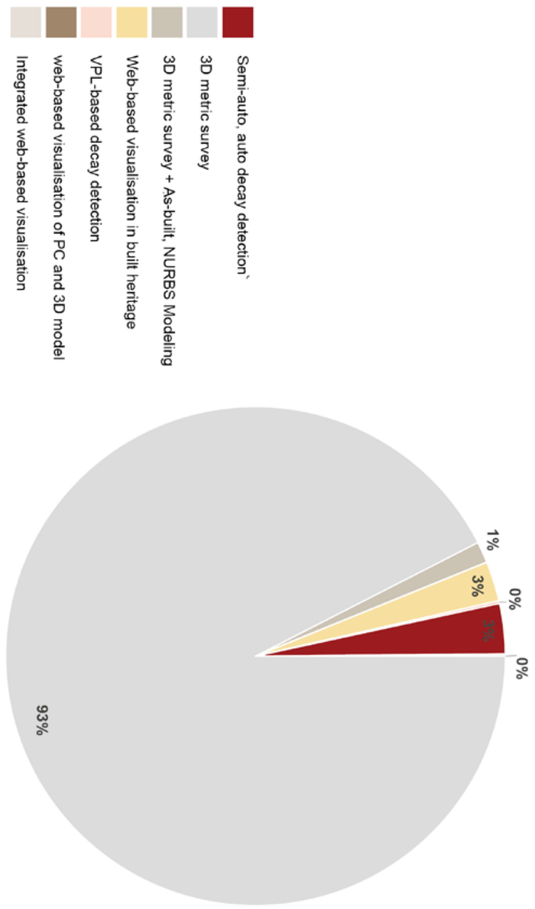


Figure 1.2. Distribution of Scopus search for each query and its corresponding results in a pie chart.

1.6.2 Visualization of the Review Process

Following the screening process, the **most recent** and **most relevant publications** were organised in a **literature matrix** to support a comparison of their objectives, methods, main inputs, and main outcomes. Each study was evaluated based on a set of criteria from their core concepts, including the use of 3D metric survey data, Rhino or Grasshopper, visual programming languages, scan-to-BIM procedures, semi-automatic decay analysis, web-based visualisation, and the integration of them in the same environment. To facilitate visual comparison, the results were classified as **Yes**, **Partial**, or **No** and illustrated through a **colour-coded** system. Green indicates that it was fully addressed; yellow indicates that it was only partially addressed, and red indicates that it was absent. This comparative visualisation helped to understand the methodological patterns.

	Year	Short reference	Title	key concept	3d metric survey	main software Rhino / Grasshopper	VPL	scan to bim	Decay analysis	Web-based	Model + point cloud in same viewer	3D decay / defect in web	Survey documentation	Measurement / section tools in web	Decay detection Automation level	Main output	Source URL
1	2026	Lasorella et al.	Integrated Digital Environments for the Knowledge and Management of Low-Accessible Cultural Heritage: A Multiscale Web-Based Framework	Web point-cloud + decay	Yes	No	No	Partial	Yes	Yes	Partial	Yes	Yes	Partial	Semi-automatic	Multiscale web environment with point-cloud-based conservation mapping	https://doi.org/10.3390/heritage9040133
2	2026	Lanzara & Improta	Scan-to-Scoring: An Algorithmic Model for Conservation Maintenance Records	VPL risk/condition scoring	Yes	Partial	Yes	Yes	Yes	Partial	No	No	No	No	Semi-automatic	Colour-coded risk scoring on point clouds/BRep/HBIM	https://doi.org/10.5194/isprs-archives-XLVIII-2-W12-2026-231-2026
3	2026	Sanz-Honrado et al.	Seg4D: An Open-Source Solution for Supporting the Diagnosis of Historic Constructions from 3D Point Clouds	Automated point-cloud diagnosis	Yes	No	No	No	Yes	No	No	No	No	No	Automatic / semi-automatic	Open-source damage detection(machin learning) and segmentation in point-cloud environment	https://doi.org/10.5194/isprs-archives-XLVIII-2-W12-2026-439-2026
4	2025	Vignali et al.	Interactive Visualization Tools for Managing the Monitoring System of the Piazza del Duomo UNESCO Site in Pisa	Rhino/GH + web monitoring	Yes	Yes	Yes	Partial	No	Yes	No	No	No	Yes	Semi-automatic	Web-embedded 3D information model and sensor visualization	https://doi.org/10.3390/heritage8010005
5	2025	Gaspari et al.	Collaborative Defect Annotation on 3D Seamless Open-Source Framework	Web defect mapping	Yes	No	No	No	Yes	Yes	Partial	Yes	Yes	Partial	Manual / collaborative	Shared web platform for defect annotation on 3D survey products	https://doi.org/10.5194/isprs-archives-XLVIII-G-2025-505-2025
6	2025	Sánchez-Aparicio et al.	A Holistic Solution for Supporting the Diagnosis of Historic Constructions from 3D Point Clouds	Automated point-cloud diagnosis	Yes	No	No	No	Yes	No	No	No	No	No	Automatic / semi-automatic	Segmentation and damage diagnosis directly on 3D point clouds	https://doi.org/10.3390/rs17122018
7	2024	Lanzara et al.	VPL Geometry Processing for Open Multilevel and Multiscalar Databases	VPL + diagnostics + web	Partial	Partial	Yes	Partial	Partial	Yes	Partial	Partial	Yes	No	Semi-automatic	Grid/cell-based diagnostic geolocation on open web platforms	https://doi.org/10.5194/isprs-archives-XLVIII-2-W8-2024-273-2024
8	2024	Aricò et al.	Scan-to-BIM Process and Architectural Conservation	Point cloud + HBIM + decay	Yes	No	No	Yes	Yes	No	No	No	Yes	No	Manual / assisted	Decay map generated in HBIM	https://doi.org/10.3390/heritage7110294
9	2023	Brown et al.	Visualizing Digital Architectural Data for Heritage Education	Rhino + point cloud + web	Yes	Yes	No	No	No	Yes	Yes	No	Yes	Yes	Manual	Potree + Three.js viewer with Rhino reconstructions and point clouds	https://doi.org/10.2352/EI.2023.35.1.VDA-393
10	2023	Croce et al.	H-BIM and Artificial Intelligence: Classification of Architectural Heritage for Semi-Automatic Scan-to-BIM Reconstruction	AI/VPL point-cloud classification	Yes	Yes	Yes	Yes	No	No	No	No	No	No	Semi-automatic	Classified point clouds managed between processing and Rhino modelling	https://doi.org/10.3390/s23052497
11	2022	Bruno et al.	VERBuM—Virtual Enhanced Reality for Building Modelling	Web HBIM	Yes	No	No	Yes	No	Yes	Partial	No	Yes	Partial	Manual / assisted	HBIM, meshes, point clouds, VR	https://www.itcon.org/papers/2022_02-ITcon-Bruno.pdf
12	2021	Croce et al.	From the Semantic Point Cloud to Heritage-Building Information Modeling: A Semiautomatic Approach Exploiting Machine Learning	point cloud + HBIM	Yes	Partial	Partial	Yes	No	No	No	No	No	No	Semi-automatic	Classified point cloud supporting HBIM reconstruction	https://doi.org/10.3390/rs13030461
13	2021	Lercari et al.	Building Cultural Heritage Resilience through Remote Sensing: An Integrated Approach Using Multi-Temporal Site Monitoring, Datafication, and Web-GL Visualization	Web point-cloud monitoring	Yes	No	No	No	Partial	Yes	Yes	Partial	Yes	Partial	Assisted	Potree/WebGL point-cloud environment	https://doi.org/10.3390/rs13204130
14	2019	Malinverni et al.	Modelling in HBIM to Document Materials Decay by a Thematic Mapping to Manage the Cultural Heritage	HBIM + decay	Yes	No	No	Yes	Yes	No	No	No	Yes	No	Manual / assisted	Semantic/thematic decay mapping in HBIM	https://doi.org/10.5194/isprs-archives-XLII-2-W11-777-2019
15	2018	Shotton	Living in the Clouds: Conceptual Reconstructions of Harbour Structures	Rhino + point cloud + web	Yes	Yes	No	No	No	Yes	Yes	No	No	Partial	Manual	Rhino reconstructions over web point clouds	https://doi.org/10.1108/JCHMSD-08-2017-0052
16	2017	Chiabrando et al.	Modeling the Decay in an HBIM Starting from 3D Point Clouds: A Followed Approach for Cultural Heritage Knowledge	Point cloud + HBIM + decay	Yes	No	No	Yes	Yes	No	No	No	Yes	No	Manual / assisted	Decay mapped in desktop HBIM	https://doi.org/10.5194/isprs-archives-XLII-2-W5-605-2017
17	2014	Stefani et al.	Developing a toolkit for mapping and displaying stone alteration on a web-based documentation platform	Web + decay mapping	Partial	No	No	No	Yes	Yes	No	Yes	Yes	Partial	Manual / assisted	Web-based 3D documentation and stone mapping	https://doi.org/10.1016/j.culher.2013.01.011

Table 1.3. Comparative literature review matrix of the selected studies and their workflow criterias.

Table 1.3. Comparative literature review matrix of the selected studies and their workflow criterias. (continued)

1.7 Research gap

The **study** and the **comparison** of the selected academic articles show that several components of our proposed workflow have already been investigated individually. Numerous studies address 3D metric survey and point-cloud generation, while the others focus on **scan-to-BIM techniques**, **architectural modelling, decay detectio**n, or **web-based visualisation**. However, these key concepts are generally developed within **separate** methodological and environmental contexts. Point clouds are frequently used for geometric reconstruction but are not directly connected to editable condition-mapping practices. Similarly, **semi-automatic** or **automatic decay detection** studies often rely on **external** computer-vision, machine-learning, or image-processing environments, with **limited integration** into software **commonly** used for **architectural modelling** and also **limited integration** into **web-based presentation**. The review also indicates **limited** use of **Grasshopper** as the principal analytical environment for semi-automated decay documentation. Visual Programming Languages are usually applied to geometric generation, parametric modelling, or just data management, but their potential for extracting, mapping, and organising visible decay information within a reality-based architectural model remains not explored. Web-based platforms are increasingly used for the visualisation of point clouds and 3D models. Nevertheless, these platforms do not always integrate survey evidence, architectural geometry, diagnostic results, orthophotos, photographs, and methodological information in the same environment. Therefore, the identified research gap is **not** the absence of methods for individual documentation and analysis tasks. Instead, it is the lack of an **integrated**, reproducible, and architecture-oriented workflow connecting:

_ Multi-sensor metric survey data;
_ As-built NURBS modelling;
_ VPL-based decay analysis;
_ Web-based visualisation.

2. Case Study

The study of **cultural heritage** needs a **multidisciplinary vision**, which means historical aspects, architectural analysis, and digital documentation are totally connected. Therefore, Inaccurate, incomplete, or unreliable information can lead us to incorrect documentation and then may negatively affect **digital strategies** and **modelling outcomes**. For this reason, before defining the methodological framework of the thesis, it is essential to present a complete understanding of the case study. The cultural heritage examined in this thesis is the **Church of Sant'Antonio dei Cappuccini**, located in the **Valle d'Itria**, near the city of **Martina Franca**, in southern Italy, in **Puglia**. This church is a significant example of a religious heritage that has gone through multiple historical phases, from its origins as a Basilian monastic settlement to its last transformation to the Capuchin style. The value of this case study is not only in its historical and artistic field, but it is also in its architectural complexity and its transformations over time, which made it suitable for an HBIM-oriented investigation with a focus on understanding its geometry, construction phases, and the relationship between **original historical documentation** and **digital representation**. In conclusion, this chapter presents the church to support the following phases in this theis.

Figure 2.1. Aerial view of the Church of Sant' Antonio dei Cappuccini and its surrounding context.

2.1 Site location and environmental context

The identification of the **site location** and environmental context, illustrates a fundamental step for understanding the current condition of the church. The **Church of Sant'Antonio dei Cappuccini** is located in Valle d'Itria (Puglia, southern Italy), between Martina Franca and Locorotondo. The site is placed in the middle of a landscape which is characterized by undulating Topography and a strong historical connection to agricultural and religious activities of the Apulian region.

The church is a part of a **religious complex** that includes the former Capuchin convent, around an internal courtyard. This configuration of the complex shows a clear relationship between built volumes and open spaces, which reflects the functional and symbolic requirements of monastic architecture. It is located in a **semi-urban** area **outside the city**, and this environment features mostly open areas and low-density development; so the location fully matches Capuchin principles to ensure both accessibility and a suitable isolation from urban areas.

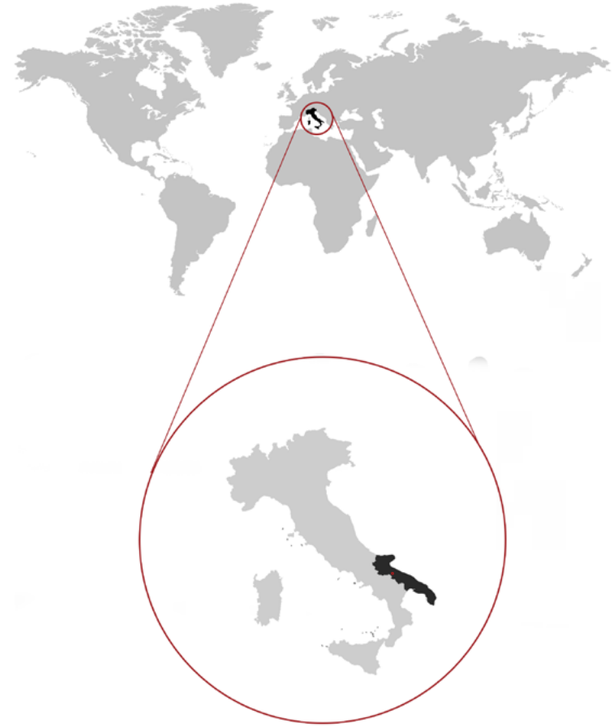


Figure 2.2. Geographical location of the case study in Puglia, Martina Franca, southern Italy.

In addition, from an environmental perspective, the site is under the **typical Mediterranean climatic condition,** which is defined by **intense solar radiation** and **high-temperature** summers, combined with **high humidity**, mild winters. These kinds of environmental conditions apply continuous **thermal** and **moisture-related stress** to the building. The main material of the church, which is a local porous limestone (calcarenite), has a high capacity to absorb moisture, so the repeated seasonal cycles of wetting and drying create the salt crystallization on and inside the stone surface (efflorescence and sub-efflorescence). Over long periods, these processes could cause a loss of material cohesion and surface erosion. Besides the masonry structures, the internal wooden elements of the church are also sensitive to environmental conditions. The refined wooden altars, choir, and ornamental furnishings are also affected by variations in temperature and relative humidity, which can cause dimensional changes in them. In conclusion, the interaction between **climatic** happenings and the **structural characteristics** of the masonry has created differential thermal expansion and moisture-induced movements. These effects together have contributed to visible morphological changes and deformations, including out-of-plumb walls, cracks, and local sagging of elements or etc. In these situations, the accuracy of documentation of these geometric irregularities is essential for the modelling phase, because they reflect the long-term environmental impact and structural behaviour of the building.



Figure 2.3. (a) Exterior view of the church: main façad.



Figure 2.3. (b) Interior view of the church: nave interior



Figure 2.4. Urban context and site location of the church in Martina Franca (Source: Elaborated by the author using data from the Open Data Portal of the Apulia Region).

2.2 Historical background of case study

This part will focuse on the **historical background** of the church of Sant'Antonio and its environmental context.

2.2.1 Historical Background of Martina Franca

Where the urban and architectural development was significantly happened between the late 16th and 18th centuries. In this period, the city experienced a phase of growth and architectural consolidation, becoming an important local center within the edge of territorial system of southern Puglia. The historic urban design developed around religious institutions, newly constructed residences, and public spaces, reflecting the social and cultural of the time.
In the 18th century in particular, Martina Franca was characterized by an active building culture, supported by local commiunity and religious orders. Then, the using of late-Baroque architectural language, comibined to local materials and construction traditions, contributed to defining the identity of this town and its surrounding territory.

2.2.2 Historical Background of the Church of Sant'Antonio

The **Church of Sant'Antonio dei Cappuccini** is a result of a long process of **constructions, transformation, and reuse** for different aims. The earliest phase of the site is related to a settlement established by **Basilian monks**, who followed the **Byzantine rite** and were connected to the **Monastery of San Nicola di Casole** near Otranto, founded in **1099**. During this period, the Basilian community developed a **religious and agricultural complex**, including an **underground crypt** that has a painted image of the **Madonna dell'Odegitria**. The cult associated with this image became widespread throughout the surroundings and was a really important part in the shaping of the **religious identity of Puglia**,and also, contributing to the naming of the **Valle d'Itria** during the **Early Modern era**. According to local historical sources, this devotion played a key role in the religious identity of Puglia and contributed to the name of the Valle d'Itria during the Early Modern period (Martina Cultura, n.d.). Then in the **16th century**, the site underwent a major transformation with the interventions of the **Capuchin Friars**,and inspired by the **Franciscan tradition**. The Capuchins decided to start to build a **new church and convent** directly on the site of the **Ex-Basilian settlement**, with maintaining the religius field of the place redefining its **architectural aspects** and **monastic configuration**. During this phase, the image of the Madonna dell'Odegitria was **transferred** from the undeground to the new constructed church, while the **underground structures** mostly fell into abandonment (Martina Cultura, n.d.).

The construction of the current church was **completed in 1590**, as indicated by the **date engraved on the facade** of the main portal. Then next architectural interventions shaped the building; For example, in **1698**, the **façade was renovated** based on a design idea by a Capuchin friar who was also an **architect and master stonemason**. Then another significant phase occurred in **1757**, with the construction of the **bell gable** on the left part of the church. It was characterized by the **Baroque style** features. These construction phases and stylistic transformations have been documented in local historical sources and are confirmed by recent academic studies which reflect the **progressive architectural layering** of the church and its environment. (Martina Cultura, n.d.; Alfio et al., 2025). The religious field remained active for several centuries and played a **religious and social key role** within the local context. Following the religious orders during the **Napoleonic period** and later during the **unification of Italy in the 19th century**, the complex again experienced some **changes in use and function**. Despite these transformations, the church has preserved its main architectural adjustments, including its **longitudinal plan**, **deep lateral chapels**, and **refined interior wooden decorations**, which are identified in recent academic research as elements of particular historical and artistic relevance which also one the essential parts of this research is identifing them to have a clear vision for the next steps in **documenting and modeling them based on the reality**. Overall, the historical development of the Church of Sant'Antonio dei Cappuccini reflects a **layered process** in which religious traditions, architectural choices, and historical events have interacted over the time. This evolution, documented mostly through local historical sources and validated by recent academic literature; however, the **historical documents related to this church is limited**, which makes a comprehensive reconstruction of its architectural history particularly challenging. But still they can provide a framework for understanding the **architectural complexity** of the building and support its selection as a **case study for advanced digital documentation and diagnosis analysis**.



Figure 2.5. Historical illustration of Capuchin monks, c. 1880



Medival Period



Presence of early **religious activity** in the regio related to the foundation of the Monastery of San Nicola di Casole in Puglia.

Establishment of a Basilian **monastic settlement** following the Byzantine rite.

Creation of a hypogeal crypt with a painted image of the Madonna dell'Odegitria.

Diffusion of the cult of the Madonna dell'Odegitria in Apulia and the Valle d'Itria.

16th Century

- **1589**

Construction of the present church, as the date date engraved on the main portal. Realization of wooden interior decorations (altars, pulpit, choir, tabernacle).

Execution of the **high altar** altarpiece (Assumption) by Antonio D'Orlando.

17th Century

- **1676**

Painting of Madonna of the Graces and Saint Felix of Cantalice by Nicola Gliri.

- **1698**

Renovation of the church façade by Friar Angelo Bruni.



18th Century

- **1757**

Construction of the campanile a vela with Baroque features.

- **1780**

Construction and decoration of the Volto Santo Chapel. Paintings by Domenico Carella.

19th Century

Suppression of religious orders and functional change of the convent.



20th Century

Extensive alterations to the **convent** and loss of original monastic layout.

Present

Lack of historical documentation, supporting the **conservation planning**

Figure 2.6. Historical development of the Church of Sant'Antonio dei Cappuccini during 7 century.

3. Survey Methodology

In this context, reliable **3D architectural modelling** and **condition analysis** depend on accurate and complete **metric documentation**. For this reason, the survey of the **Church of Sant'Antonio dei Cappuccini** was planned by combining different **acquisition techniques**, each selected according to the characteristics of the building and the accessibility of its spaces. The **exterior areas** were documented through **UAV photogrammetry**, while the **interior spaces** were recorded using a handheld **Mobile Mapping System**. **GNSS measurements** were also used to establish **Ground Control Points (GCPs)** to provide **topographic control** and to support the **spatial accuracy** of the final datasets.

This chapter describes the **instruments**, **fieldwork procedures**, and **data processing** stages adopted during the survey. It also explains the **generation** and **registration** of the point clouds and the orthophotos , and the evaluation of data density and accuracy. The resulting datasets form the following chapters.

3.1 Introduction

This chapter describes the **surveying methodology** for the digital documentation of the **Church of Sant'Antonio dei Cappuccini** in Martina Franca, which was conducted in collaboration with the Geomatics laboratory of Politecnico di Bari.

The survey is the first operational phase of the research, since the quality of the following modelling strategy and **VPL-based analysis** steps strongly depends on the reliability of the acquired spatial data. For this reason, the survey was planned not only like a simple data collection activity but also as the basis for creating a high accuracy **geometric reference** of the architectural complex.

This church has a complex configuration, including external façades, internal vaulted spaces, side chapels, altars, decorative elements, and irregular masonry surfaces. In these conditions, we have to plan a survey strategy that is able to document both the general architectural form and also the local geometric details. Also, some parts of the building were difficult to access or not fully visible with a single acquisition. For this reason, a **multi-sensor approach** was chosen; combining aerial (**UAV) photogrammetry** and handheld **Mobile Laser Scanning (MMS)** methods to have a more complete result of the building.

Based on this methodology, **UAV photogrammetry** was used to document the external surfaces and also the architectural context around the church, while handheld **laser scanning (MMS)** was used to acquire the internal spaces; then the integration of these two datasets made it possible for us to overcome the limits of each individual technique and to reduce the loss of geometric information during the modelling phase. The survey was also supported by a **GNSS-based topographic framework**, which allowed the final dataset to be **georeferenced** and placed in a consistent reference system.



In conclusion, the chapter is written based on the main phases of the survey framework. First, the objectives of the survey are described in relation to the general aims of the thesis. Then, the instruments and acquisition techniques are explained. Finally, the accuracy assessment and the finalized high-fidelity reference dataset are discussed. Therefore, this dataset provides the geometric basis for the next **NURBS-based modelling**, **diagnostic analysis**, and **HBIM-oriented documentation** and this multi-sensor method could be a defined workflow for case studies with similar limitations.

Figure 3.1. Field activities during the metric survey of the Church of Sant'Antonio dei Cappuccini: (a) survey equipment preparation and (b) interior data acquisition.

3.2 Survey objectives

The main objective of this survey was to create a reliable **digital copy** of the **Church of Sant'Antonio dei Cappuccini** and its complex. Then this digital representation is aimed at supporting the following phases of the research, including the **as-built NURBS-based modelling**, the **VPL-based diagnostic analysis**, and the organization of information. In this case, the survey is considered a **3D metric survey** activity, as well as the first step for transforming the physical building into an interpretable digital reference for future architectural analysis. The case study was selected because of its historical and architectural value. The church, located in Martina Franca, presents a layered architectural design and includes elements with particular importance, such as the altars and their handcrafted wooden decorations. For this reason, the survey had to record not only the geometric form of the building, but also the specific architectural and decorative features and paintings that define its cultural value. The aim was therefore to obtain a dataset able to include both geometric interpretation and future analysis and monitoring works, at the same time.

A second objective was to document the **real geometry** of the church with sufficient accuracy for generating **2D drawings** and **3D architectural models**, because, despite the high heritage value of the church, no complete official documentation was available to use for the conservation plans. Mostly, historic masonry buildings include irregular surfaces, local deformations, non-standard geometries, and constructive discontinuities, but these aspects are usually simplified in standard modelling workflows, since they are essential to have as-built documents. Therefore, this survey focuses on capturing the real **morphological condition** of the building, including façades, vaulted spaces, side chapels, altars, connections, and masonry surfaces.

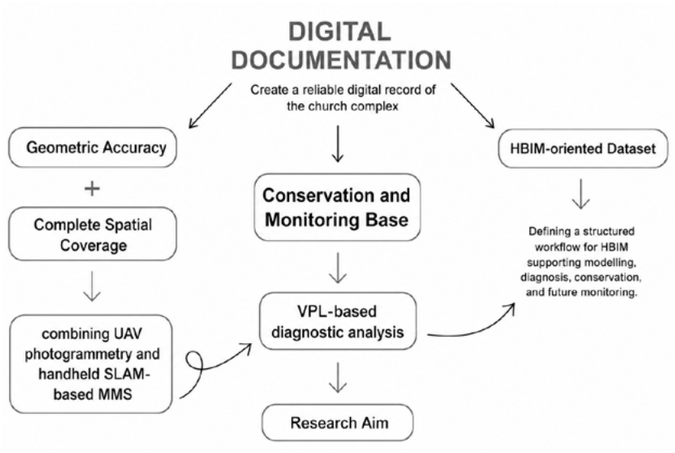


Figure 3.2. Main objectives and methodological framework of the digital documentation process.

Another important objective was to achieve complete coverage of both the external and internal parts. The complexity of the building and the limited accessibility of some areas made it impossible to rely on a single acquisition method, so the combination of UAV photogrammetry and the MMS technique allowed the research to reduce missing data and to produce a more complete representation of the church, without losing information needed for the subsequent phases. For the internal spaces, the survey relied on handheld Mobile Laser Scanning (MMS) based on the SLAM algorithm, establishing a dynamic data acquisition workflow. The survey also aimed to create a multi-scale geometric dataset. The church includes both large architectural volumes and smaller, detailed elements, such as decorative parts, vault intersections, altars, and irregular masonry surfaces. These elements require different levels of resolution. For this reason, the acquisition strategy had to support both the overall documentation of the building and the detailed recording of selected areas. This objective was necessary because the following modelling phase needed a point cloud dense enough for the reconstruction of complex within NURBS surfaces. A further objective was to produce a metric base useful for conservation, monitoring, and heritage management. The digital documentation of the church can support the understanding of its current state of conservation and can be used as a reference for future comparison. In this way, the survey data are useful not only for the present thesis workflow but also for tracking possible changes over time, supporting restoration decisions, and improving the management of cultural heritage through HBIM-based systems.

Finally, the survey can establish a high-fidelity point cloud.



Figure 3.3. Field operation of the survey

Figure 3.4. UAV photogrammetric survey of the church exterior.

3.3 Survey workflow

This section is related to the **computational workflow** that shows the transformation of the raw spatial data acquired from both the **UAV photogrammetric survey** and the handheld **Mobile Laser Scanning (MMS)** into a unified geometric model. The **post-processing** phase is critical for **co-registration** of the different multi-sensor datasets, finding the systematic errors, and finally ensuring that the output meets the **geometric reliability** required for the project's purposes.

The whole chapter is divided into three main phases; First, the specific instrumentation, sensor configurations, and field acquisition techniques for acquiring the raw data. Second, the post-processing operations include **point cloud registration** through the **Iterative Closest Point (ICP)** algorithm, **noise filtering**, and **dataset optimization**. Finally, the **accuracy assessment** is done using topographic **Check Points (CPs)** to evaluate the metric reliability and analyze the distribution of **residual errors** of the integrated dense cloud.

Figure 3.5. Multi-sensor 3D metric survey strategy combining UAV photogrammetry, topographic control, and handheld MMS.

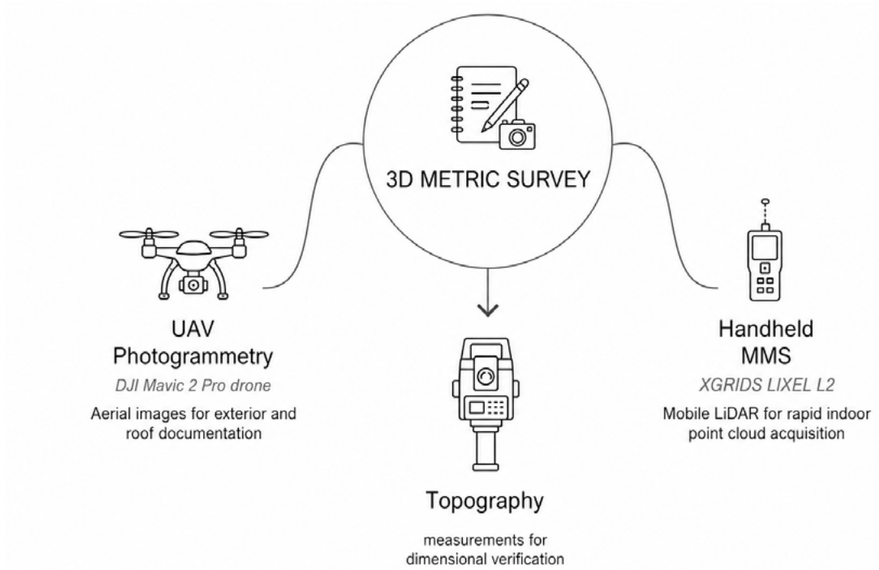




Figure 3.6. Distribution of GCPs used for georeferencing the UAV. The (11) Ground Control Points (GCPs) were measured using a total station from a GNSS-georeferenced topographic network.

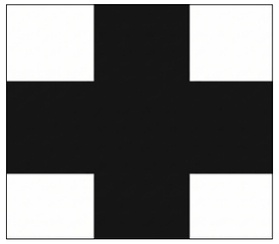


Figure 3.7. GCPs Typology.

3.3.1 Instruments and Techniques

To achieve a complete and multi-scale digital documentation of the **Church of Sant'Antonio dei Cappuccini**, a **multi-sensor data acquisition** strategy was conducted. This approach combines **aerial photogrammetry** for the exterior envelope with handheld **Mobile Laser Scanning (MMS)** for the intricate interior spaces. The technical specifications of the instruments and the specific techniques used in the on-site survey are described here:

1. Topographic Control and Georeferencing Framework

To integrate these two different datasets (the aerial photogrammetric cloud and the internal point cloud) into a unique reference system, a **topographic control network** was mandatory. For the georeferencing framework, we used a **Leica GNSS Viva 12 receiver**. This instrument uses advanced **SmartTrack+** technology with 120 channels, ensuring high-reliability tracking of multiple satellite signals (GPS, GLONASS, and Galileo). The topographic field survey was conducted in **Post-Processing Kinematic (PPK)** mode to acquire the spatial coordinates of the main topographic vertices (network stations) distributed strategically around the church. The GNSS raw data in **Rinex format** was post-processed using **Leica Infinity** proprietary software by referencing the baseline measurements to the nearest permanent GNSS reference station.



Figure 3.8. The instruments used for topographic control and georeferencing: (a) Leica Viva TS12 total station and (b) Leica Viva GNSS receiver.

This **PPK** configuration guarantees an absolute high-precision phase measurement accuracy of **5 mm + 0.5 ppm** horizontally and **10 mm + 0.5 ppm** vertically. In addition, from these georeferenced vertices, a **Leica Viva TS12 robotic total station** was used to measure the 11 **Ground Control Points (GCPs)**. These 11 certified GCPs served as the absolute coordinate baseline to register the photogrammetric model in the official **RDN2008-UTM33N (EPSG:6708)** reference system, providing the exact metric controls needed to validate the final multi-sensor dataset.

GNSS Technology	**Advanced measurement engine**	
	Leica patented SmartTrack+ technology	• Jamming resistant measurements • High precision pulse aperture multipath correlator • Excellent low elevation tracking technology • Very low noise GNSS carrier phase measurements with <0.5 mm precision • Minimum acquisition time
	No. of channels	120 channels
	Reacquisition time	<1 sec
	GNSS Measurements	
	Satellite signals tracking	GPS: L1, L2, L2C, L5 (CA, P, C code) GLONASS: L1, L2 (C/A, P narrow Code); Galileo (Test); GIOVE-A, GIOVE-B; Galileo: E1, E5a, E5b, Alt-BOC; Compass; SBAS: WAAS, EGNOS, GAGAN, MSAS
Measurement Performance	**Accuracy***	
	DGPS/RTCM	Typically 25 cm (rms)
	RTK Rapid static (phase) Static mode after initialization	Horizontal: 5 mm + 0.5 ppm (rms) Vertical: 10 mm + 0.5 ppm (rms)
	RTK Kinematic (phase) Moving mode after initialization	Horizontal: 10 mm + 1 ppm (rms) Vertical: 20 mm + 1 ppm (rms)
	Post Processing (phase) Static with long observations	Horizontal: 3 mm + 0.5 ppm (rms) Vertical: 6 mm + 0.5 ppm (rms)
	Post Processing (phase) Rapid static mode	Horizontal: 5 mm + 0.5 ppm (rms) Vertical: 10 mm + 0.5 ppm (rms)
	On-The-Fly initialization	
	Reliability†	Better than 99.99% using Leica SmartCheck+ technology
	Time for initialization	Typically 8 sec
	RTK baseline range	up to 50 km

Table 3.1. Technical specifications and measurement performance of the Leica Viva GNSS receiver.

2. Aerial Photogrammetric Infrastructure (UAV)

For the digital documentation of the roofs, high-altitude external surfaces, and the architectural environment around the church, an **Unmanned Aerial Vehicle (UAV)** was used. The equipment used was a **DJI Mavic 2 PRO** multi-rotor drone. This lightweight UAV (maximum take-off weight of 907 g) provides high operational flexibility and a maximum flight time of approximately 31 minutes, which was sufficient to do a complete programmatic flight plan over the monumental complex. The drone is equipped with an integrated **Hasselblad L1D-20c** camera, featuring a **1-inch CMOS sensor** for capturing high-resolution images of **20 million pixels** (photo size 5472 × 3648). The optical configuration includes a 10.26 mm focal length with an adjustable aperture from f/2.8 to f/11 and an approximate 77° Field of View (FOV). During the field operations, a total dataset of **519 high-resolution images** was acquired. The flight paths combine **vertical and oblique imagery** to fully capture the vertical masonry walls and avoid data gaps in structural connections. The photogrammetric processing relies on **Structure from Motion (SfM)** and **Multi-View Stereo (MVS)** algorithms to reconstruct the external **3D point cloud**.

Features	Specifications
UAV Platform	
Max. take-off weight	907 g
Maximum Speed (P-Mode)	48 km/h / 13.4 m/s
Flight time	~31 min
Camera: Hasselblad L1D-20c	
Sensor	1" CMOS; Effective pixels: 20 million
Photo size	5472 × 3648
Focal length	10.26 mm
Field of view	approx. 77°
Aperture	f/2.8–f/11
Shooting speed	Electronic shutter: 8–1/8000 s

Table 3.2. Technical specifications of the DJI Mavic 2 Pro UAV and Hasselblad L1D-20c camera.



Figure 3.9. DJI Mavic 2 Pro UAV used for exterior photogrammetric acquisition.

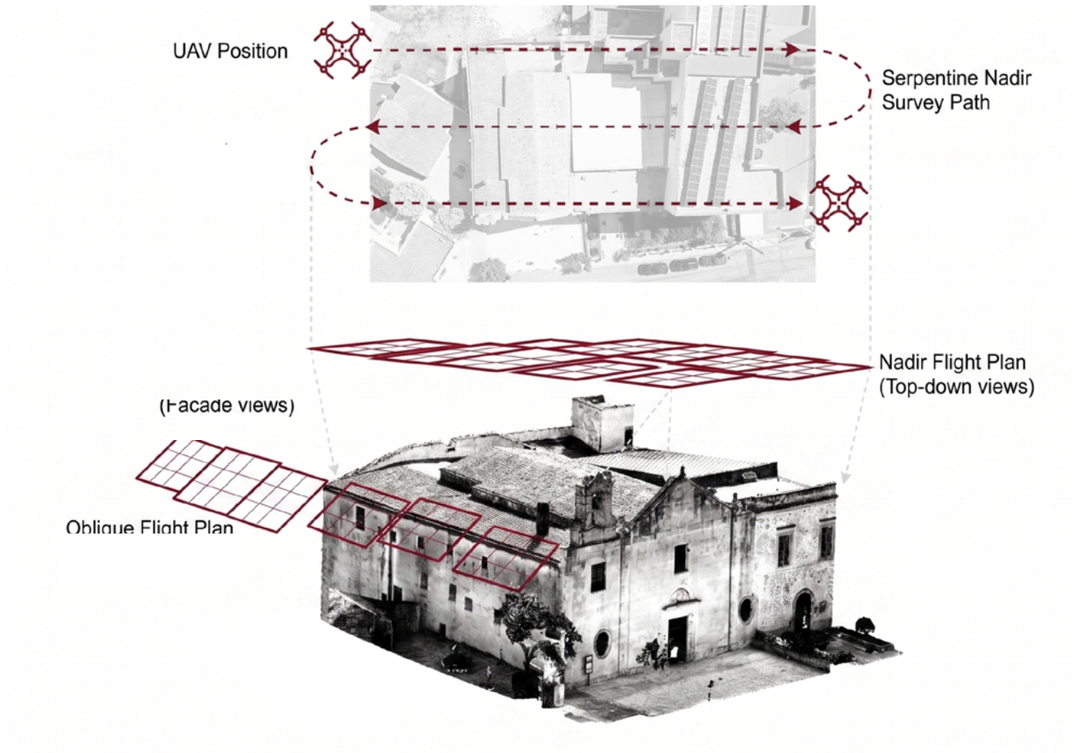


Figure 3.10. UAV flight configuration: (a) serpentine nadir survey path, (b) nadir image acquisition, and (c) oblique façade acquisition.

3. Indoor LiDAR Surveying via Handheld MMS

The indoor environments characterized by complicated architectural elements such as vaults, side chapels, and handcrafted wooden altars required a continuous acquisition system to minimize data loss. For this purpose, a handheld **Mobile Laser Scanning** system, specifically the **XGRIDS LIXEL L2** model, was used. This hardware utilizes advanced **LiDAR** technology based on **Time of Flight (TOF)** distance measurements with multi-echo acquisition capabilities. Operating in mobile mapping mode, the system stands out for its high portability and ability to perform rapid and continuous surveys in complex, articulated heritage environments without the operational constraints of traditional fixed tripods, significantly reducing field acquisition times compared to conventional static **TLS**. This LiDAR technology is able to do a dynamic data collection with a high acquisition frequency of over **640,000 points/second**, a measurement range between **0.50 m and 120 m**, and a comprehensive sensor field of view of **360° × 270°**. These performed parameters ensured a precise acquisition, even in dark and not accessible indoor spaces. The positioning and registration process of the handheld MMS system is based on integrated inertial localization and **Simultaneous Localization and Mapping (SLAM)** technology. The **SLAM algorithm** makes it possible to maintain continuous geometric alignment between different scans, which represents a fundamental requirement for indoor historical contexts. In addition, unlike aerial photogrammetry, which demands longer computational processing times for 3D point cloud reconstruction using **SfM/MVS algorithms**, this LiDAR-based MMS hardware provided a registered point cloud almost immediately after the tracking mission, so it can optimize the overall data processing time consumption. As a result, the internal survey produced a point cloud of **more than 50 million points**.



Figure 3.11. XGRIDS LIXEL L2 handheld MMS.

Features	Specifications
Handheld MMS Platform	
Device model	XGRIDS LIXEL L2
Operating mode	Mobile mapping mode
Weight	approx. 1.6 kg
Dimensions	approx. 180 × 130 × 400 mm
Internal storage	1 TB SSD
Operating time	approx. 90 min
Protection level	IP54
Operating temperature	-20°C to +50°C
LiDAR Performance	
Measurement principle	Time-of-Flight LIDAR
Laser class	Class 1 (905 nm)
Acquisition frequency	320,000 points/second
Field of view	360° × 270°
Relative accuracy	approx. 1.3 mm
Absolute accuracy	approx. 3 cm RMSE
Point cloud density	up to 1,000,000 pts/m²
Point cloud thickness	approx. 5 mm
Imaging and Data Output	
Sensor integration	LiDAR + visual cameras + IMU
Camera system	360° panoramic 48 MP camera
Output formats	LAS, E57, LCC, 3D Tiles

Table 3.3. Technical specifications of the XGRIDS LIXEL L2 handheld Mobile Mapping System. (XGRIDS, 2024)

3.3.2 Post-Processing of Point Clouds

After the on-site acquisition phase, the raw data from the **UAV photogrammetric survey** and the handheld **Mobile Laser Scanning** survey had to be processed in different software and environments. The main goal of this phase was to transform the separate point clouds from different techniques into a clean, accurate, and **unified point cloud**, which is suitable for the following process. First, the external photogrammetric dataset was imported into **Agisoft Metashape**. This software uses **Structure from Motion (SfM)** and **Multi-View Stereo (MVS)** algorithms to reconstruct three-dimensional geometry from overlapping images. In this survey, the 519 high-resolution UAV images were aligned in post-processing to generate the **dense point cloud** of the external parts of the church (include all the facades and roof). The point cloud was then **georeferenced** using the coordinates of the **Ground Control Points** measured with a **Total Station**. The topographic network was then tied to the global coordinate system thanks to **GNSS measurements**. In this way, the external point cloud was placed in the **RDN2008-UTM33N** reference system, **EPSG:6708**. Then, for the internal point cloud, which was acquired with the **XGRIDS LIXEL L2** handheld MMS system, the original software of the device was used. In this process, a registered indoor point cloud was generated based on the **SLAM trajectory** of the scanner. Since the indoor acquisition was carried out without a GNSS signal, the internal point cloud was later **co-registered** with the external georeferenced point cloud to create a complete representation of both the interior and exterior parts of the architectural complex. After the first part of post-processing, the internal and external point clouds were imported into **CloudCompare** software. This environment was used as the main environment for **point cloud integration**, cleaning, filtering, optimization, and section generation. The two clouds were first aligned and merged. The co-registration was done through the **Iterative Closest Point (ICP)** algorithm, commonly known as ICP. This algorithm improves the alignment between two overlapping point clouds by reducing the distance between corresponding areas. In this case, **ICP** was used to connect the photogrammetric external cloud with the MMS internal cloud through the common parts visible in both point cloud, which is the main frontal facade. Also, after the co-registration of the UAV and MMS datasets in the Cloud Compare software using the Iterative Closest Point algorithm.

CloudCompare

XGRIDS

Metashape

When the registration was finished, the full point cloud was cleaned in order to remove elements that were not useful for the architectural analysis and NURBS modeling part of the research. These elements included noise, isolated points, outliers, artefacts, and objects outside the scene. This step was essential because raw point clouds contain unnecessary information caused by reflections, acquisition limits, moving objects, or environmental conditions. In addition, several filtering methods were applied, including Statistical Outlier Removal, Radius Outlier Removal, and filtering based on intensity values.



Figure 3.12. Subsampling and preparation of the integrated point cloud for subsequent processing.

These operations could improve the readability of the geometry and prepared the dataset for our purpose. After, the cleaned point cloud was gone through **subsampling** operations. The aim of subsampling was to reduce the density and weight of the dataset without losing the main geometric information of the building. This step was important because the complete point cloud of the indoor and outdoor areas of the church was very huge, with more than **40 million points** just for the external photogrammetric cloud and more than **50 million points** for the internal laser scanning cloud. Mostly, a **high-density** point cloud is useful for documentation, but when it is difficult to manage in further phases, it needs to be subsampled. The first subsampling method used in this workflow was **Voxel Grid downsampling**. This method divides the point cloud into small cubic cells called **voxels**. Then, the points inside each voxel are replaced by one representative point, usually the **barycentre** of the points. In the formula, **p̄v** represents the representative point of the voxel, **Nv** is the total number of points contained in the voxel, **pj** is a single point inside the voxel, and **j** is the index used to identify the points inside that voxel.

$$\bar{p}_v = \frac{1}{N_v} \sum_{j=1}^{N_v} p_j$$

The **UAV point cloud** was used as the reference dataset (since it has higher accuracy), while the **MMS point cloud** was aligned to it. The **ICP process** was applied considering a theoretical overlap of **60%**, since the two datasets shared only one main facade of the church. The scale was kept fixed at **1.0** in order to preserve the original metric properties of both datasets. The final **RMS value** obtained after registration was **0.013 m**, computed on **307,097 points**. This value shows a residual alignment error of approximately **1.3 cm** between the two point clouds in the overlapping areas, which can be considered a reliable value.

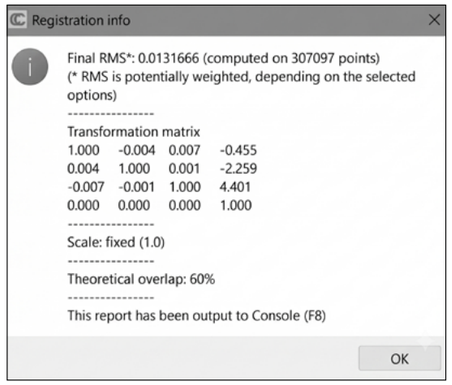


Figure 3.13 ICP registration of the UAV and MMS point clouds in CloudCompare.

Parameter	Value
Reference dataset	UAV photogrammetric point cloud
Aligned dataset	MMS point cloud
Registration method	ICP
Final RMS	0.013 m
Points used	307,097
Theoretical overlap	60%
Scale	Fixed, 1.0

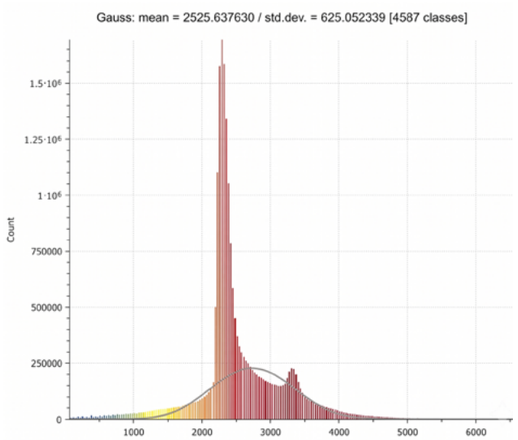
Table 3.4. ICP registration parameters and results for the UAV and MMS point clouds.

The second subsampling method was **Poisson-disk sampling**.This method is based on a **minimum distance** between selected points. In the formula, pi and pj represent two different points in the point cloud, while ||pi − pj|| represents the **Euclidean distance** between these two points. The symbol rmin indicates the predefined minimum radius, or the minimum allowed distance between two sampled points. The condition i ≠ j means that the comparison is made between two different points. This method helps to avoid points that are too close to each other and creates a more **uniform distribution** of the PointCloud. Figure Poisson-disk sampling formula and symbol definition.

$$\|p_i - p_j\| \geq r_{\min} \text{ for all } i \neq j$$

In this research, **Voxel Grid downsampling** was mainly useful for regular and less detailed areas, because it reduced the weight of the PointCloud while keeping a homogeneous distribution. In more complex areas, such as vaults, altars, imposts, intersections, and connections between architectural elements, **Poisson-disk sampling** was more appropriate because it helped to preserve the local geometric detail. This combination of different strategies made the unified PointCloud easier to manage without losing the **morphological information**.

The accuracy of the processed point cloud was evaluated through the **topographic control network** acquired during the survey. The external photogrammetric model was georeferenced using the **11 Ground Control Points** measured with the **GNSS survey** in **PPK mode**. This photogrammetric processing reached an **RMSE of about 0.03 m**. Therefore, the final external **UAV point cloud** can be considered reliable for the architectural scale of the research and suitable for the following **NURBS-based modelling**, **diagnostic analysis**, and **HBIM-oriented documentation** phases. Then, the **surface density analysis** was calculated in **CloudCompare** using a radius of **0.10 m** to assess if the UAV photogrammetric point cloud provides sufficient point density for the purposes of this research or not; since the subsequent diagnostic analysis are based on **orthophotos** from the photogrammetric UAV, it was necessary to evaluate the density and distribution of the it in order to define its suitability for generating reliable orthophotos of surfaces. The analysis was illustrated on **21,032,380 points** and produced a **mean surface density of 2525.64 points/m²**, with a **standard deviation of 625.05 points/m²**.



The histogram shows that most density values are concentrated around the main peak, approximately between **2200 and 2600 points/m²**, so generally we can see a consistent point distribution across the surfaces. Higher density values are visible in specific areas, mainly along roof edges, vegetation, complex geometries, and zones with stronger **image overlap**. Lower density values are associated with areas affected by **occlusion**, weaker visibility, or less favorable acquisition geometry.

Figure 3.14. Point-cloud surface density distribution obtained from the processed UAV dataset.

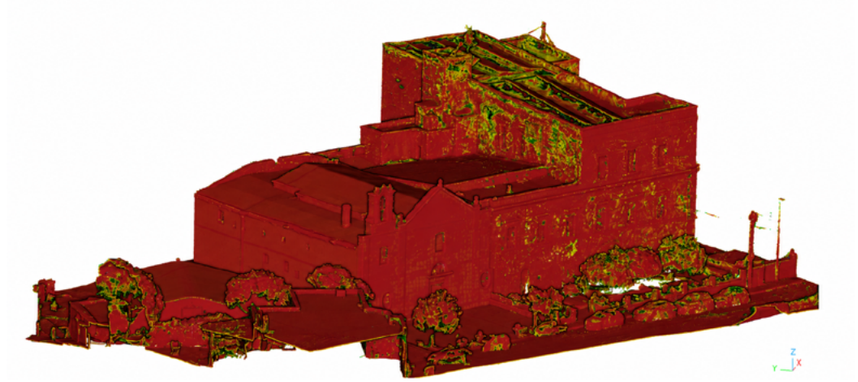


Figure 3.15. Spatial visualization of point-cloud density across the exterior survey dataset.

Overall, the results confirm that the **UAV PointCloud** provides a sufficiently dense representation of the architectural surfaces and can therefore be considered suitable for the generation of **orthophotos** and for supporting the **VPL-based diagnostic analysis** carried out in this study. In conclusion, the **post-processing phase** represents one of the fundamental steps between the field survey and the **HBIM processing**. Through registration, cleaning, filtering, subsampling, segmentation, and section extraction, the raw survey data were transformed into a **high-fidelity geometric reference**, and the final dataset provided the **metric and morphological base** for the thesis.

4. Architectural Characteristics

In this context, reliable **3D architectural modelling** and **condition analysis** depend on accurate and complete **metric documentation**. For this reason, the survey of the **Church of Sant'Antonio dei Cappuccini** was planned by combining different **acquisition techniques**, each selected according to the characteristics of the building and the accessibility of its spaces.The exterior areas were documented through **UAV photogrammetry**, while the interior spaces were recorded using a handheld **Mobile Mapping System**. **GNSS measurements** were also used to establish **Ground Control Points (GCPs)** to provide **topographic control** and to support the **spatial accuracy** of the final datasets.

This chapter describes the **instruments**, **fieldwork procedures**, and **data processing stages** adopted during the survey. It also explains the generation and registration of the **point clouds** and the **orthophotos** , and the evaluation of **data density** and **accuracy**. The resulting **datasets** form the following chapters.

4.1 General composition

The **Church of Sant'Antonio dei Cappuccini** presents a typical architectural style of **Capuchin religious buildings** which are characterized by simplicity, focus on being functional, and a distinct spatial organization of the spaces.

Capuchin architecture is grounded in **Franciscan principles**. According to mendicant regulations, architectural form is a way for a spiritual purpose, indicating compact volumes, limited decorative symbols, and a focuse on internal spaces rather than external representation for the public. Vertical elements are carefully controlled and reduced to essential components, and it usually avoids monumental towers as a response, such as a bell tower. Furthermore, Capuchin religious buildings commonly develop through progressive construction processes, so they will have some results in **irregular geometries**. These features define a framework in which architecture serves religious practice while accommodating transformation over time (Legendziewicz et al., 2025).

The church, as is told in the previouse chapter, is part of a larger **religious complex** that includes the **former convent**, organized around an **internal courtyard**, although the original monastic layout that has been partially altered over time.

From a spatial perspective, the church is developed according to a **longitudinal plan** with a **single tripartite longitudinal nave**. The internal space is designed by a series of **lateral chapels**, six of them, which are arranged along the nave, creating a clear rhythmic division of the interior. This linear organization shows the axial development of the church and visual attention to the **main altar** and making it the main focal point of the church.

Besides, in the exterior design, the **facades** are constructed by a sober and neutral architectural language, which continues the Capuchin principles. It presents a simple composition with a few decorative elements and a **baroque-style bell tower**. The **main facade**, which has the main entrance, is centrally positioned and marked by an inscription dating the completion of the church. On the left side of the facade, there is a **campanile a vela**, which illustrates a distinctive vertical element in the overall volumetric composition, and one of the goals is the recognizability of the church in the surrounding landscape.



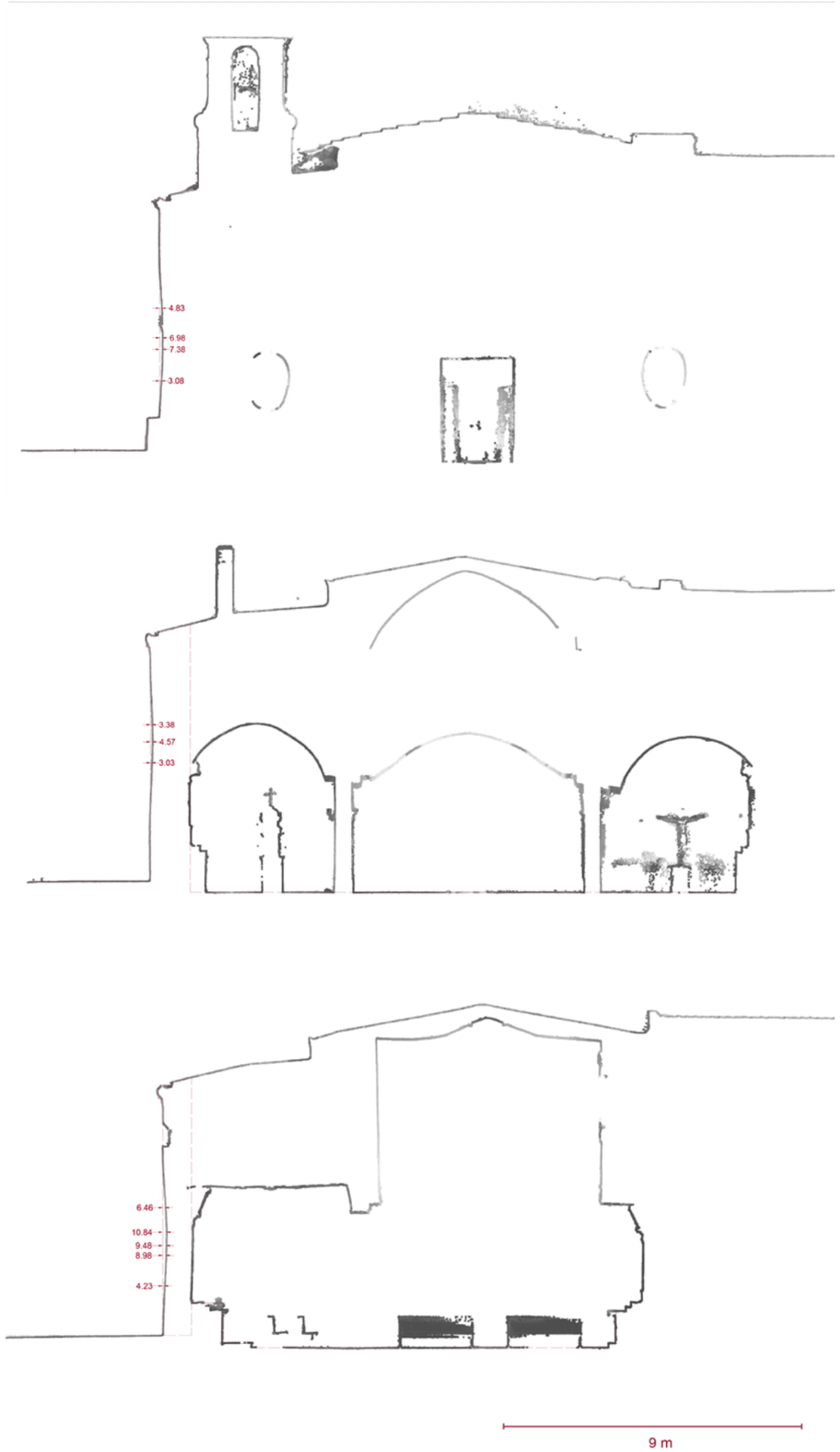
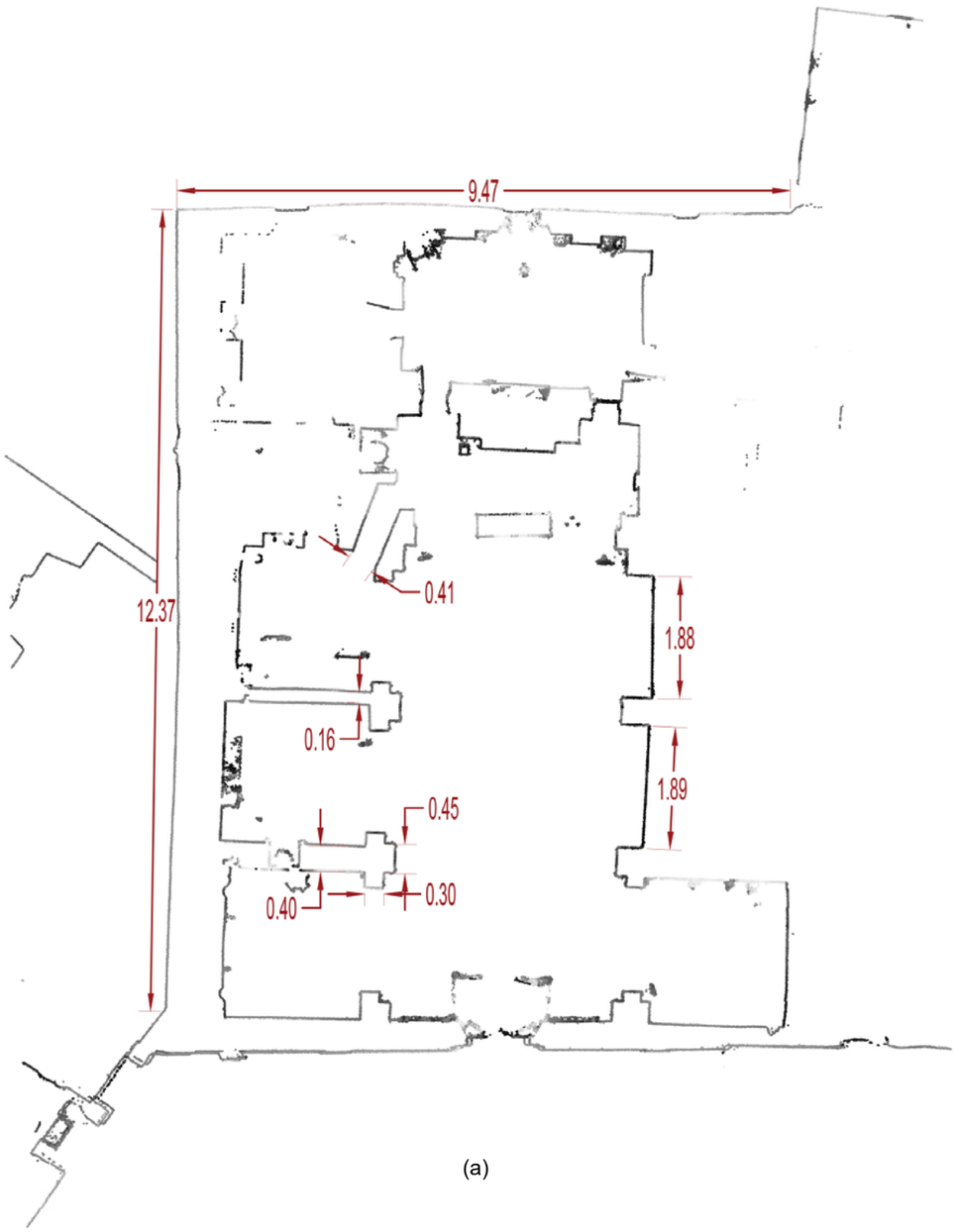
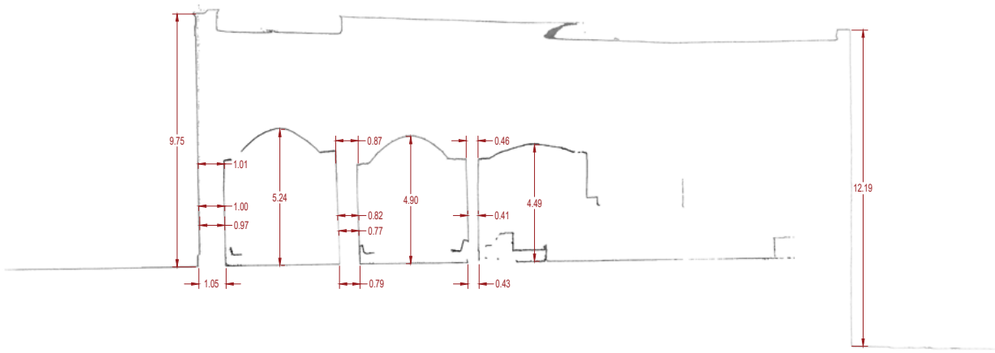


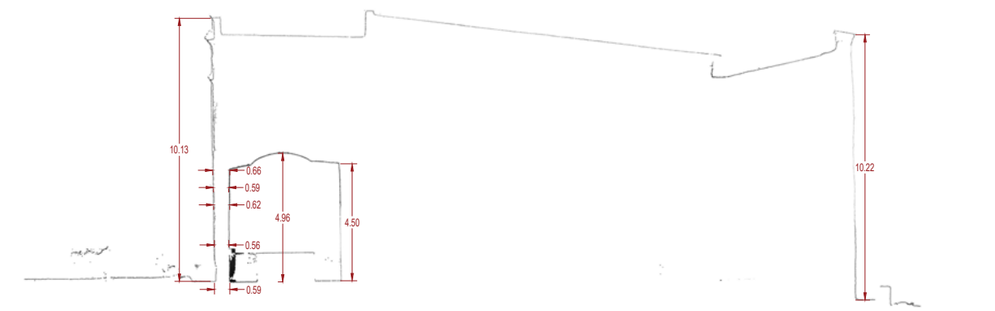
Figure 4.1 Survey-based plan and sections illustrating the deformation of the lateral (left side) wall of church.



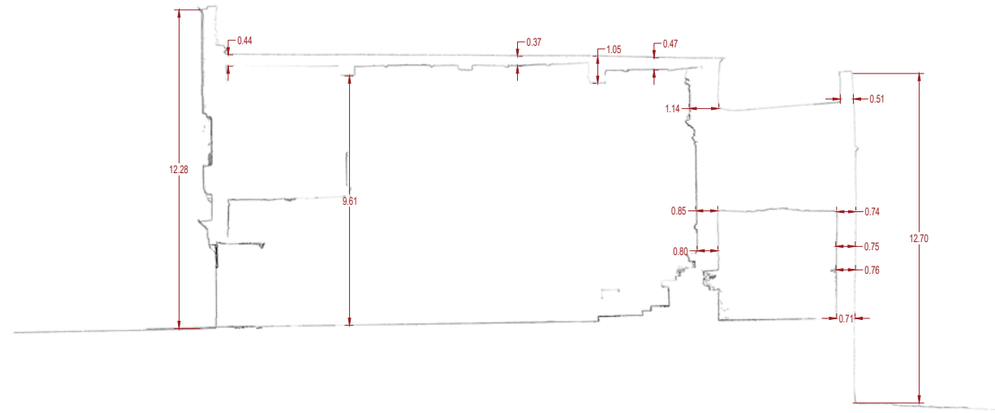
(a)



(b)



(c)



(d)

Figure 4.2. Survey-based plan and sections generated from the combination of the UAV and MMS survey dataset, illustrating the general architectural composition of church. (a) Ground floor plan; (b,c,d) Transversal and longitudinal cross-sections.

4.2 Exterior Architectural Characteristics

The building is designed as a **longitudinal, rectangular volume** with limited formal articulation and a distinct absence of elaborate decorative elements. This volumetric idea emphasizes **functional clarity** and preserves the spiritual character of the church, and also can shift architectural focus from external representation to the internal design.

The **main facade** is organized according to a clear **axial symmetry**, then we can see the entrance, which is centrally positioned. Besides, openings are few and relatively small in the scale of the church, contributing to the solid and introverted masonry. The external surfaces are constructed in **local limestone**, and there is some evidents signs of aging and **surface weathering**. These material conditions are documented in the survey and can improve the reading of the facade as the main historical surface, shaped over time.

The only important element of the external composition is the **campanile a vela**, located on the left side of the main facade. Designed as an open bell gable. So, it creates a vertical language that marks the roofline without ruining the overall simplicity of the church. The presence of some decorative stone elements on the upper part of the main facade, such as volutes and finials, captured a controlled **Baroque influence** .

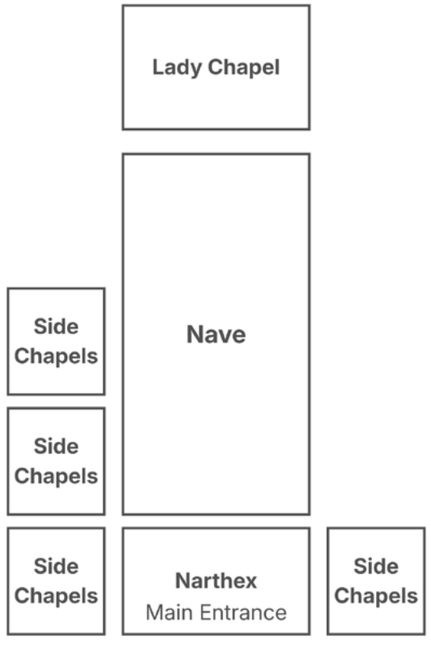


Figure 4.3. Schematic spatial organization of the nave, narthex, side chapels, and Lady Chapel.

In addition, the analysis of the **left elevation** highlights that this facade is almost entirely free of unnecessary elements and is defined by a **compact masonry surface**, with having only small and irregularly distributed openings. These openings appear to respond primarily to functional requirements and needs rather than compositional or aesthetic intentions. It again shows the **introverted nature** of the complex. Also, the variation in wall finishes, discoloration, and surface degradation of this facade suggests multiple construction and maintenance phases. Based on the **photogrammetric survey** with drone conducted in collaboration with Politecnico di Bari, the analysis of photos revealed a strong functional relationship between the church and the adjacent **conventual structures**.

The results shows that the church works not as an isolated building, but as one part of a **larger complex**, where spaces, accessibilities, and the uses are closely connected. The lateral analysis of the church exhibits **irregular geometries** and different heights in the roof, and **heterogeneous construction techniques**, indicating successive phases of **addition, transformation, and reuse**.

Moreover, the visible differences in roof levels and the junctions between volumes indicate an **additive construction logic**, where every spaces was attached to the original structure again and again over the time.

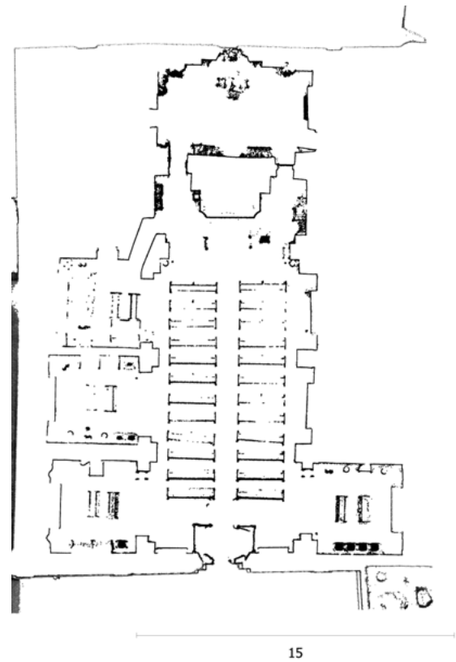


Figure 4.4. Floor plan of the church extracted from the interior point cloud (MMS technique).



Figure 4.5. UAV aerial view of the church and the adjoining convent complex and environment.

4.3 Interior Architectural Characteristics

About the longitudinal interior layout of the Church of Sant'Antonio dei Cappuccini, it includes a single nave and 6 sequences of chapels, which 3 of them are Left Side Chapels, 1 of them is Right Side Chapels, the other is Lady Chapel, which is the main and biggest chapel in the main axis of the building and behinde the Nave, and the last one is the chapel where is the **main entrance** and it is like a bridge between outside and the interior spritual area. The circulation is strongly oriented toward the **main altar** and guides both movement and visual attention along the principal axis of the church. This **axial organization** is made by a combination of **arches and vaults**, which have structural role and maintaining visual continuity at the same time. One of the most significant features of the interior is the **vaulted ceiling system**. The nave and chapels are covered by a series of connected vaults, combining modified **barrel vaults** and **intersecting geometries**. Although the general rhythm of the vaulting system appears coherent, with a closer observation, we can recognise the variations in curvature, thickness, and alignment between the bays. These irregularities suggest the coexistence of different historical phases and traditional building techniques, rather than a strict and standardized design approach.



Figure 4.6. Interior architectural views: (a) main nave



(b) vaulting system



(c) side chapel area

A main interior feature is the huge use of **carved wooden elements**, particularly in the main altar, lateral altars, pulpit, choir, and tabernacle. These furnishings can form a coherent decorative system and act as a visual point of view in compare with a simple architectural setting in the exterior. Their integration with the masonry walls and vaulted system demonstrates a relationship between functional architectural space and artistic ideas, characteristic of **Capuchin style interiors**. The main nave differs in depth and the rich decorative signs, reflecting variations in devotional function and construction chronology. In addition, some chapels preserve traces of earlier layers, while in the others, we can find the existence of symbols from **18th century painted cycles** and **Baroque decorative features**.

In overall, decorative elements are integrated into the **structural framework** and do not operate independently. Paintings are framed religious scenes that are embedded within the vault surfaces, contributing to a language that enhances aestetics of the church without having conflicts with the **Cappucin principals**. Also, the interior color palette remains controlled, with light toned plaster surfaces contrasted by darker painted lines and also stone architectural elements.

From a geometric and structural perspective, the interior area is characterized by a **light asymmetries** and **non-uniform alignments** in arches, vaults, and supporting elements. While it is not immediately shown, these deviations become apparent through a detailed survey and **digital documentation**. Finding out about these characteristics is crucial for an accurate **digital (HBIM) representation**, as they reflect the **real construction logic**, **material behavior**, and every transformations of the building, rather than an **idealized architectural model**.

4.4 Analysis of architectural geometric forms

4.4.1 Vaulting system

The **vaulting system** of the **Church of Sant'Antonio dei Cappuccini** is recognised by a non-uniform composition of **masonry vaults**, creating **continuous shells** rather than a **skeletal rib-based structure**. This configuration is a classical system **vault typology**, which is described in masonry vault theory books, where the vault behaves as a **structural surface** transferring loads to the walls and piers and then to the ground.

The analysis and classification of the vault types in this research is based on a direct observation of the interior in the survey, analysis of the **3D point clouds**, and then a comparison with classical masonry vault typologies specially as discussed in Heyman's **The Stone Skeleton** book. The main nave is covered by a **longitudinal barrel vault**, which is modified with **lunettes**. This identification is supported by the existence of a **continuous curved surface** that is extending along the longitudinal axis of the church, with also the curvature developed in a single direction only. Then, the lack of intersecting vault surfaces and the lack of diagonal groin lines could confirm that the nave vault is not a **groin vault**. Besides, the **lunettes** locally just modify the geometry of the **barrel vault** with a few openings and connections to the outside, but it is important to notice that they do not change its structural behaviour, which remains like a **single curved masonry shell** transferring **horizontal thrust** to the vertical elements such as walls.

For the side chapels, in the left and right side of the church, **groin vaults** are present. These vaults are constructed by the perpendicular intersection of two **barrel vaults** with similar height and produce recognizable diagonal groins. Also, in some transitional and secondary spaces, we can see **groin vaults**, but they are limited, and their aim is to localized bays where the conditions require a more useful distribution of loads to the supports. An important note is that these **groin vaults** do not characterize the **main nave** but only appear in some specific connecting zones in the building. Ultimately, the **Lady Chapel** and **Narthex (Main Entrance)** are largely covered by **pavilion (cloister) vaults**. We can identify these types of vaults by curved surfaces rising from the support walls toward a central point, forming a **double curved geometry**. Their identification is based on the non-square plan but rectangular plan of the chapels and on the absence of groin lines or intersecting barrel geometries. So, structurally, these vaults behave as a **unique shell system**, and distributing loads toward the walls rather than concentrating them on the specific arches, like **groin vaults** system. In the entire **vaulting system**, slight **geometric irregularities** can be observed, including variations in curvature, bay dimensions, and alignments. These features are normal and common when we have **traditional construction techniques**, **progressive building phases**, and **long-term structural adjustments**. From a methodological perspective, the recognition of these non-ideal geometries is crucial for **HBIM modelling**, as we want to continue with a **reality-based approach** that would be capable of representing the actual form and behavior of the **masonry vaults** in a comparison with simplified ideal shapes.

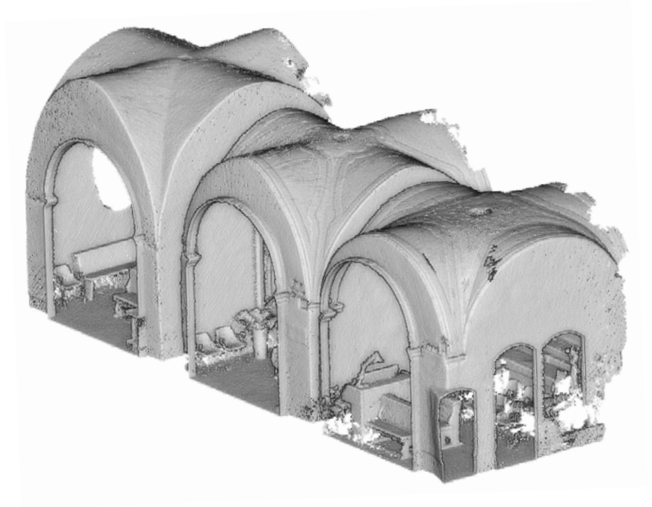


Figure 4.7. 3D point-cloud view of the side chapels vaulting system.

4.4.2 Openings Geometry

The **geometric analysis** of the openings, based on our **survey** and also **point cloud data**, shows that these elements are mainly designed by a very simple and primary geometric forms. Mostly, they are **rectangular**, with straight vertical and horizontal edges, while it has two **circular openings** on the **main facade**. The overall composition reflects a **geometry-oriented design approach**, where openings are just functional voids between a massive masonry and not as some decorative architectural elements. The rectangular windows and doors are especially on the left and back facades where connected to the convent; their **height-to-width ratios** are generally consistent, although differences in dimensions and spacing are compeletly clear in the observation. These variations show a **non-modular system** and highlight that the openings were created over time according to the functions that users need. Also, note that small **geometric deviations**, such as differences in sill height, lintel alignment, and positioning, are visible when we extracted sections from the **point cloud data**. In the next type of openings, a specific geometric exception is represented by the **circular windows (oculi)** located on the main façade of the church. These openings introduce a **curved geometry** within a largely rectilinear composition. Our sections show that the oculi have an almost circular profile, although irregularities in radius and centering can be seen. These deviations and the **non-ideal geometry** could be likely related to **construction techniques** and **material behavior**, not intentional design choices. Also, from another point of view, both rectangular and circular openings are deep within the wall thickness. Generally, the geometry of the openings can be described as non-uniform and adaptive by simple shapes, but with localized **geometric irregularities**. Understanding this concept is essential for an **HBIM representation** with high accuracy, because they cannot be modeled using ideal or repetitive **parametric objects** and therefore require a direct export from the surveyed data. In conclusion, the combination of studying the exterior and interior **architectural features** of the case study can highlight the **geometric complexity** of the building, **material layering**, and **spatial order**.The absence of solid modularity and the presence of localized deformations (which was clearly highlited in the survey) confirm that an **idealized modelling approach** could fail to capture the reality of this church. Also, from a material perspective, the building is primarily constructed using **local stone**, while **wood** is extensively used for interior furnishings and decorative elements. The combination of these materials, together with the long term effects of weather conditions,as it disscoused in the aspect of the environment of the region, has contributed to the slight irregularities in walls, vaults, and decorative components that are observable and represent key aspects for accurate **architectural documentation**.



Figure 4.8. All the façade openings typologies, Extracted from UAV photogrammetry dataset.

4.4.3 Facade Orthophotos

The orthophotos of the chuch are generated from UAV photogrammetric data through the 3Dreshaper software.

Main Facade Material:
Local porous limestone (Calcarenite)

Bell gable and portal decoration Material:
Local porous limestone (Calcarenite)



Figure 4.9. Orthophoto of the main façade generated from UAV photogrammetry dataset.



Figure 4.10. Orthophotos of the back façades generated from UAV photogrammetry.



Figure 4.11. Orthophotos of the lateral façade generated from UAV photogrammetry.

4.5 Building diagnosis

In this section, the **decay mapping** analysis of 2 main facades, will be conducted to have a dataset (based on the traditional and manual techniques) to compre with the final results of the proposed workflow (based on VPL-based workflow).

4.5.1 Decay detection with manual technique

Visual inspection of both facades shows several **decay patterns**, which are documented and classified according to the **ICOMOS-ISCS Illustrated Glossary** (ICOMOS, 2008) on **Stone Deterioration Patterns**. The identification of each **decay typology** was based on direct visual evidence during the **on-site survey** and supported by **orthophotos** generated from the **UAV dataset point cloud**.

On the **left facade**, **five decay categories** were identified and mapped:

Soiling was the most distributed decay pattern on the facade, presenting as a very thin layer of exogenous particles that is primarily atmospheric dust and airborne pollutants, giving a dirty appearance to the stone and render surfaces without structural degradation of the substrate. According to the **ICOMOS-ISCS glossary** (ICOMOS, 2008), soiling differs from a crust in that it lacks visible thickness and coherence, though with increasing adhesion, it can gradually evolve into a **black crust** formation. The evidence for this classification was the homogeneous grey-dark superficial deposit observed particularly on horizontal and sub-horizontal surface areas, consistent with particle settlement patterns driven by atmospheric pollution, incomplete rain washing, and aerosol deposition.

Discoloration was recorded as a non-uniform color variation and patchy surface appearance. Based on the **ICOMOS-ISCS** definition, discoloration represents a modification of one or more color parameters like hue, value, and chroma of the original material. In this case, the evidence pointed toward differential moisture absorption, varying degrees of solar exposure across the facade orientation, and natural material ageing as primary causes. The patchy appearance, without associated material loss or surface deformation, confirmed its classification as discoloration rather than staining or biological colonization.

Biological Colonization (Lichen) was identified as dark green to grey-green vegetation patches distributed across the facade surface. The **ICOMOS-ISCS glossary** (ICOMOS, 2008) defines lichen as a symbiotic organism composed of a fungus and a green alga or cyanobacterium, forming rounded millimetric to centimetric crusty or bushy patches with a leathery appearance. Lichen growth is generally favored under clean air conditions and persistent seasonal humidity, both of which are consistent with the environmental context of the surveyed building.

Patch Repair was documented as localized repaired plaster and render areas presenting a notably different color and surface texture from the surrounding original material. These areas represented previous maintenance interventions. In addition, we need to notice that the presence of patch repair is indirect evidence of pre-existing underlying decay processes, such as detachment, scaling, or material loss that had previously required intervention.

On the **main facade**, **five decay** categories were identified and mapped:

Soiling was again extensively documented as **grey-dark** superficial deposits without material loss, distributed broadly across the facade surfaces. The causal evidence included atmospheric pollution, airborne particle deposition, and incomplete rain washing, all of which are consistent with the building's urban exposure conditions.

Discoloration appeared as a non-uniform color variation between individual stone blocks, resulting in a visually patchy surface appearance. The differential moisture absorption capacity of adjacent building materials, combined with variable solar exposure across the facade geometry and natural material ageing, was identified as the primary contributing factor.

Differential Weathering was recorded in zones where adjacent stone blocks exposed to comparable environmental conditions exhibited different weathering intensities and surface conditions. According to the **ICOMOS-ISCS** framework, differential erosion, closely related to differential weathering, occurs when deterioration does not proceed at the same rate across the stone surface, resulting in irregular surface topography and relief formation. On the main facade, the evidence was the visible contrast in surface texture and degree of material loss between adjacent masonry units sharing similar exposure conditions.

Black Crust / Deposit was documented as localized dark deposits concentrated in sheltered zones of the facade, particularly in areas protected from direct rainfall and water runoff. The **ICOMOS-ISCS glossary** (ICOMOS, 2008) defines **black crust** as a coherent collection of materials, atmospheric particles trapped within a gypsum matrix ($CaSO_4 \cdot 2H_2O$). The characteristic grey-to-black coloration, the spatial correlation with sheltered facade areas away from rain impact zones, and the coherent and adherent nature of the deposit provided the diagnostic evidence for this classification, distinguishing it from simple soiling or biological colonization.

Erosion was documented through the observable loss of original surface detail, resulting in rounded edges, softened carved profiles, and the progressive disappearance of sharp geometric definition on decorative architectural elements. The **ICOMOS-ISCS glossary** defines erosion as the loss of original surface leading to smoothed shapes, with sub-types including differential erosion, rounding, and roughening. On the main facade, the evidence was particularly clear on sculptural and carved stone elements, where fine surface detail had been progressively lost, consistent with long-term exposure to physical and chemical weathering agents.

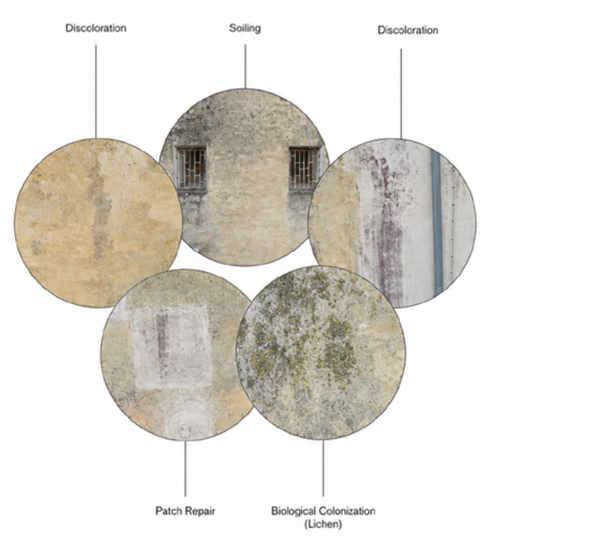
Decay	Evidence on Façade	Probable Cause	Color code
Soiling	Grey-dark superficial deposits without material loss	Atmospheric pollution, airborne particles, dust deposition, incomplete rain washing	#6B6B6B
Discoloration	Non-uniform color variation between blocks	Differential moisture absorption, solar exposure, ageing, chemical alteration	#D8C7A3
Differential Weathering	Different weathering intensity on stones exposed to similar conditions	Variations in porosity, stone properties, orientation to wind and rain	#B58B5C
Black Crust / Deposit	Localized dark deposits	Atmospheric pollutants, carbonaceous particles, moisture retention	#2E2E2E
Erosion	Rounded edges, softened carved details, loss of sharp geometry	Rainwater action, wind erosion, limestone dissolution, long-term weathering	#C8A27A

Table 4.1. Decay categories, visual evidence, probable causes, and colour codes for the main façade.

Decay	Evidence on Façade	Probable Cause	Color code
Soiling	Grey-dark superficial deposits on the façade surfaces	Atmospheric pollution, airborne particles, dust deposition, incomplete rain washing	#6B6B6B
Discoloration	Non-uniform colour variation and patchy surface appearance	Differential moisture absorption, solar exposure, ageing	#D8C7A3
Patch Repair	Localized repaired plaster/render areas with different color	Previous maintenance interventions and material replacement	#CFCFCF
Biological Colonization (Lichen)	Dark green vegetation	Long-term exposure, seasonal humidity	#7FAF5F

Table 4.2. Decay categories, visual evidence, probable causes, and colour codes for the lateral façade.





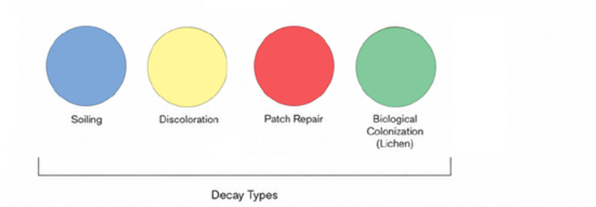
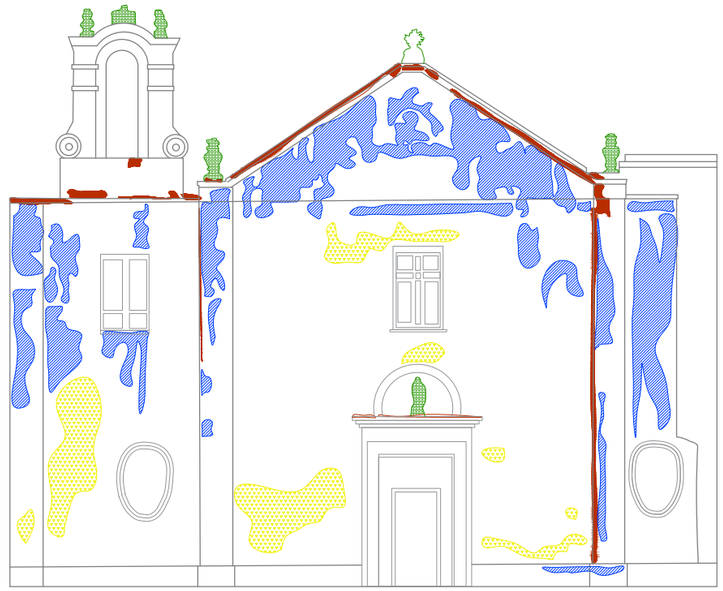


Figure 4.12. Manual decay map of the lateral façade with representative surface samples.





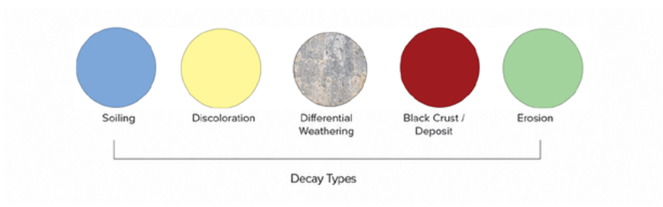


Figure 4.13. Manual decay map of the main façade with representative surface samples.

5. Geometric Modeling

After the **point cloud generation**, **co-registration**, and **post-processing** of the **multi-sensor survey data** (described in Chapter 3), this chapter will explain the generation of an **as-built model** in **3D Rhinoceros** software. The objective of this part of the thesis was not to produce an **idealised reconstruction** of the church, but to generate a **real geometric and editable representation** of the church capable of preserving the main irregularities, asymmetries, and discontinuities recorded by the survey data to be a reference for future conservation planning, such as **mesh-based structural analysis** or **Restoration design visualization** or to be a base for **3D decay mapping**.

This **modelling workflow** included **point cloud optimisation and segmentation**, extraction of a large number of sections for each component, reconstruction of **analytical curves**, and generation of **NURBS surfaces** through different **modelling commands**. The **modelling strategy** was adjusted for each architectural element according to their **geometric complexity**. In general, regular components were reconstructed using simplified profiles and repeated geometric rules, while vaults, openings, junctions, and decorative elements required denser sections and local modelling procedures.

The most important part was about balancing **geometric accuracy**, **model complexity**, and **editability**. The result is not only as a three-dimensional representation of the church, but also as a geometric reference for the **VPL-based diagnostic analyses**, **data integration**, and **web-based visualisation** developed in the following chapters. In the final part of the chapter, the correspondence between the **NURBS model** and the **reference point cloud** is evaluated.

5.1 Modeling Strategies

General modelling concept

The **modelling workflow** follows a **geometry-first approach** which the **point cloud** is the main metric reference throughout this reconstruction phase. **NURBS geometry** is based on mathematically defined curves and surfaces controlled by **degree**, **knot distribution**, and **control points**. This type of representation is usually suitable for **built heritage** because it can combine **continuous surface description**, **local editability**, and compatibility with the native modelling and **visual-programming environment** of **Rhinoceros** and **Grasshopper**. The selection of **NURBS** was therefore not only a representational of **geometric information** choice but also a **methodological requirement** for the later stages of the research. In fact, the overall logic of this workflow can be summarised as:

1. The optimised **point cloud** segmented and sectioned in **CloudCompare**.
2. The selected **sections** were exported while preserving their **spatial coordinates**.
3. The sections were imported into **Rhinoceros**.
4. Interpreted through **lines**, **arcs**, and **interpolated curves**.
5. The spaces between these profiles were converted into surfaces using different **NURBS commands** such as **Loft**, **Sweep 1 Rail**, **Sweep 2 Rails**, **Revolve**, **Network Surface**, and **Patch**.

The number and orientation of sections, the type of curve, and the selected **surface-generation operation** were different according to the morphology and complexity of the **architectural element**. The workflow also avoided the application of a **uniform reconstruction process** to different building components.

	Stage	Primary environment	Input	Main operation	Output and modelling purpose
Fig . 5.2	**Data preparation and segmentation**	CloudCompare	Complete point cloud **(Ext: 5,066,009 pts / Int: 24,897,415 pts)**	Extraction of functional portions of exterior and interior parts	Manageable local datasets for every component
Fig . 5.3	**Section generation**	CloudCompare	Local point cloud portions	Longitudinal, transverse, horizontal, vertical, and oblique cutting planes	Representative point cloud profiles
Fig . 5.4 (a)	**Section transfer**	CloudCompare Rhino	Selected profiles	Export and import without changing coordinates	Three-dimensional reference sections in Rhino
Fig . 5.4 (b)	**Curve reconstruction**	Rhinoceros	Imported point cloud sections	Lines, arcs, interpolated curves, and fitted curves	Editable surface generators
Fig . 5.4 (c)	**Surface generation**	Rhinoceros	Curves	Loft, Sweep, NetworkSrf, Revolve, Patch, and boundary-based surfaces, as appropriate	NURBS surfaces for each element
	Local adjustment	Rhinoceros	NURBS surfaces	Boundary control, trimming, joining, and local connecting surfaces	Coordinated architectural components

Table 5.1. Main stages of the as built NURBS modelling workflow using point cloud as the refernece.

Separate management of the interior and exterior point clouds

The exterior **UAV photogrammetric point cloud** and the interior **MMS point cloud** had already been **georeferenced** during the **registration phase**. However, they are intentionally not merged into a **single point cloud object**. With this decision we preserved the original characteristics of each source and had a better **operational control** in **Rhinoceros**. Also, the interior and exterior point clouds were different in **acquisition geometry**, **density**, **radiometric information**, **occlusion patterns**, and **local accuracy**; so a permanent merge would have increased the **computational load**, complicated the interpretation of overlapping areas, and made it difficult to isolate a part to be the reference for a specific component. Therefore the two point clouds were imported into **separate locked layers** and could be active selectively. The **exterior point cloud** is used for generating the façades, roof geometry, bell gable, external wall surfaces, openings, and adjoining built elements. The **interior point cloud** was used for the nave, lateral chapels, interior walls, floors, arches, vault systems, openings, and altar areas. Because the datasets had their **registered coordinates**, they could still be displayed whenever the relationship between internal and external geometry needed to be checked.

Adaptive section generation in CloudCompare

This **NURBS model** was not generated by **direct automatic surface fitting** to the complete **point cloud**. Instead, some representative **sections** were first generated in **CloudCompare**. These **sectioned point clouds** were then converted into a controlled set of profiles that could reconstruct the curves as the base for the **3D model**. **Longitudinal sections** were used to describe changes along the main axis of the nave, façades, roofs, and elongated components. **Transverse sections** documented the width, wall relationships, arch profiles, and vault curvature across the building. **Horizontal sections** supported the interpretation of wall thicknesses, plan irregularities, openings, and changes in alignment at different heights. **Vertical sections** were used for façades, wall inclinations, openings, roof slopes, and internal elevations. **Oblique or locally oriented sections** were used wherever standard axes could not describe complex curved geometries. The **spacing between sections** was not fixed in every space of the church. Regular or approximately planar elements required fewer profiles, because their overall geometry could be illustrated with a limited number of sections. In contrast, areas characterised by **changing curvature** and intersections required **denser local sectioning**. This is particularly noticeable around **vault imposts**, the intersections between the nave **barrel vault** and its **lunettes**, **side-chapel vaults**, arches, openings, cornices, and the main altar. The **section spacing** was therefore reduced wherever the geometry changed rapidly and increased where the morphology remained stable. Additionally, the **direction of the sections** was also adapted to the local geometry. For vaults, sections were oriented to capture the **intrados profile**, the longitudinal shape of the surface, and the configuration of intersections. For arches and openings, profiles were generated through the **intrados**, **extrados**, and side boundaries. For roof surfaces, sections were positioned across slopes, ridges, and eaves. For complex decorative elements, multiple **local section families** were combined to make more informative profiles without unnecessarily increasing the number of curves in geometrically simple areas.

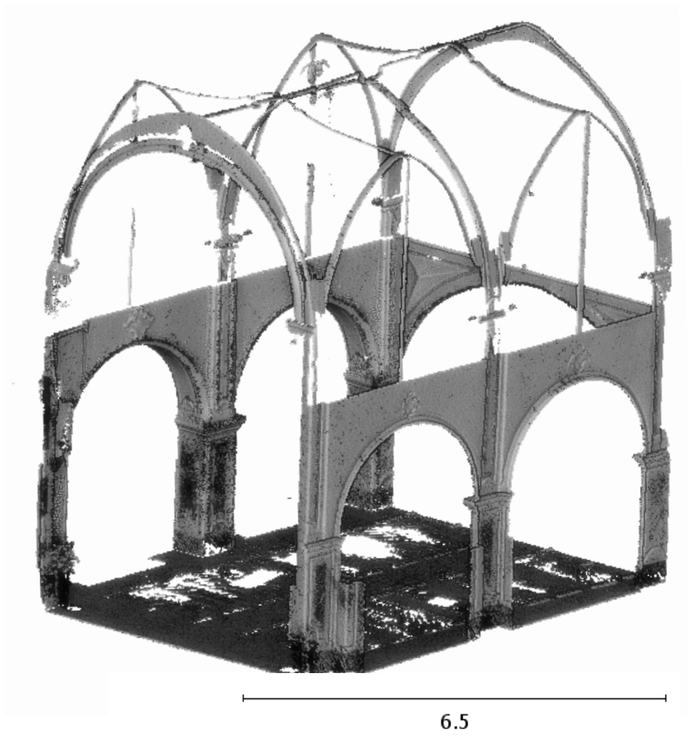


Figure 5.1. Section profiles from the point cloud in CloudCompare.

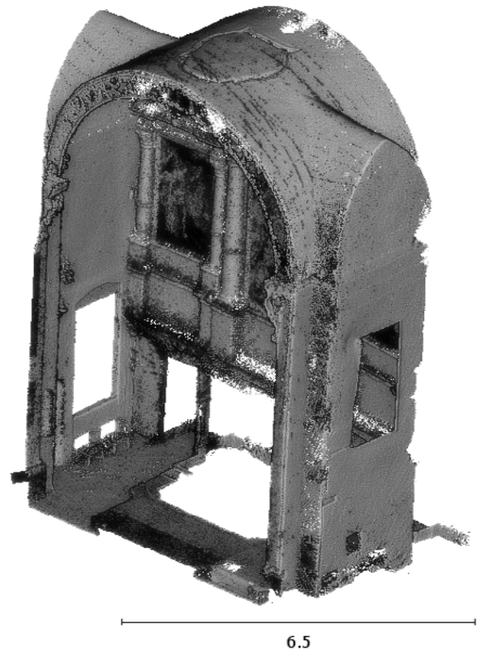


Figure 5.2. The selected point cloud of the main alter in CloudCompare before section generation.

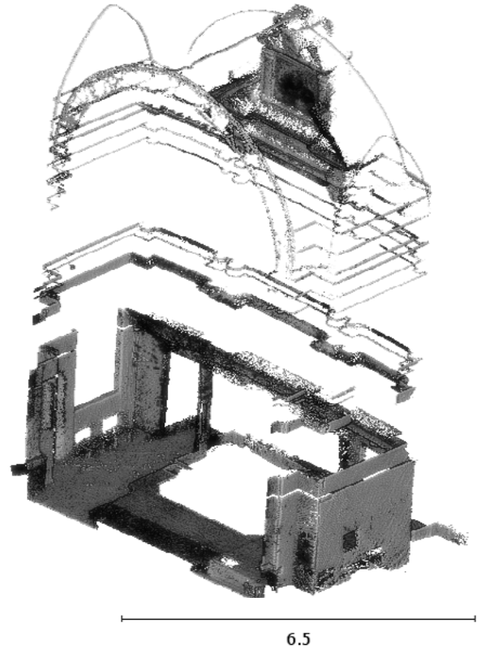


Figure 5.3. The selected point cloud of the main alter in CloudCompare after section generation.

NURBS Surface Generation Strategies

Once the sections were established and vectorized in the curves elements in Rhino, they were converted into continuous NURBS surfaces. Since no single modeling command could be used for the structural complexity of the entire church; surface generation were selected based on the topology of the curves, the degree of geometric variation, and the fidelity that they had to the survey data with a visual point of view. In this process, surfaces were never changed to ideal verticality, horizontality, or orthogonality; all historical irregularities tolerance were preserved. The main NURBS operations that were applied to generate the surfaces:

1. Planar Surfaces: Applied to walls, floors, and roof slopes using boundary curves, maintaining their actual surveyed inclinations and local deviations.

2. Loft: Used for elements with gradually changing cross-sections, such as wall transitions, vaults, and broad arch surfaces. Denser intermediate profiles were introduced wherever geometric curvature changed rapidly.

3. Sweep 1 Rail & 2 Rails: Sweep 1 Rail generated linear elements with uniform profiles, such as cornices and mouldings. Sweep 2 Rails provided dual-boundary control for complex, non-uniform arches and vault transitions.

4. Revolve: Strictly limited to geometrically verified axisymmetric components. When survey data revealed asymmetry, Loft or Sweep was used instead to prevent artificial symmetrization.

5. Network Surface: Employed for complex, bi-directional curvatures, specially for vault configurations where a single directional sweep or loft was insufficient.

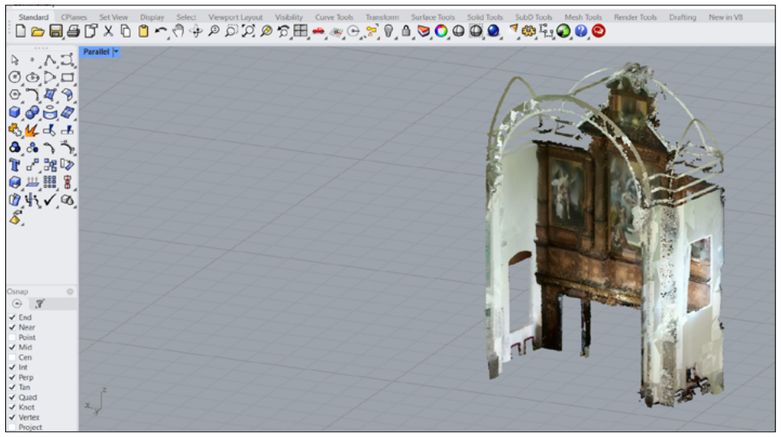
6. Patch: Reserved exclusively for irregular transitions or partially incomplete zones.



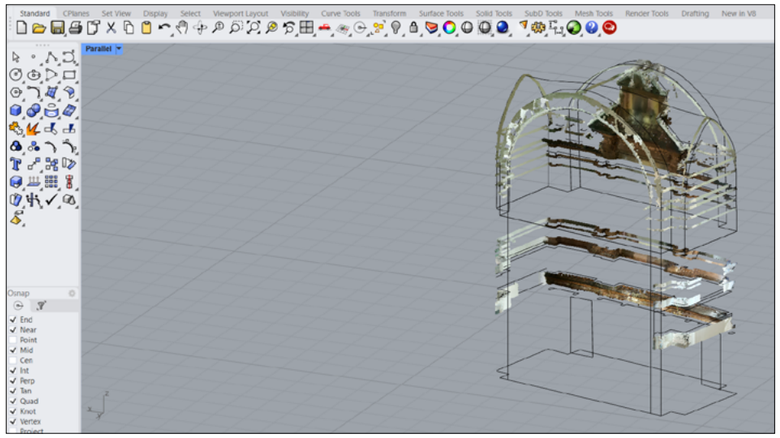
(a) (b) (c)

Figure 5.4. Reconstruction of the selected architectural element (main alter) in front view: (a) point-cloud reference, (b) extracted profiles, and (c) reconstructed NURBS geometry.

(a)



(b)



(c)

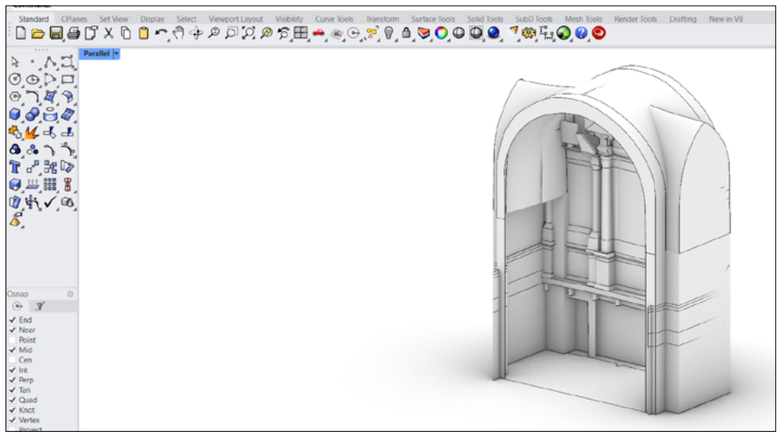


Figure 5.5. Reconstruction of the selected architectural element (main alter) in 3D view: (a) point-cloud reference, (b) extracted profiles, and (c) reconstructed NURBS geometry.

Architectural Modeling System (Exterior and Interior)

The geometric modelling of the church had a clear and structured path. The interior and exterior parts were modelled separately for better control, but both were kept in the same coordinate system. The same 4 rules were followed for all architectural elements: **1.** Preserving the existing irregularities and deformations, **2.** Avoiding automatic symmetry, **3.** Simplifying very small decorative details that were not necessary for any analysis, **4.** Respect to the point cloud as the main source for decisions.

Then the modelling was organised into these main steps:

1. Main walls and boundaries

The modelling started with the main exterior walls, interior wall surfaces, and floor levels. These elements defined the general spatial limits of the church and provided the reference levels needed for modelling the roofs and vaults. Mostly, the exterior walls were modelled using the UAV photogrammetric data, while the interior surfaces were based on the handheld laser scanner data.

2. Roofs and vault systems

The exterior roofs and gables were reconstructed using ridge lines, eave profiles, and transverse sections. Separate NURBS surfaces were created where different roof slopes or volumes.

For the interior, the nave was modelled as a barrel vault with lunettes. The lunettes and the vaults of the side chapels were treated as separate surfaces because their geometry was different from the main barrel vault. Commands such as Loft and Network Surface were used to control these complex geometries and keep their real form.

3. Openings, arches, and architectural connections

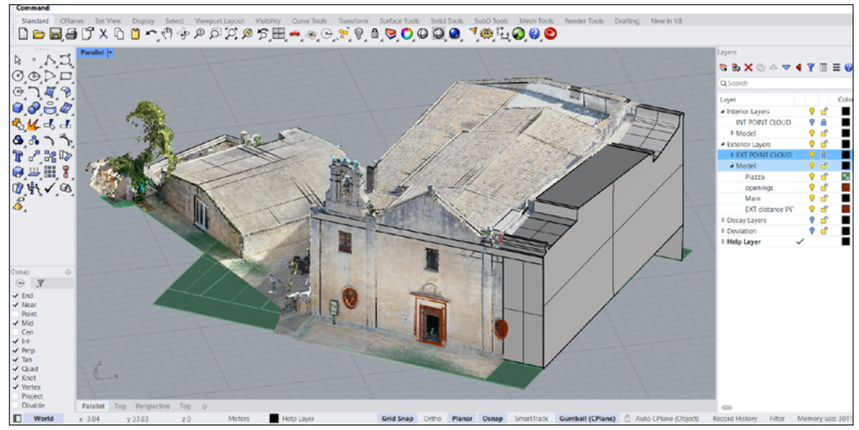
Doors, windows, and arches were modelled using separate profiles for the intrados, extrados, and depth. Free form NURBS curves were the best choice when the point cloud showed asymmetry or deformation, instead of forcing the geometry into regular circular arcs.

4. Complex and adjoining elements

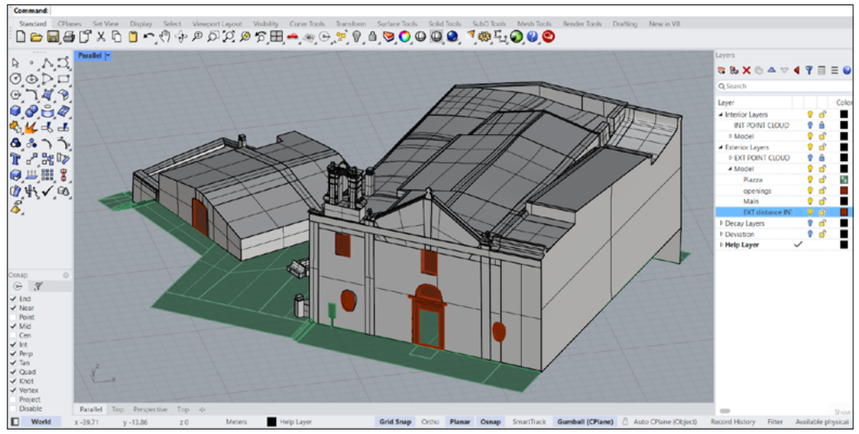
More complex elements, such as the main altar, the bell gable, and the adjoining building volumes, were divided into smaller and more manageable components. Cornices, recesses, supports, and other main parts were modelled separately and then combined with the rest of the 3D model. Their main architectural form and connections were preserved, while very small decorative irregularities were simplified to keep the model lighter and more suitable for analysis and web-based visualisation.

In addition, the **interior and exterior models** were constantly displayed together to verify their relationship. The comparison focused on **wall thicknesses**, **opening positions**, **floor and roof levels**, and other locations where the two datasets provided **geometric evidence** at the same time. Since the **source point clouds** were registered but not merged, this **combined visualisation** provided a practical control while preserving the advantages of separate data management. Finally, the modelling stage established a controlled transition from the **3D metric survey data** to a **NURBS as-built geometry**.

(a)



(b)



(c)

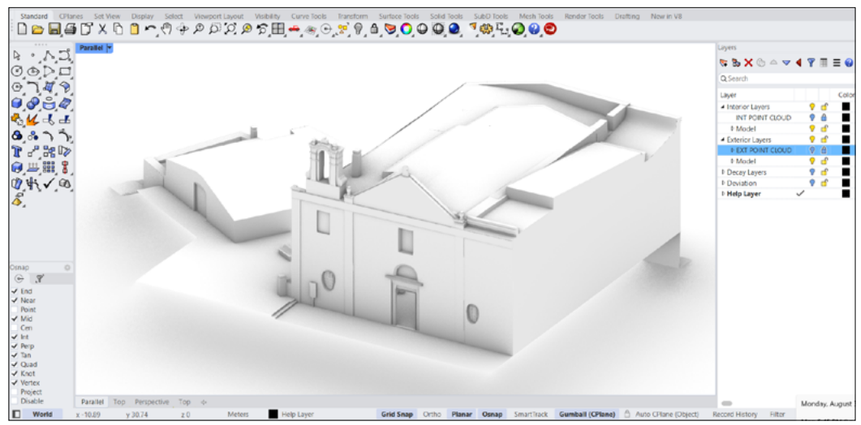
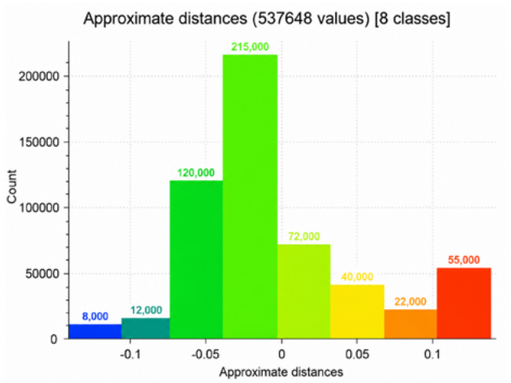


Figure 5.6. Final development of the exterior as-built NURBS model: (a) point-cloud reference and initial geometry, (b) reconstructed architectural components, and (c) final assembled model.

5.2 Accuracy validation

After finishing the modelling process, to evaluate how our model was built in the as-built condition, the geometric accuracy validation was performed through two distinct evaluations: the exterior model, the interior model with their corresponding point clouds.

For the exterior model evaluation, the distance computation shows a high overall metric correspondence with the photogrammetric UAV point cloud. The analysis illustrates a low mean distance of 2.0 cm (Avg dist = 0.02 m). As shown in the error distribution analysis, over 85% of the exterior point cloud falls within a tight tolerance band of ±5 cm. The heat map indicates that the primary massing and planar surfaces of the exterior model were reconstructed with high metric fidelity, while the localized deviations and higher errors are strictly confined to window areas, complex architectural transitions, and areas with high scanning noise.



(a)

Metric	Result
Avg dist.	0.020371
Sigma	0.142198
Max error	0.182412

Table 5.2. Statistical results of the exterior model-to-cloud analysis.

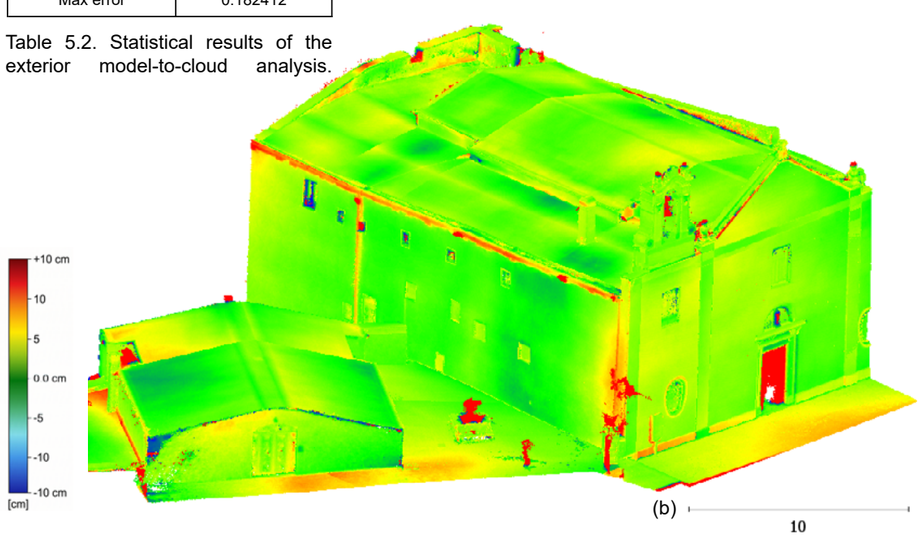
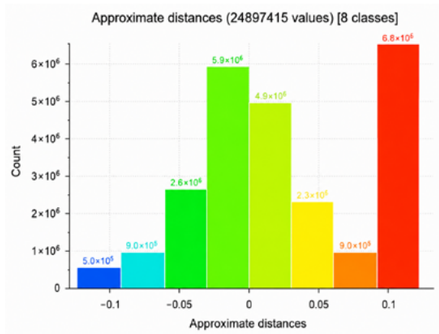


Figure 5.7. Exterior model-to-cloud analysis: (a) deviation distribution and (b) spatial deviation map.

Then, for the interior model evaluation, the distance computation was again used for the metric correspondence between the complex vaulting system and the MMS point cloud dataset. The analysis shows a mean distance (Avg dist) of 0.035 m (3.5 cm) close to zero, with a maximum error within 10 cm (0.1 m). As it is shown in the error distribution analysis, the majority of the interior point cloud (over 75%) is closely concentrated within the ±5 cm tolerance, like the exterior model; while localized deviations and higher errors are strictly confined to complex vaulted geometry, intersection joints, the floor of the interior model, and areas with scanning noise. In summary, the comparative analysis shows a high degree of metric fidelity, with the majority of deviations within a ±5 cm tolerance. This analysis confirms the geometric reliability of the overall 3D modelling workflow based on sectioning.



(a)

Metric	Result
Avg dist.	0.035398
Sigma	0.096203
Max error	0.151242

Table 5.3. Statistical results of the interior model-to-cloud analysis.

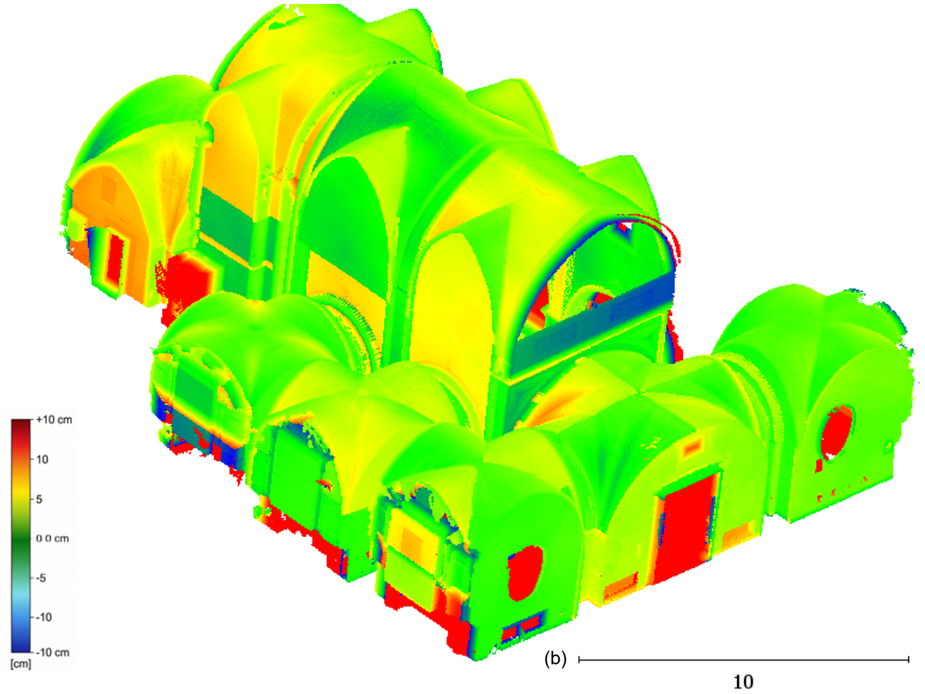
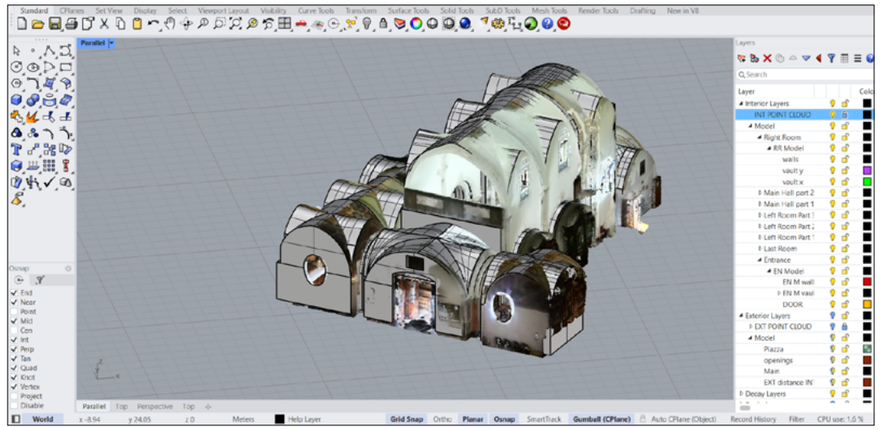


Figure 5.8. Interior model-to-cloud analysis: (a) deviation distribution and (b) spatial deviation map.

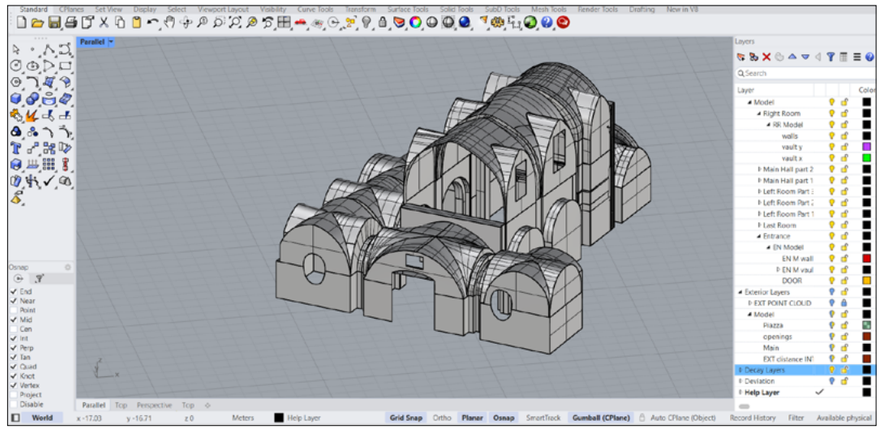
5.3 Model limitation and challenges

The main limitations of this workflow are related to the role of the modeller, the requirements of subsequent **visual analysis**, and the approximation introduced by **NURBS surfaces**. Firstly, the reliability of the **3D model** is influenced by the limitations of the **acquisition methods**. For example, the interior **mobile scanning** can be affected by local errors because of long trajectories or repetitive spaces. **Photogrammetric data** can also be less reliable in zones affected by **occlusion**, reflective surfaces, or limited image coverage, or even based on the lighting situation; as a result, **point density** varied according to accessibility, influencing the amount of interpretation required during curve and surface reconstruction. In this case study, some architectural elements were partly hidden by furniture, altars, equipment, or inaccessible areas, which means the **point cloud** did not provide a 100% complete dataset of the permanent structure. In this phase, missing geometries were reconstructed only when neighbouring sections provided a reliable base; otherwise, the geometry was simplified rather than completed through unsupported assumptions. **Point cloud cleaning** also required careful attention to avoid removing valid points near edges or leaving temporary objects that could distort and change **section profiles**. Although this method provided strong geometric control, its results depended heavily on the spacing and orientation of the selected sections. An **adaptive strategy** helped to solve this matter by using wider spacing in regular areas and denser sections around complex elements like vaults and arches, but in any case, the section selection remained partly dependent on the **modeller's visual judgement**. The transformation of **point cloud sections** into **NURBS curves** also required some arrangements. For each section, it was necessary to decide whether the profile must be represented by a **regular geometric curve** or needed a more **free-form shape**. Small variations also had to be evaluated carefully to understand whether they represented actual irregularities or only **noise** in the point cloud. Another important aspect for the operator is controlling the number of **control points**. Using too few points could remove relevant deformations, while using too many could make the geometry unnecessarily complex and unstable. Therefore, the process cannot be considered automatic, and its reproducibility depends on clearly defining the **modelling tolerances** and **simplification criteria**.Avoiding **automatic mirroring** improved the representation of the actual **as-built condition** but increased modelling time. Repeated elements had to be checked independently whenever the point cloud showed local differences in dimensions or alignment. While time-consuming, this approach was essential for accurate **diagnostic analysis**. **NURBS surfaces** provided a continuous and editable representation, but they are still a close estimate of the actual scan data and not an exact copy. Complex areas such as **vault-lunette intersections** often required multiple adjoining surfaces, and achieving the perfect mathematical continuity was neither always possible nor consistent with actual construction realities. Finally, while the **geometric NURBS model** was structured, it did not automatically construct a complete **HBIM model**, as Rhino surfaces lack inherent **semantic classes**, **material data**, and **object relationships**; therefore, if transferring this complex geometry to **BIM platforms** was needed, it could sometimes cause **geometric simplification**. For this reason, the model should be understood as an accurate **geometric foundation**.

(a)



(b)



(c)

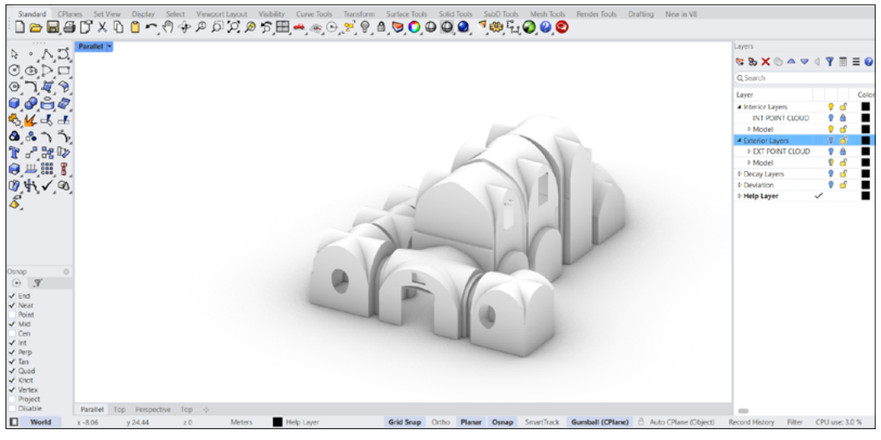


Figure 5.9. Final development of the interior as-built NURBS model: (a) point-cloud reference and initial geometry, (b) reconstructed architectural components, and (c) final assembled model.

6. VPL-Based Analysis

This chapter will present the **Visual Programming Language (VPL)-based workflow** that is developed for **semi-automated decay mapping** using **Rhinoceros** and **Grasshopper**. In this part, based on the **RGB value information** extracted from **orthophotos** generated through the **UAV photogrammetric survey** of the church's exterior façade (One of the church's exterior façades was selected for the application of the proposed workflow), **adjustable parameters** are used to create **editable boundaries** of the decay areas recognised on the façade and then transfer them onto the **3D façade model**. In summary, the chapter describes the working environment, the **decay-mapping process** developed in Grasshopper, the outputs of the proposed workflow, and its final definition.

6.1 Environment and Tools

In general, **Visual Programming Languages (VPLs)** are a graphical method for building **computational strategies** through the connection of visual elements rather than through the use of written code. These operations can be represented by **components**, with the relationships between **inputs, functions, and outputs** which are defined through **connecting wires**, and at the end, the resulting **graph** makes the process visible and allows the user to understand how data are performing throughout the system. Specifically, in **architectural applications**, VPL is similar to **parametric thinking**. For example, a **parametric process** is not only defined by the final result, but by the **relationships and rules** used to generate that result; so, in this case, the operator first establishes a **logical workflow**, identifies the essential inputs, and defines the connections between them, then the final output is one possible situation of an expanded system that can be modified by changing its **parameters**. As discussed by Wirz (2010), the value of this **parametric approach** is in the possibility of maintaining the **process structure** while adjusting separated conditions without reconstructing the entire process.



Figure 6.1. Basic input–process–output logic of a Visual Programming Language workflow.

This logic is based on the concept of the **algorithm**, and its objective is not limited to solving a single isolated case. Instead, this kind of workflow could remain applicable to comparable case studies where the general logic is the same while the input data or control parameters are changed. This feature is completely relevant to **heritage documentation**, where the same analytical problem may happen to different façades, architectural elements, survey datasets, or even different case studies, although the dimensions and physical conditions are not the same. Several VPL platforms are currently used in the architecture context, but the most common examples are **Grasshopper**, within **Rhinoceros**, and also **Dynamo**, which is associated with the **Autodesk** and **Revit** environments. For this thesis, **Rhinoceros 8** and its integrated **Grasshopper** environment were selected as the main tools, because the survey data, the as-built NURBS model, and the analytical results could be managed together. **Rhinoceros** was already used in the previous modelling phase to reconstruct the geometry of the **Church of Sant'Antonio dei Cappuccini**, so continuing the analytical work (decay mapping) in the same environment reduced the need to transfer complex geometric information between separate software.

Grasshopper here is used to define the **computational and parametric logic** of the **decay mapping** instead of drawing each boundary manually. It created a repeatable link between the **image data**, **adjustable parameters**, and the **three-dimensional geometry** of the façade. Since the workflow works as a **dataflow graph**, any change to the inputs automatically updated the final result based on the experts' goals. This possibility of controlling the process through **numerical parameters** was one of the main reasons for selecting a **VPL-based approach**. Parameters such as the **dimensions of the analysed area**, the **density of image sampling**, and the **level of similarity** between selected colors could be modified without rebuilding the complete workflow. This made it possible to test different settings, compare their effects, and also to be adaptable to other parts of the building, since in this thesis we focused only on one facade to apply our approach.

In conclusion, the workflow combines the **orthophoto**, **point cloud**, and **3D model** to support a **semi-automated mapping process**. The main logic in **Grasshopper** was that the **façade image** was sampled, the selected **colour values** were compared with a **reference colour**, and an **adjustable tolerance** was used to identify similar areas. These areas were then converted into **contours**, transformed to match the **façade geometry**, and projected onto the **3D surface** as **editable decay boundaries**. In this way, the final **decay map** can be checked directly on both the **original survey data** and the **actual geometry** of the building and allows the detected **decay areas** to be evaluated directly in relation to both the **original survey evidence** and the **actual 3D model** of the building.

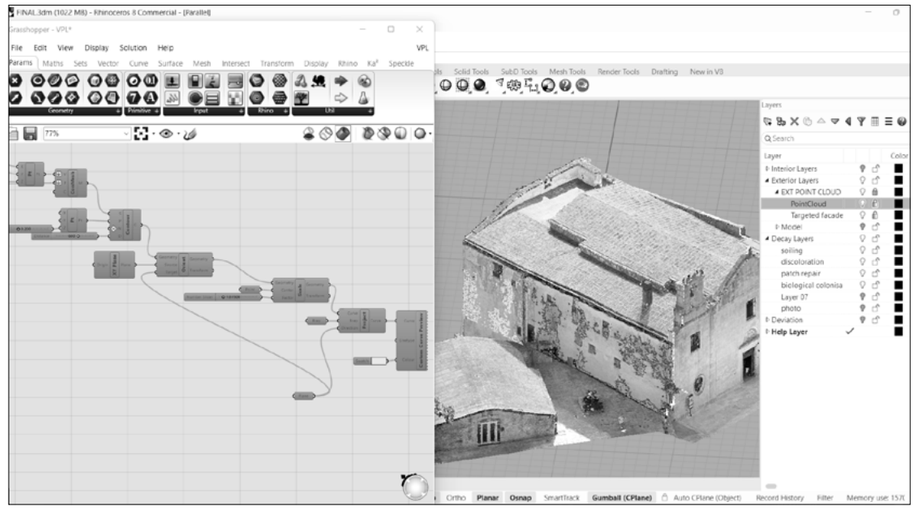


Figure 6.2. Integrated Rhinoceros–Grasshopper environment used for the decay-mapping workflow to show the interface.

6.2 RGB-Based Decay Detection

This proposed operation was applied to the **north-western façade** of the church as the test area where its **orthophoto** shows several visible surface decay and allowed the complete process to be developed and evaluated. Before starting the computational process, the decay conditions of the façade were identified by the operator and organised into four **degradation classes**:

- **Soiling**
- **Discoloration**
- **Patch Repair**
- **Biological Colonization**

One representative color was chosen and assigned to each category in the **reference raster**. The workflow did not automatically diagnose the type of decay directly from a raw image. Instead, the classes are defined based on the **restoration expert decision**, while **Grasshopper** supported the extraction and mapping and transferring their boundaries through a **repeatable computational procedure**. Then each degradation class was generated separately, and its final curves were assigned to an independent **Rhino layer** with a different color. The layers were named **soiling**, **discoloration**, **patch repair**, and **biological colonisation**. This organisation allowed each category to be displayed, hidden, edited, verified, or exported separately in different formats. The **Grasshopper workflow** was developed through several connected components in which each component received specific input data, performed one specific operation, and then transferred its result to the next stage. The complete process is explained in following stages:

Stage 1: Definition of the Orthophoto Extent

In the first stage, the physical extent of the orthophoto in the Grasshopper environment was established. A **Rectangle component** was used to create a two-dimensional boundary corresponding to the dimensions of the image (the orthophoto of the selected façade). The main inputs were **X Size = 34.95 m** and **Y Size = 18.40 m**. These values were the fixed dimensions of the orthophoto and were not used as detection parameters and they should not be changed during the process, and the purpose was to reproduce the image with its correct real scale and establish the **spatial limits** of the analysed area. In fact, the Rectangle component received the X and Y values and generated a rectangular boundary on the **World XY plane**. Since at first, the orthophoto existed on a horizontal plane, the **image processing stage** was first developed in this two-dimensional reference system and at the last stage it will be projected on the **three-dimensional model** of the church. Then the output of this stage was therefore a rectangle measuring **34.95 by 18.40 meters**, corresponding to the orthophoto values.

Stage 2: Generation of the Sampling Mesh

Then the rectangle was connected to a **Mesh Plane component**. The function of this component was converting the rectangular area into a regular **mesh** formed by **vertices** and **faces**. The mesh provided the sampling structure that is needed to read the colour information in the raster image. The main inputs were **B - Boundary**, representing the rectangle defining the orthophoto extent; **W - Width Count**, set to 600; and **H - Height Count**, set to 600. The **Width Count** and **Height Count** can control the number of divisions in the two directions. In the first try, the values were set to 600 and 600 but a higher number of divisions creates more sampling points and can represent smaller image variations, so the results could be more precise, but it also increases the amount of data and the computational time. Then a lower number reduces the calculation load but may simplify or remove small decay areas. Accordingly, the selected values must respect a balance between the visible detail of the orthophoto and the performance of the Grasshopper. Unlike the fixed dimensions of the orthophoto, the **sampling density** can be adjusted according to the image resolution, the dimensions of the façade, and the required level of detail, and the output was a regular mesh covering the orthophoto area.

Stage 3: Extraction of Mesh Vertices and Faces

After, the sampling mesh was connected to a **Deconstruct Mesh component**. This component could divide the mesh into its basic geometric information; So, its principal outputs included **V - Vertices**, representing the sampling points distributed within the orthophoto; **F - Faces**, defining the connectivity structure of the mesh; **N - Normals**, describing the orientation of the mesh elements; and **C - Colors**, containing all the color information attached to the mesh. In this workflow, the vertices and faces were the main outputs that we needed. The vertices were used as the locations for image sampling, while the original faces were later reused to reconstruct a new mesh. The vertices were also deconstructed into their X, Y, and Z **coordinates**. Their original X and Y values were important because they represented the exact location of each sample within the orthophoto.

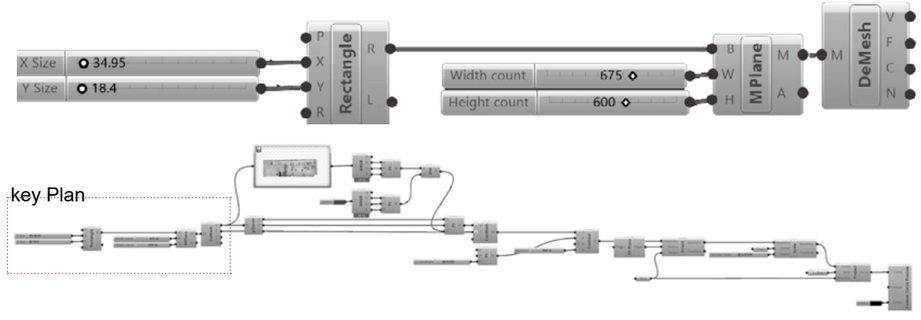


Figure 6.3. Grasshopper workflow for defining the orthophoto extent, generating the sampling mesh.

Stage 4: Image Sampling

In the next stage, we had to connect the **mesh vertices** to the **Image Sampler component**. The selected **raster image** (the **orthophoto**) was loaded into this component, and each mesh vertex was used as a sampling location. The **Image Sampler** was a relationship between the position of each vertex and the corresponding pixel or **RGB value** in the orthophoto. Its input therefore was the sample points generated by the mesh, while its output had a color value for each point. This operation exchanged the raster image into a collection of **color data** connected to geometric positions. In this case, instead of examining the orthophoto as a single image, the workflow evaluated it through a **sampling grid**.

Stage 5: Separation of the RGB Channels

The color output of the **Image Sampler** was connected to a **Split ARGB component**. Digital colors contain four numerical channels: **A - Alpha**, for transparency; **R - Red**; **G - Green**; and **B – Blue**. This **Grasshopper component** shows these values in a range from 0 to 1. In this workflow, the **Alpha channel** was not used because transparency was not part of our **decay detection logic** and only the **Red**, **Green**, and **Blue** outputs were used; and after that, the **RGB values** were connected to a **Construct Point component**: Red was connected to X, Green was connected to Y, and Blue was connected to Z. This component was used as a method for combining the three **RGB channels** into one **three-dimensional numerical vector** to be comparable with our **reference colors**.

Stage 6: Definition of the Reference Color

The **Color Swatch component** was used to define the color that represents the **decay class**. The selected color was again connected to a **Split ARGB component** and then converted into a second **three-dimensional RGB point**. Since some differences could happen based on the **image resolution**, color transitions, surface texture, illumination, and the way the reference raster had been prepared, the reference color was combined with an **adjustable tolerance** in the following stage. The same path was repeated separately for **soiling**, **discoloration**, **patch repair**, and **biological colonization** and each class has its own representative color and final display layer.

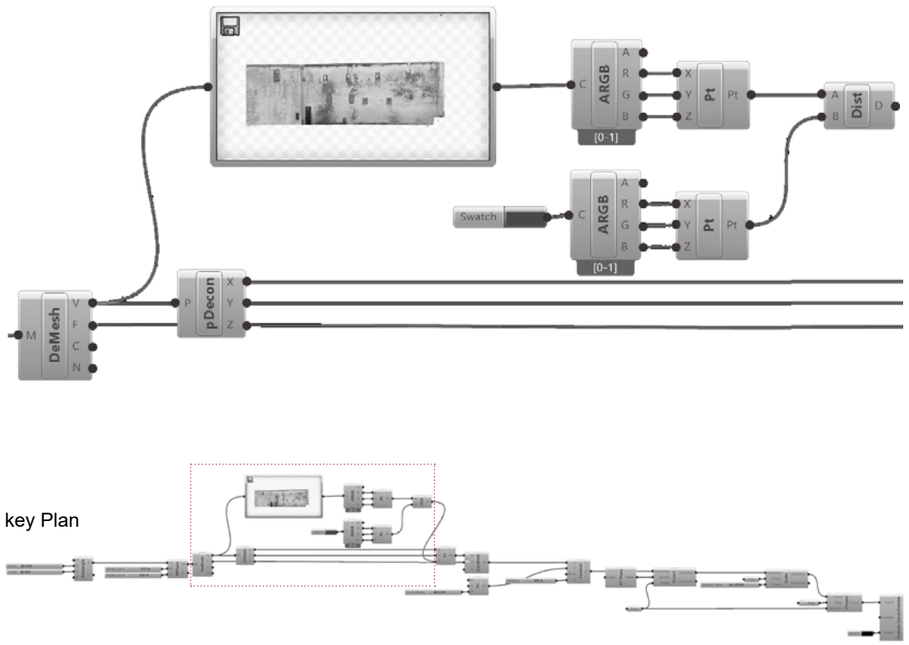


Figure 6.4. Grasshopper workflow for image sampling and the RGB processing.

Stage 7: Calculation of RGB Color Distance

The two **RGB points** were connected to a **Distance component**. One input from the **RGB vector** extracted from each sampled point from the orthophoto, while the second input received the RGB values of the selected **reference color**. The output of the Distance component is not a physical distance measured on the façade. It is a numerical representation of color difference in **RGB space**. It means a value close to zero shows that the sampled color is very similar to the reference color, and a larger value indicates a bigger difference.

$$d_i = \sqrt{(R_i - R_r)^2 + (G_i - G_r)^2 + (B_i - B_r)^2}$$

Stage 8: Construction of a Distance Mesh

The mesh vertices were deconstructed into **X, Y, and Z coordinates**. The X and Y positions were the same, while the **RGB Distance values** were assigned as the new Z coordinates. In this way, the color difference was the height; so, the pixels closer to the reference color remained at lower values, and larger color differences produced higher values. Then the new points were then combined with the **original mesh faces** to create a new mesh. This step made it possible to convert the color analysis into a **numerical surface** which **contour curves** could be extracted from it.

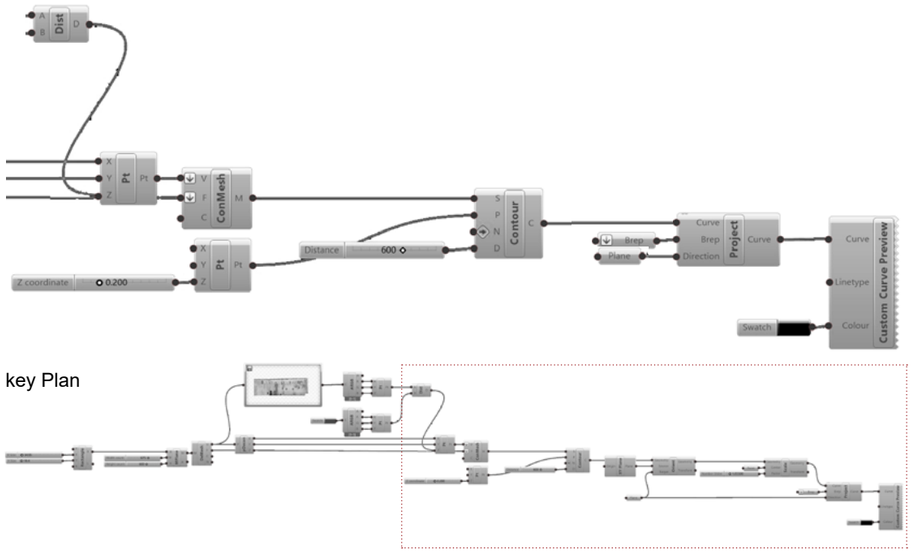


Figure 6.5. Grasshopper workflow for tolerance-based contour extraction.

Stage 9: The Tolerance and Contour Extraction

The new mesh then was connected to a **Contour component**. The purpose of this part was to generate the curves corresponding to the selected level of color similarity. The main inputs were **S - Shape**, receiving the distance mesh; **P - Base Point**, defining the elevation of the first contour; **N - Direction**, defining the direction of the contour planes; and **D - Distance**, defining the interval between the planes. First, the Z coordinate of the base point was set to 0.20 (this value is normalised on a scale from 0 to 1, where 0 corresponds to an exact color similarity and 1 to the maximum color variation); this value represented the selected **RGB tolerance** for the first test. This number means the contour is generated approximately to locations where the color distance from the reference value was equal to 0.20. This tolerance is an **adjustable parameter**. A smaller value selects a narrower range of colors and usually creates more limited boundaries, and a larger value has a wider range of similar colors but could also increase false selections at the same time. Therefore, the final value had to be calibrated by comparing the curves with the original image according to the visual characteristics of each **decay category**.

Stage 10: Projection onto the Three-Dimensional Façade

For the final stage, the curves must be connected to the target façade **Brep** with a **Project component**. The main inputs were **Curve**, receiving the decay boundaries; **Brep**, receiving the target façade surface; and **Direction**, defining the projection direction towards the façade. Finally, as the outputs, the curves were projected onto the façade **Brep** and transferred from the 2D image plane to their correct position on the **3D model**.

Stage 11: Visualisation and Layer Management

Finally, the **projected curves** were connected to **Custom Curve Preview** to control their color and appearance in the **Rhino** viewport. After visual checking by the **operator**, the accepted curves could be baked into Rhino and illustrate decays in **separate layers** and it made it possible to **display**, **compare**, and **modify** each degradation class **independently**.

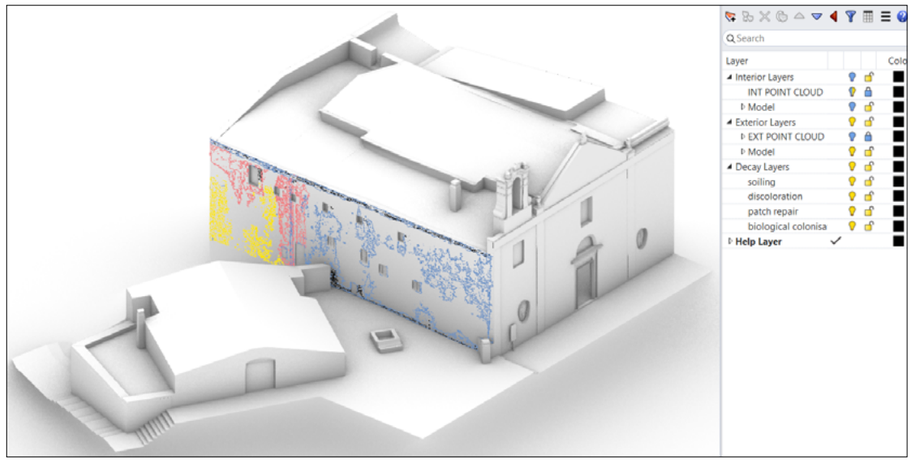


Figure 6.6. 3D visualisation and layer management of the projected decay boundaries in Rhinoceros.



Figure 6.7. Projected decay boundaries on the analysed façade in elevation view.

6.3 Final Semi-automatic Workflow Definition

This defined workflow can be considered as a semi-automated and also operator-controlled method for converting color information from an orthophoto into editable metric decay boundaries positioned on a three-dimensional façade. In summary, this method combines three main groups of inputs: the orthophoto and its dimensions, the analytical parameters such as sampling density, reference color, and RGB tolerance, and additionally the three-dimensional target geometry. Grasshopper samples the image, compares the RGB values with a reference color, and extracts boundaries according to the tolerance in their corresponding position on the façade of the 3D model.

Here, the user is responsible for defining the decay classes, selecting their representative colors, adjusting the tolerance, identifying false selections, and checking the final curves in comparison with the survey data. Manual correction can also be applied when it is necessary. This distinction by user is essential because color similarity alone cannot provide a complete and accurate decay diagnosis. Sometimes, similar colors may represent different conditions because of lighting, shadows, moisture, texture, image noise, or material variations.

One of the biggest advantages of this workflow is its flexibility. Different results can be tested by changing the reference color, RGB tolerance, or sampling density without manually redrawing the complete decay map. Additionally, the same Grasshopper pathway can also be applied to another façade by replacing the orthophoto and its target geometry.

Another advantage is that these results can be exported in different formats. For example, exporting to **DWG** can provide a base for quantitative analysis. If converted into closed curves, their area and different dimensions can be calculated and compared with the total façade area. These calculations are considered a possible extension of the present workflow rather than its main output. The data can also be converted into **JavaScript Object Notation** (JSON) format which is a lightweight, text-based data-interchange format for integration with other digital environments. JSON file can save the curve coordinates together with attributes such as decay category, identification, display properties, and additional descriptive information. This creates a connection between the Grasshopper analysis and the web-based visualisation developed in this thesis, where the decay boundaries can be displayed directly on the three-dimensional model and managed by category.

This method also has limitations because its reliability depends on the quality of the orthophoto, sampling density, reference color, RGB tolerance, and correspondence between the image and the three-dimensional geometry. For this reason, visual verification and manual adjustment remain essential parts of the process.

Overall, the workflow is a **direct connection** between image-based survey data, visual programming, editable vector geometry, and the three-dimensional model. Its main goal is not the full automation of decay diagnosis, but a transparent and adjustable method that supports the specialist in identifying, mapping, editing, and transferring the surface conditions across different digital documentation environments.

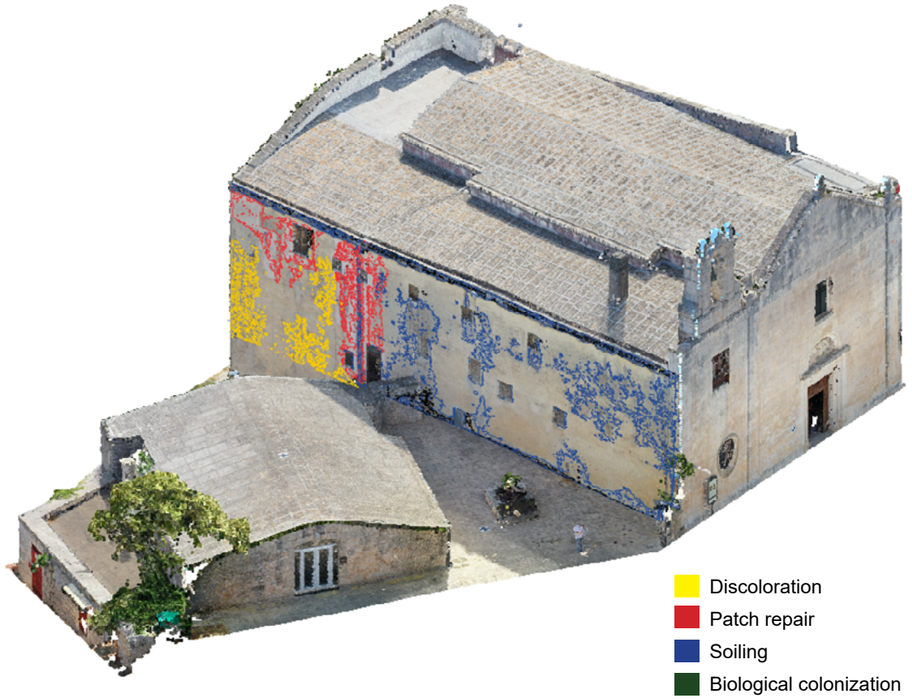


Figure 6.8. Final three-dimensional decay map integrated with the survey-based model.



Figure 6.9. Final VPL-based Soiling decay map of the analysed façade in elevation view.

6.4 Evaluating the Mapping Methods: Manual vs. Semi-Automated

To visually evaluate the results of the proposed VPL-based workflow, this section presents a comparison with the traditional and manual technique, which is conducted in chapter 2. The following figures illustrate the results of both methods applied to the same lateral exterior facade of the Church of Sant'Antonio dei Cappuccini.

(a)



(b)

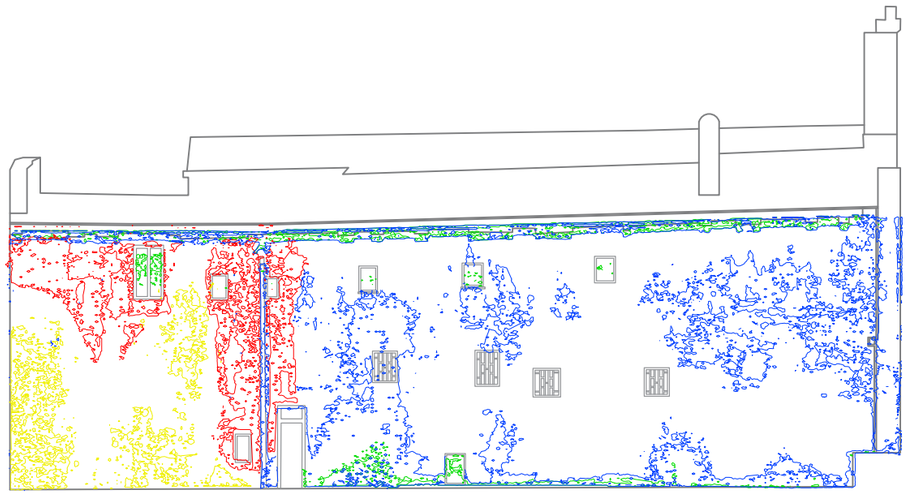


Figure 6.10. Overall visual comparison of the complete decay mapping on the analyzed facade: (a) traditional manual mapping, (b) VPL-based semi-automated extraction.

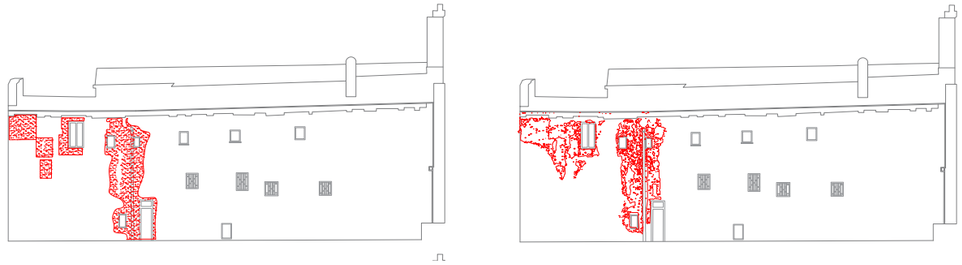


Figure 6.11. Comparative evaluation of the Patch Repair pattern distributionon on the analyzed facade: (a) manual operator interpretation, (b) Semi-automated VPL-based decay mapping

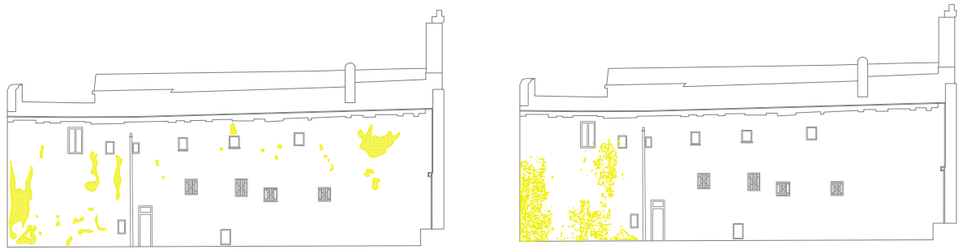


Figure 6.12. Comparative evaluation of the Discoloration pattern distributionon on the analyzed facade: (a) manual operator interpretation, (b) Semi-automated VPL-based decay mapping

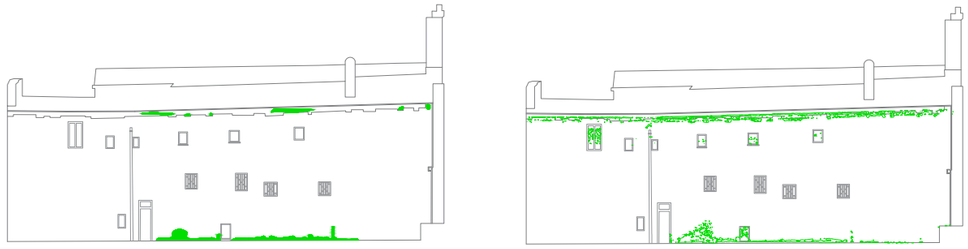


Figure 6.13. Comparative evaluation of the Biological Colonization pattern distributionon on the analyzed facade: (a) manual operator interpretation, (b) Semi-automated VPL-based decay mapping

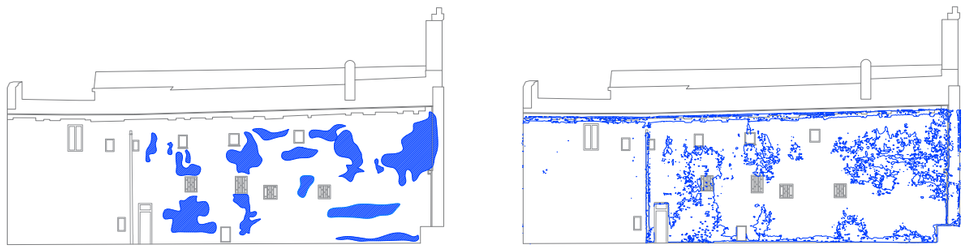


Figure 6.14. Comparative evaluation of the Soiling pattern distributionon on the analyzed facade: (a) manual operator interpretation, (b) Semi-automated VPL-based decay mapping

7. Final Outputs

After all the phases of this thesis: **3D metric survey**, **NURBS modelling**, **VPL-based decay mapping**, and **data integration**, the proposed workflow produced a complete set of results connecting the physical condition of the **Church of Sant'Antonio dei Cappuccini** with its **digital representation**. Finally, the different datasets, including **point clouds**, the **architectural model**, **orthophotos**, **decay maps**, and **survey documentation**, were prepared for integrated **web-based visualisation**.

7.1 From Questions to Findings

The main objective of this thesis is **to bridge the gap between different digital heritage disciplines.** Traditionally, 3D surveys data, architectural modeling, and decay diagnosis exist in isolated software environments. Through the case study of the **Church of Sant'Antonio dei Cappuccini**, an integrated workflow through Rhinoceros and Grasshopper was developed and tested. This workflow could **successfully connect** 3D metric survey data, as-built NURBS modeling, and diagnostic analysis to support conservation planning for built heritage. By building the methodology around Rhinoceros software and applying it to our case study, the study answered its core research questions, illustrating how reality-based digital documentation can move outside of the isolated software environments into a reproducible platform. The first sub-question of **how to develop an as-built NURBS model from point-cloud data while preserving the historic building's non-standard characteristics** is answered directly by the modeling methodology developed in Chapter 4. In this scenario, rather than relying on automated surface fitting or idealized BIM families that force geometric regularization, the workflow used an adaptive, section-based approach. Actually, by extracting targeted longitudinal, transverse, and vertical profiles from the registered UAV and MMS point clouds, the reconstruction captured the actual as-built morphology, including wall out-of-plumbness, localized deformations, and non-uniform vault curvatures. This ensures that the resulting NURBS model works as a real geometric foundation and not a simplified generalization. The next sub-question of **how Visual Programming Languages can be utilized for semi-automated decay mapping without relying on external computer-vision software** is resolved by the Grasshopper workflow specified in Chapter 5. This parametric dataflow samples **orthophoto** colors, converts RGB channels into numerical vectors, and computes color distances against a reference swatch; then the system translates raster information into editable vector boundaries with a controllable tolerance.

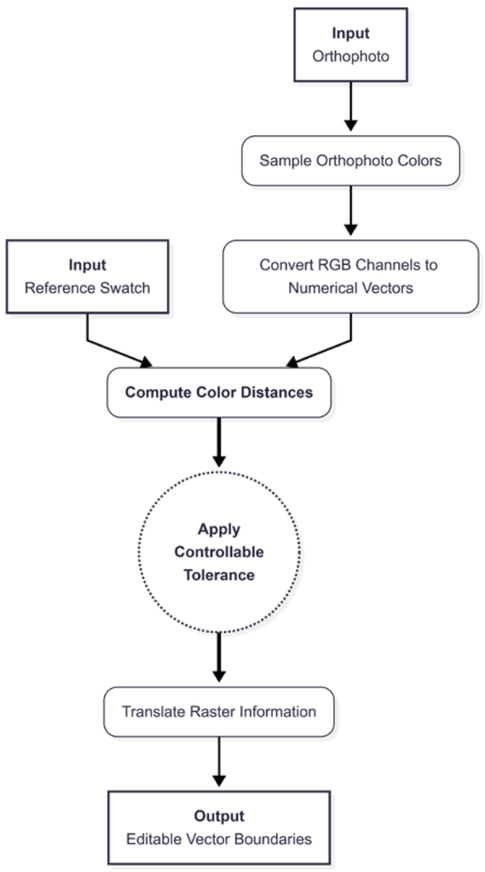


Figure 7.1. The final proposed workflow of VPL-based decay mapping in Grasshopper environment.

This approach avoids the "black box" limitations of heavy machine learning algorithms with providing an operator-controlled and transparent process where restoration experts can adjust sampling densities and tolerances according to specific surface conditions without wasting a lot of time. Then the question of **how diverse architectural datasets can be integrated within an accessible digital environment** is answered by the web-based visualization framework developed in the final stages of the research. By deploying a custom-coded platform using **HTML, CSS, JavaScript,** and **WebGL** libraries, the workflow bridges the gap between heavy desktop software and non-specialist stakeholders. The platform tries to transform a passive 3D viewer into a real-time collaborative tool, allowing on-site inspectors and project managers to exchange data and coordinate with each other. The next sub-question about **the efficiency and accuracy of the parametric workflow of decay mapping** is addressed through the comparative evaluation presented in Chapter 5. The results confirm that the Grasshopper-based semi-automated workflow significantly reduces the time required for decay mapping compared to traditional manual 2D CAD drafting. Essentially, this high efficiency is achieved without sacrificing metric reliability, as the vector boundaries remain directly tied to the calibrated orthophoto pixels and surveyed geometry.

7.2 Web-Based Visualization

One of the most important challenges in the built heritage context is sharing complex digital data with professionals who may not have advanced and licensed architectural software. To answer this, the final stage of this thesis focused on developing a customized, web-based visualization platform. Instead of relying on commercial, closed-source platforms, this interactive website is designed and coded from scratch using HTML, CSS, and JavaScript and was then published on GitHub Pages. Since the whole workflow of this thesis relies on the Rhino (Grasshopper) environment, it is an interoperable workflow; in this case, we could export every data set in a computer science language. For example, for the VPL-based decay analysis layer in Rhino, we export them as a JSON file to be usable in coding in the correct position on the 3D model. In summary, this platform performs as a central hub where the architectural geometry (3D model), survey data (point cloud), and diagnostic analysis (decay mapping of the facade) come together in an accessible environment.

The website offers several practical features designed specifically for heritage documentation and analysis. These are the platform's key options:

Layered Interactive 3D Viewer:
Using WebGL technologies (utilizing libraries like Three.js), the viewer allows users to smoothly navigate massive point clouds and reconstructed NURBS models directly in their web browser. This gives stakeholders a clear and immediate sense of spatial awareness without requiring specialized software.

Layer Management System:
The interface features a flexible sidebar menu that is coded to let users independently turn different data layers on or off, manage the opacity, colors, and also the visual style of each dataset. For instance, the site loads the exterior point cloud by default to immediately illustrate the context of the church. After that, users can overlay specific Grasshopper-generated decay boundaries directly onto the 3D geometry to visually verify the analytical results.

Advanced Decay Layer Controls:
On the platform, there are decay maps for four specific degradation classes: Biological Colonisation, Patch Repair, Discoloration, and Soiling. In addition, several customized options are added; users can adjust the color of each decay layer using a color picker, change the opacity, and change the boundary line thickness for better visual clarity against the underlying geometry.

Theoretical Data & Indicative Treatments:
By clicking on any decay layer, an "Analysis Inspector" panel will open. This feature can provide a useful theoretical context, including a description, probable causes, how it was identified, and some suggested treatment strategies. (It is crucial to highlight that these treatment proposals are not definitive expert conservation diagnoses and are just some potential suggestions to show the website's feature as an informational tool.)

http://santantoniochurch.tech/

Figure 7.2. QR code for direct access to the web-based visualization platform.

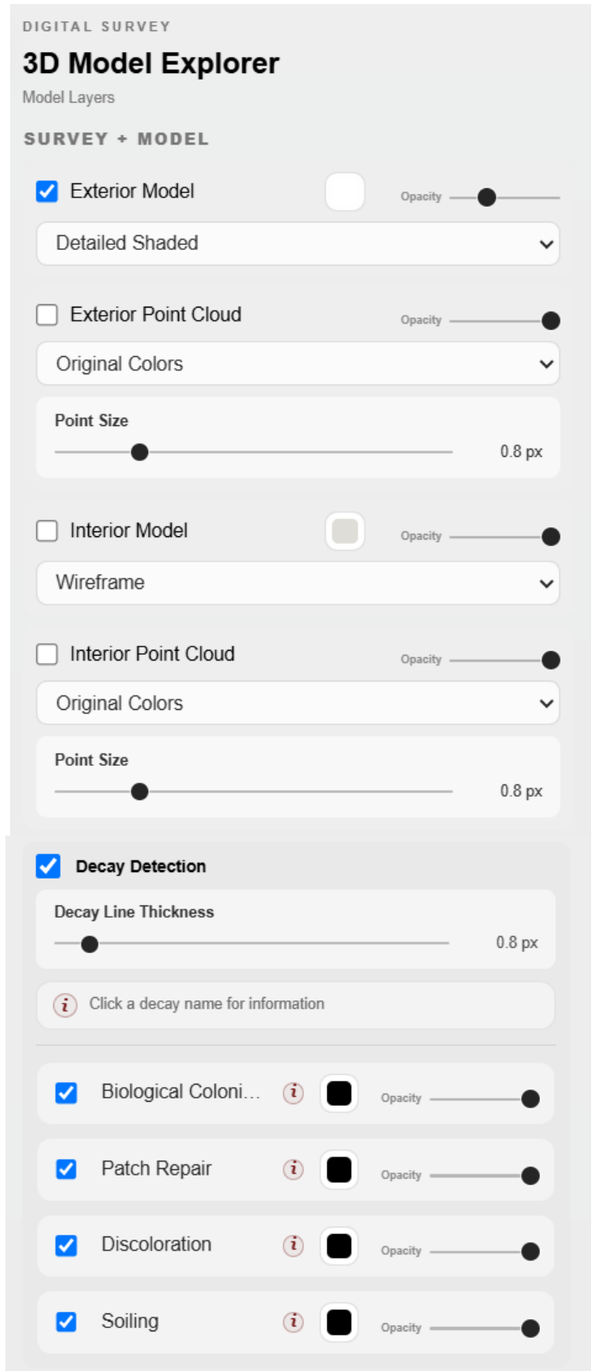


Figure 7.3. The web platform's layer management system and advanced decay controls.

Measurement Tools:
Another practical feature is the ability to take precise measurements directly within the 3D space. Users can measure distances or angles on the models or point clouds or decay layers and even easily switching between units (meters, centimeters, millimeters). These measures will be recorded in a separate panel, and users can customise the name of each measurement. It helps track specific cracks or openings and manage or clear them as needed.
Interactive Section Box:
To deeply analyze interior spaces and evaluate wall thicknesses, or to see the connections between spaces, a dynamic section box is designed. By using reflexive push-and-pull handles in resize, move, or rotate modes, users can slice through the 3D models and point clouds to interactively inspect different cross-sections of the structure.
Archival Documentation:
In the other hand, the website includes the theoretical context of the project, survey metadata, diagnostic parameters, and details about the survey team and the equipment used in the survey (UAV, MMS, and GNSS). There is also a complete gallery of fieldwork photos and orthophotos and some photos of the exterior and interior parts of the church. This approach ensures that no contextual data is lost when transferring information between different environments.
Mobile-Optimized Interface:
In the end, because heritage conservation frequently requires on-site field inspections, CSS and JavaScript are fully optimized to perform also on mobile devices. This helps the tool remain completely functional and easy to use on a smartphone or tablet while standing in front of the actual building.

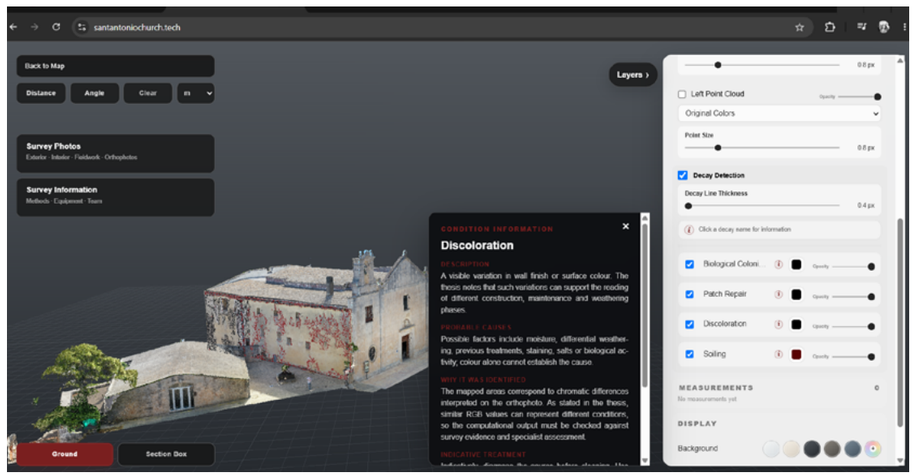


Figure 7.4. The interactive 3D viewer displaying a specific decay analysis inspector panel.

7.3 Conclusion

First of all, this thesis tried to highlight the critical importance of keeping digital documentation as close to reality as possible, and then by integrating multi-sensor surveys with NURBS modeling and VPL analysis, the research provides an interoperable, editable, and highly accurate record of the Church of Sant'Antonio dei Cappuccini. The final web integration ensures that this valuable data does not remain locked inside specialized and licensed software, but rather becomes an interactive, collaborative tool for future conservation planning.

Also, **the accessibility and reproducibility of the workflow** are validated by the lightweight web-based framework and the structured VPL scripts. By avoiding heavy and complicated black-box commercial software and instead using a simple web viewer that runs directly in the browser via GitHub Pages, the method becomes easy to repeat and reuse. It gives architects, on-site restorers, and heritage specialists, even those without advanced computer skills, a practical, user-friendly tool for managing conservation projects. However, an important distinction must be made regarding the VPL analytical part of this thesis. The proposed semi-automated decay detection in Grasshopper workflow is designed strictly as a diagnostic support tool, not an independent diagnostic system. While parametric algorithms can extremely accelerate the repetitive tasks of extracting, mapping, and organizing the data, they do not include architectural or chemical understanding. The classification of decay, the understanding of material conditions, and the final validation of the diagnostic maps must always remain in the hands of human experts and qualified heritage specialists.

In conclusion, the main contribution of this thesis is not the automation of architectural diagnosis, but the establishment of a structured connection between reality-based documentation, computational analysis, architectural modelling, and interactive visualization, and the workflow provides a base for further development towards more advanced and interdisciplinary approaches in the digital heritage documentation context.

7.4 Discussion and Limitations

The significance and innovation of this thesis lies in showing how digital survey data can support heritage conservation more than just a simple documentation. Instead of treating point clouds and 3D models as static records, the proposed workflow uses them as an active sources of information for analysis and understanding. By combining as-built NURBS modelling integrated with Grasshopper-based visual programming, the workflow can represent the irregular geometry and decay conditions of historic buildings without forcing them into idealized forms. At the same time, the web-based platform makes the resulting information easier to access and share among different professionals, providing a practical environment for exploring the survey data, architectural model, and condition-related information, and also has the oppurtunity to be available for adding extra information from different stalkholders. While this integrated workflow offers a strong foundation for heritage documentation, recognising and evaluating **its limitations** is another essential part of this thesis.

First, the NURBS modeling process, while highly accurate, is not fully automated and can be time-consuming. Therefore, unless high precision is strictly required for specific goals like Finite Element Method (FEM) analysis, it might not always be the most efficient strategy to choose, and simplification can sometimes make the process more practical and faster. **Second,** the VPL-based decay mapping relies heavily on the quality of the RGB information. Environmental factors during the UAV survey, such as sunlight situation, shadows, or even surface moisture, can easily alter color values. Consequently, the Grasshopper algorithm might misunderstand a dark shadow as "soiling" or "black crust," and it causes false positive selections. **A further limitation** is the critical distinction between detection and diagnosis. The workflow identifies and maps visual patterns that may indicate surface deterioration, but it does not independently determine the underlying material cause, structural significance, or specific conservation treatment required for each detected area. Therefore, the proposed framework operates strictly as a diagnostic support tool rather than a complete diagnostic system, and in the end, the final interpretation is still dependent on expert assessment.

7.5 Future Research Perspectives

The proposed workflow and methodology in this thesis open several doors for future developments in this context of **built heritage** and its **digitalisation era**. From a geometric point of view, the highly accurate as-built **NURBS model** provides a perfect baseline for other advanced analyses, such as **Finite Element Method (FEM) analysis**, to study the structural behavior of the irregular **vaulting systems**. Analytically, future research could aim to solve the current limitations of **RGB-based detection** by integrating **Machine Learning (ML)** algorithms or using **AI** directly into the **Grasshopper** environment to have a unique workflow. Also, **decay detection** can be done through both texture and colors, rather than relying just on RGB color values, and it could resolve current limitations regarding shadows and lighting variations and improve the reliability of the mapping process. Regarding the designed **web-based visualization platform**, the capacity of the platform for **stakeholder integration** can be expanded in future works. Future versions could introduce **role-based interactive tools**. By creating customized environments for different specialists, and allowing structural engineers, art historians, and restoration teams to simultaneously add annotations, upload lab test results, or edit decay boundaries directly on the browser, the website would evolve from a visualization and reporting tool into a fully comprehensive, multi-disciplinary **management system** for conservation planning of built heritage. Furthermore, one of the key strengths of the proposed workflow is its **high replicability**. The proposed methodology is designed to be highly replicable and can be easily adapted to other historical case studies. Additionally, regarding different **3D metric survey techniques**, future research could improve this method by integrating **Terrestrial Laser Scanning (TLS)**. While the current survey methods are efficient, TLS could provide higher **point cloud density** and **sub-millimeter accuracy**, which will increase point cloud accuracy and as a result, also the **VPL-based decay mapping** quality.

Bibliography

Acosta, E., Spettu, F., & Fiorillo, F. (2022). A procedure to import a complex geometry model of a heritage building into BIM for advanced architectural representations. The International Archives of the Photogrammetry, Remote Sensing and Spatial Information Sciences, XLVI-2/W1-2022, 9–16. https://doi.org/10.5194/isprs-archives-XLVI-2-W1-2022-9-2022

Alfio, V. S., Costantino, D., Fallah, M., Restuccia Garofalo, A., Pepe, M., & Piumatti, P. (2025). Integrated workflow for 3D modelling of historic architecture: A multi-sensor approach. In 2025 IMEKO TC26 International Conference on Metrology for Archaeology and Cultural Heritage (pp. 1–6). https://doi.org/10.21014/tc26-2025.001

Alshawabkeh, Y., & Baik, A. (2023). Integration of photogrammetry and laser scanning for enhancing scan-to-HBIM modeling of Al Ula heritage site. Heritage Science, 11, 147. https://doi.org/10.1186/s40494-023-00997-2

Aricò, M., Ferro, C., La Guardia, M., Lo Brutto, M., Taranto, G., & Ventimiglia, G. M. (2024). Scan-to-BIM process and architectural conservation: Towards an effective tool for the thematic mapping of decay and alteration phenomena. Heritage, 7(11), 6257–6281. https://doi.org/10.3390/heritage7110294

Bolognesi, C. M., & Bassorizzi, D. (2023). Scan to BIM processes: Heritage accuracy versus BIM semantic. The International Archives of the Photogrammetry, Remote Sensing and Spatial Information Sciences, XLVIII-M-2-2023, 267–272. https://doi.org/10.5194/isprs-archives-XLVIII-M-2-2023-267-2023

Brown, C. J., Yao, S., Zhang, X., Brown, C. J., Caven, J. B., Krusche, K. U., & Wang, C. (2023). Visualizing digital architectural data for heritage education. Electronic Imaging, 35(1), 393-1–393-7. https://doi.org/10.2352/EI.2023.35.1.VDA-393

Brunetti, O. (2012). Martina Franca nel Settecento: Strutture architettoniche e immagine urbana. Edifir Edizioni.

Bruno, S., Scioti, A., Pierucci, A., Rubino, R., Di Noia, T., & Fatiguso, F. (2022). VERBUM—Virtual enhanced reality for building modelling (virtual technical tour in digital twins for building conservation). Journal of Information Technology in Construction, 27, 20–47. https://doi.org/10.36680/j.itcon.2022.002

Caciora, T., Ilieș, A., Herman, G. V., Berdenov, Z., Safarov, B., Bilalov, B., Ilieș, D. C., Baias, Ș., & Hassan, T. H. (2024). Advanced semi-automatic approach for identifying damaged surfaces in cultural heritage sites: Integrating UAVs, photogrammetry, and 3D data analysis. Remote Sensing, 16(16), 3061. https://doi.org/10.3390/rs16163061

Chiabrando, F., Lo Turco, M., & Rinaudo, F. (2017). Modeling the decay in an HBIM starting from 3D point clouds: A followed approach for cultural heritage knowledge. The International Archives of the Photogrammetry, Remote Sensing and Spatial Information Sciences, XLII-2/W5, 605–612. https://doi.org/10.5194/isprs-archives-XLII-2-W5-605-2017

Croce, V., Caroti, G., De Luca, L., Jacquot, K., Piemonte, A., & Véron, P. (2021). From the semantic point cloud to heritage-building information modeling: A semiautomatic approach exploiting machine learning. Remote Sensing, 13(3), 461. https://doi.org/10.3390/rs13030461

Croce, V., Caroti, G., Piemonte, A., De Luca, L., & Véron, P. (2023). H-BIM and artificial intelligence: Classification of architectural heritage for semi-automatic scan-to-BIM reconstruction. Sensors, 23(5), 2497. https://doi.org/10.3390/s23052497

Cusniriuc, V. T., & Martillo Flores, J. (2019). Bonavalle: Rilievo metrico 3D, HBIM e VPL per la salvaguardia del patrimonio architettonico [Master's thesis, Politecnico di Torino].

de Cadilhac, R. (2022). Old monasteries and new cemeteries: The case of the Capuchins in Conversano, Italy. Conservation Science in Cultural Heritage, 22(1), 405–424. https://doi.org/10.6092/issn.1973-9494/17363

Di Luggo, A., Campi, M., Repola, L., Cera, V., Scandurra, S., Pulcrano, M., & Falcone, M. (2019). Evaluation of historical heritage documentation: Reality based survey and derivative models. The International Archives of the Photogrammetry, Remote Sensing and Spatial Information Sciences, XLII-2/W17, 115–122. https://doi.org/10.5194/isprs-archives-XLII-2-W17-115-2019

Galantucci, R. A., Musicco, A., Verdoscia, C., & Fatiguso, F. (2025). Machine learning for the semi-automatic 3D decay segmentation and mapping of heritage assets. International Journal of Architectural Heritage, 19(3), 389–407. https://doi.org/10.1080/15583058.2023.2287152

Gaspari, F., Barbieri, F., Fascia, R., & Pinto, L. (2025). Collaborative defect annotation on 3D seamless open-source framework. The International Archives of the Photogrammetry, Remote Sensing and Spatial Information Sciences, XLVIII-G-2025, 505–511. https://doi.org/10.5194/isprs-archives-XLVIII-G-2025-505-2025

Heyman, J. (1995). The stone skeleton: Structural engineering of masonry architecture. Cambridge University Press. https://doi.org/10.1017/CBO9781107050310

ICOMOS International Scientific Committee for Stone. (2008). Illustrated glossary on stone deterioration patterns. ICOMOS.

Laasch, H., Patankar, Y., Tennenini, C., Medic, T., Flatt, R. J., & Wieser, A. (2025). Machine learning-based detection of stone degradation using TLS, photographs and HBIM: A case study on the Lausanne Cathedral. In STONE 2025: Proceedings of the 15th International Congress on the Deterioration and Conservation of Stone (pp. 545–551).

Lanzara, E., Fatigati, G., Guardascione, S., & Rapicano, M. T. (2024). VPL geometry processing for open multilevel and multiscalar databases. The International Archives of the Photogrammetry, Remote Sensing and Spatial Information Sciences, XLVIII-2/W8-2024, 273–280. https://doi.org/10.5194/isprs-archives-XLVIII-2-W8-2024-273-2024

Lanzara, E., & Improta, I. (2026). Scan-to-scoring: An algorithmic model for conservation maintenance records. The International Archives of the Photogrammetry, Remote Sensing and Spatial Information Sciences, XLVIII-2/W12-2026, 231–238. https://doi.org/10.5194/isprs-archives-XLVIII-2-W12-2026-231-2026

Lasorella, M., Rondinelli, M. F. L., Guida, A., & Fatiguso, F. (2026). Integrated digital environments for the knowledge and management of low-accessible cultural heritage: A multiscale web-based framework. Heritage, 9(4), 133. https://doi.org/10.3390/heritage9040133

Lau-Kee, D., Billyard, A., Faichney, R., Kozato, Y., Otto, P., Smith, M., & Wilkinson, I. (1991). VPL: An active, declarative visual programming system. In Proceedings of the 1991 IEEE Workshop on Visual Languages (pp. 40–46). IEEE Computer Society.

Legendziewicz, A., Grodzka, E., Marcinów, A., & Błaszczyk, K. (2025). Between modesty and modernity: The transformations of the architecture of the Franciscan church in Żagań between the second half of the thirteenth century and the beginning of the sixteenth century. Arts, 14(1), 11. https://doi.org/10.3390/arts14010011

Lercari, N., Jaffke, D., Campiani, A., Guillem, A., McAvoy, S., Jiménez Delgado, G., & Bevk Neeb, A. (2021). Building cultural heritage resilience through remote sensing: An integrated approach using multi-temporal site monitoring, datafication, and WebGL visualization. Remote Sensing, 13(20), 4130. https://doi.org/10.3390/rs13204130

Malinverni, E. S., Mariano, F., Di Stefano, F., Petetta, L., & Onori, F. (2019). Modelling in HBIM to document materials decay by a thematic mapping to manage the cultural heritage. The International Archives of the Photogrammetry, Remote Sensing and Spatial Information Sciences, XLII-2/W11, 777–784. https://doi.org/10.5194/isprs-archives-XLII-2-W11-777-2019

Markiewicz, J., Kot, P., Georgopoulos, A., Bocheńska, A., Muradov, M., Hess, M., Czajkowski, K., Zawieska, D., & Antoniou, A. (2025). Transforming architectural heritage documentation: Developing integrated European recommendations for safeguarding and preservation. npj Heritage Science, 13, 622. https://doi.org/10.1038/s40494-025-02200-0

Martina Cultura. (n.d.). Chiesa di Sant'Antonio dei Cappuccini. https://martinacultura.altervista.org/wordpress/?p=18

Nieto-Julián, E., Bruno, S., & Moyano, J. (2024). An efficient process for the management of the deterioration and conservation of architectural heritage: The HBIM project of the Duomo of Molfetta (Italy). Remote Sensing, 16(23), 4542. https://doi.org/10.3390/rs16234542

Pepe, M., Restuccia Garofalo, A., Costantino, D., Tana, F. F., Palumbo, D., Alfio, V. S., & Spacone, E. (2024). From point cloud to BIM: A new method based on efficient point cloud simplification by geometric feature analysis and building parametric objects in Rhinoceros/Grasshopper software. Remote Sensing, 16(9), 1630. https://doi.org/10.3390/rs16091630

Perfetti, L., Spettu, F., Achille, C., Fassi, F., Navillod, C., & Cerutti, C. (2023). A multi-sensor approach to survey complex architectures supported by multi-camera photogrammetry. The International Archives of the Photogrammetry, Remote Sensing and Spatial Information Sciences, XLVIII-M-2-2023, 1209–1216. https://doi.org/10.5194/isprs-archives-XLVIII-M-2-2023-1209-2023

Remondino, F. (2011). Heritage recording and 3D modeling with photogrammetry and 3D scanning. Remote Sensing, 3(6), 1104–1138. https://doi.org/10.3390/rs3061104

Sánchez-Aparicio, L. J., Santamaría-Maestro, R., Sanz-Honrado, P., Villanueva-Llauradó, P., Aira-Zunzunegui, J. R., & González-Aguilera, D. (2025). A holistic solution for supporting the diagnosis of historic constructions from 3D point clouds. Remote Sensing, 17(12), 2018. https://doi.org/10.3390/rs17122018

Sanz-Honrado, P., Santamaría-Maestro, R., & Sánchez-Aparicio, L. J. (2026). Seg4D: An open-source solution for supporting the diagnosis of historic constructions using 3D point clouds—A case study application. The International Archives of the Photogrammetry, Remote Sensing and Spatial Information Sciences, XLVIII-2/W12-2026, 439–446. https://doi.org/10.5194/isprs-archives-XLVIII-2-W12-2026-439-2026

Seo, H. (2025). R–C–C fusion classifier for automatic damage detection of heritage building using 3D laser scanning. Journal of Civil Structural Health Monitoring, 15, 927–941. https://doi.org/10.1007/s13349-024-00857-y

Stefani, C., Brunetaud, X., Janvier-Badosa, S., Beck, K., De Luca, L., & Al-Mukhtar, M. (2014). Developing a toolkit for mapping and displaying stone alteration on a web-based documentation platform. Journal of Cultural Heritage, 15(1), 1–9. https://doi.org/10.1016/j.culher.2013.01.011

Shotton, E. (2018). Living in the clouds: Conceptual reconstructions of harbour structures. Journal of Cultural Heritage Management and Sustainable Development, 8(4), 405–419. https://doi.org/10.1108/JCHMSD-08-2017-0052

Tedeschi, A. (2010). Architettura parametrica: Introduzione a Grasshopper (2nd ed.). Le Penseur.

Tong, X., Zhang, C., Zhou, J., & Di Sarno, L. (2026). Defect augmented Heritage-BIM for masonry structures leveraging deep learning-based segmentation. International Journal of Architectural Heritage, 1–21. https://doi.org/10.1080/15583058.2026.2633538

Vignali, L., & Resta, C. (2025). Interactive visualization tools for managing the monitoring system of the Piazza del Duomo UNESCO site in Pisa. Heritage, 8(1), 5. https://doi.org/10.3390/heritage8010005

Wang, X., Wu, C., & Que, R. (2021). Regularized rebuild workflow of HBIM for built heritage documentation. ISPRS Annals of the Photogrammetry, Remote Sensing and Spatial Information Sciences, VIII-M-1-2021, 193–200. https://doi.org/10.5194/isprs-annals-VIII-M-1-2021-193-2021

XGRIDS Technology. (2024). LIXEL L2 Handheld Mobile Mapping System: Technical Specifications. Shenzhen XGRIDS Technology Co., Ltd. https://www.xgrids.com

Politecnico di Torino, Master’s Degree Course in Architecture For Heritage